A Thesis
For the Degree of Doctor of Philosophy

Anti-diabetic and Anti-obesity effects of Sulforaphane in Broccoli leaf extract

GRADUATE SCHOOL
JEJU NATIONAL UNIVERSITY

College of Veterinary Medicine

Sachithra S. Ranaweera

February 2021

Anti-diabetic and Anti-obesity effects of Sulforaphane in Broccoli leaf extract

Sachithra S. Ranaweera

(Supervised by Professor Han Chang-Hoon)

A thesis submitted in partial fulfillment of the requirement for the degree of

Doctor of Philosophy

2021. 02.

The thesis has been examined and approved by

.....

Thesis Director, Professor Lee Young Jae
College of Veterinary Medicine, Jeju National University

.....

Professor Jee Youngheun
College of Veterinary Medicine, Jeju National University

.....

Professor Kim Se Jae
College of Natural Science, Jeju National University

.....

Professor Kim Min Young
College of Applied Life Science, Jeju National University

.....

Professor Han Chang-Hoon
College of Veterinary Medicine, Jeju National University

College of Veterinary Medicine
GRADUATE SCHOOL
JEJU NATIONAL UNIVERSITY

Table of Contents

List of Tables vii

List of Figures viii

List of Abbreviations x

General Introduction 12

PART-I 20

Anti-diabetic effect of Sulforaphane in Broccoli leaf extract on HepG2 cells and ob/ob mice 20

1.1. Abstract 21

1.2. Introduction 22

1.3. Materials and Method 24

1.3.1. Materials and chemicals 24

1.3.2. Preparation of BLE 24

1.3.3. Broccoli extract UPLC standardization 25

1.3.4. HepG2 cell culture and treatment 25

1.3.5. Cell viability assay 26

1.3.6. 2-NBDG glucose uptake assay in insulin resistance HepG2 cells 26

1.3.7. Animals 27

1.3.8. Sample treatment 28

1.3.9. Insulin tolerance test (ITT) 29

1.3.10. Glucose tolerance test (GTT) 29

1.3.11. Blood glucose, serum insulin, and HOMA-IR 29

1.3.12. Western blot 30

1.3.13. RNA isolation, library preparation, sequencing, and data analysis 30

1.3.14. Statistical analysis 32

1.4. Results 33

1.4.1. UPLC analysis of BLE 33
1.4.2. Cytotoxicity of BLE on HepG2 cells..... 34
1.4.3. Glucose uptake in high glucose treated HepG2 cells 34
1.4.4. The phosphorylation of Akt and GSK3β in high glucose treated HepG2 cells……..... 36
1.4.5. Insulin sensitivity in ob/ob mice..... 38
1.4.6. Glucose tolerance in ob/ob mice..... 40
1.4.7. Serum parameters in ob/ob mice 42
1.4.8. The phosphorylation levels of Akt and GSK3β in ob/ob mice liver ... 44
1.4.9. Differential gene expression in ob/ob mice liver..... 46
1.5. Discussion 50
PART-II 56
Anti-obesity effect of Sulforaphane in Broccoli leaf extract on 3T3-L1 adipocyte and ob/ob mice..... 56
2.1. Abstract 57
2.2. Introduction 58
2.3. Materials and methods 61
2.3.1. Material and Chemicals 61
2.3.2. Preparation of broccoli leaf extract..... 61
2.3.3. Broccoli extract UPLC standardization. 62
2.3.4. Cell culture and differentiation 62
2.3.5. Cytotoxicity assay..... 63
2.3.6. Oil Red O staining 64
2.3.7. Measurement of triglyceride (TG) content in 3T3-L1 adipocytes..... 64
2.3.8. 2-NBDG uptake assay 65
2.3.9. Animals..... 65
2.3.10. Sample treatment 66

2.3.11. Blood glucose 66
2.3.12. Serum parameters in ob/ob mice 67
2.3.13. Tissue processing and hematoxylin & eosin (H&E) staining 67
2.3.14. Western blot analysis 68
2.3.15. RNA sequencing analysis 68
2.3.16. Statistical analysis 69
2.4. Results 70
2.4.1. UPLC analysis of BLE 70
2.4.2. Cytotoxicity of BLE in 3T3-L1 cells 70
2.4.3. Lipid accumulation and TG content in 3T3-L1 adipocytes 71
2.4.4. Glucose uptake in 3T3-L1 adipocytes 73
2.4.5. Phosphorylation of AMPK and ACC in 3T3-L1 adipocytes 75
2.4.6. Hepatic lipid accumulation in ob/ob mouse liver 77
2.4.7. AMPK signaling pathway in white adipose tissue of ob/ob mice 80
2.4.8. Serum parameters of ob/ob mice 82
2.4.9. Blood glucose concentrations of ob/ob mice 84
2.4.10. Hepatic gene expression analysis 85
2.5. Discussion 89
PART-III 95
Anti-inflammatory effects of Sulforaphane in Broccoli leaf extract on LPS-stimulated RAW 264.7 cells and ob/ob mice 95
3.1. Abstract 96
3.2. Introduction 97
3.3. Materials and Methods 100
3.3.1. Materials 100
3.3.2. Preparation of broccoli leaf extract 100

3.3.3. DPPH radical scavenging activity 101
3.3.4. RAW 264.7 cell culture and treatment 101
3.3.5. Cell viability assay 102
3.3.6. Measurement of NO production 102
3.3.7. Enzyme-linked immunosorbent assay (ELISA) 103
3.3.8. Measurement of COX-2 and iNOS protein expression 103
3.3.9. Animals experiments 104
3.3.10. Sample treatment 104
3.3.11. Total RNA isolation, library preparation, sequencing, and data analysis… 105
3.3.12. Statistical analysis 106
3.4. Results 107
3.4.1. DPPH radical scavenging activity 107
3.4.2. Effects of BLE on cell viability in RAW 264.7 cells 108
3.4.3. Inhibition of LPS-stimulated NO production in RAW 264.7 cells.... 109
3.4.4. Inhibition of LPS-stimulated COX-2 and iNOS production in RAW 264.7 cells 111
3.4.5. Inhibitory effect of SFN and BLE on TNF-α, IL-6, and IL-1β production 112
3.4.6. Differential gene expression analysis of ob/ob mice liver 115
3.5. Discussion 120
General Conclusion 125
References 128
Acknowledgement 149

List of Tables

Table 1. Up-regulated genes related to insulin signaling & glucose metabolism in ob/ob mice liver which were normalized by SFN & BLE..... 47

Table 2. Down-regulated genes related to insulin signaling & glucose metabolism in ob/ob mice liver which were normalized by SFN & BLE..... 47

Table 3. Up-regulated genes related to lipid metabolism in ob/ob mice liver which were normalized by SFN & BLE..... 86

Table 4. Down-regulated genes related to lipid metabolism in ob/ob mice liver which were normalized by SFN & BLE..... 86

Table 5. Antioxidant activity of samples expressed as IC^{50} and AEAC values..... 108

Table 6. Up-regulated genes related to inflammation in ob/ob mice liver which were normalized by SFN & BLE 116

Table 7. Down-regulated genes related to inflammation in ob/ob mice liver which were normalized by SFN & BLE..... 117

List of Figures

Fig. 1. Insulin signaling pathway..... 12

Fig. 2. Role of AMPK in the regulation of lipid and glucose metabolism. 13

Fig. 3. Obesity-induce inflammation in the pathogenesis of the metabolic syndrome 14

Fig. 4. GRN convert into SFN by the action of the enzyme myrosinase 15

Fig. 5. Hypothetical model: SFN in BLE restores the disturbed gene expression to normal level……18

Fig. 6. Hypothetical model: anti-diabetic effect of SFN and BLE…….23

Fig. 7. Preparation of BLE by PEF treatment…….25

Fig. 8. HepG2 cell culture and experiments 27

Fig. 9. Animal experiment: sample treatment 28

Fig. 10. Overview of RNA sequencing analysis 32

Fig. 11. UPLC analysis of BLE..... 33

Fig. 12. Effect of BLE on HepG2 cell viability..... 34

Fig. 13. Glucose uptake in high glucose treated HepG2 cells. 35

Fig. 14. Phosphorylation level of Akt and GSK3β in high glucose treated HepG2 cells. 37

Fig. 15. Effect of SFN and BLE on the insulin tolerance in ob/ob mice. 39

Fig. 16. Effect of SFN and BLE on the glucose tolerance in ob/ob mice. 41

Fig. 17. Effect of SFN and BLE on the insulin resistance in ob/ob mice..... 43

Fig. 18. The phosphorylation levels of Akt and GSK3β in ob/ob mice liver. 45

Fig. 19. Differential expression of genes in ob/ob mice liver. 49

Fig. 20. Anti-diabetic effect of SFN and BLE…….....55

Fig. 21. Hypothetical model: anti-obesity effect of SFN and BLE……60

Fig. 22. 3T3-L1 cell culture and treatment. 63

Fig. 23. Effect of BLE on 3T3-L1 cell viability. 70

Fig. 24. Lipid accumulation and TG content of 3T3-L1 adipocytes 72

Fig. 25. Glucose uptake in the 3T3-L1 adipocytes. 74

Fig. 26. Phosphorylation of AMPK pathway molecules in 3T3-L1 adipocytes..... 76

Fig. 27. Hepatic lipid accumulation in ob/ob mice..... 79

Fig. 28. Phosphorylation of AMPK, ACC, and the expression of HMGCR in white adipose tissue of ob/ob mice. 81

Fig. 29. Serum parameters in ob/ob mice. 83

Fig. 30. Blood glucose concentration of ob/ob mice. 84

Fig. 31. Differential gene expression analysis in ob/ob mice liver. 88

Fig. 32. Anti-obesity effect of SFN and BLE…….....94

Fig. 33. Hypothetical model: anti-inflammatory effect of SFN and BLE……..99

Fig. 34. DPPH radical scavenging activity of SFN and BLE. 107

Fig. 35. Effects of BLE on RAW 264.7 cell viability. 109

Fig. 36. Cell morphology and NO production in LPS-stimulated RAW 264.7 cells. 110

Fig. 37. Effects of SFN and BLE on iNOS and COX-2 expressions 112

Fig. 38. Production of pro-inflammatory cytokines. 114

Fig. 39. Differential gene expression in ob/ob mice liver. 119

Fig. 40. Anti-inflammatory effect of SFN and BLE…….....124

Fig. 41. SFN in BLE exerts anti-diabetic, anti-obesity, and anti-inflammatory effects by restoring the disturbed gene expression to normal level……..126

List of Abbreviations

ACC	Acetyl-CoA carboxylase
Akt	Protein kinase B
AMPK	AMP-activated protein kinase
ANOVA	Analysis of variance
BLE	Broccoli leaf extract
COX-2	Cyclooxygenase-2
DMEM	Dulbecco's Modified Eagle Medium
DPPH	2,2-diphenyl-1-picryl-hydrazyl-hydrate
ELISA	Enzyme-linked immunosorbent assay
FA	Fatty acid
FAO	Fatty acid oxidation
FBS	Fetal bovine serum
GRN	Glucoraphanin
GSK3β	Glycogen synthase kinase 3 beta
GTT	Glucose tolerance test
HMGCR	Hydroxy-3-methylglutaryl coenzyme A reductase
HOMA-IR	Homeostasis model assessment of insulin resistance index
IL-1β	Interleukin 1β
IL-6	Interleukin 6
iNOS	Inducible nitric oxide synthase
IR	Insulin resistance
IRS1	insulin receptor substrate 1

ITT	Insulin tolerance test
LDL	Low-density lipoprotein
LPS	Lipopolysaccharides
MET	Metformin
NAFLD	Non-alcoholic fatty liver disease
PEF	Pulsed electric field
PPI	Protein-protein interaction
ROS	Reactive oxygen species
SFN	Sulforaphane
T1DM	Type 1 diabetes mellitus
T2DM	Type 2 diabetes mellitus
TC	Total cholesterol
TG	Triglyceride
TNF-α	Tumor Necrosis Factor-α
UPLC	Ultra performance liquid chromatography

General Introduction

Diabetes

Diabetes mellitus is a chronic metabolic disorder characterized by chronic elevation in blood sugar levels. Type 1 diabetes mellitus (T1DM) indicates beta-cell destruction that may ultimately lead to absolute insulin deficiency [1]. In type 2 diabetes mellitus (T2DM), impaired insulin action in the form of insulin resistance (IR) leads to abnormal hepatic glucose production and decreased hepatic glucose utilization [2]. T2DM is the most common form of diabetes worldwide [3].

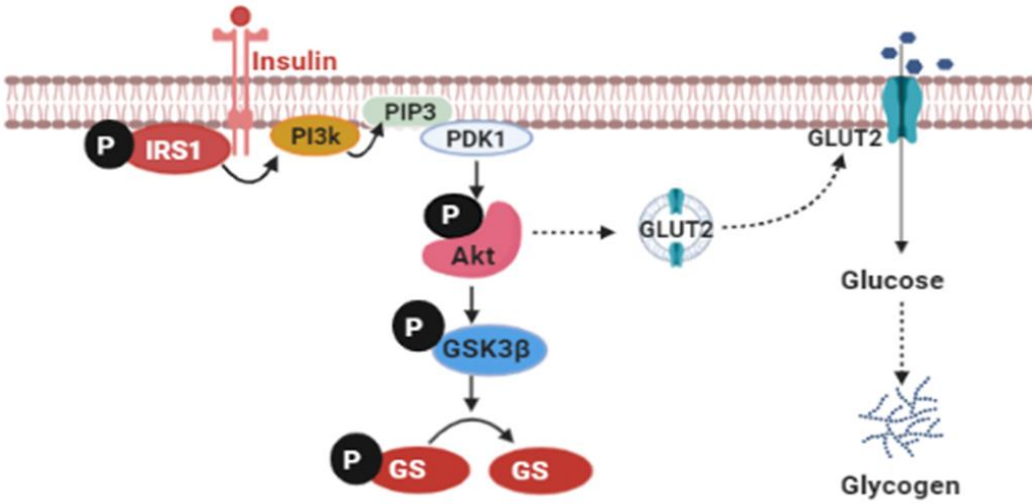

Fig. 1. Insulin signaling pathway.

Insulin receptor activation leads to phosphorylation of crucial tyrosine residues on insulin receptor substrate 1 (IRS1), following activation of the phosphatidylinositol 3-kinase (PI3K)/protein kinase B (PKB/Akt) pathway [4] (Fig. 1). Akt is one of the principal regulatory molecules associated with glucose metabolism mediated via cellular glucose uptake [5]. In addition, Akt inactivates glycogen synthase kinase (GSK3β) via phosphorylation that leads to subsequent dephosphorylation and activation of glycogen synthase (GS) [4].

Obesity

Obesity is associated with metabolic disorders including type II diabetes, hypertension, inflammation, and non-alcoholic fatty liver disease (NAFLD) [6]. Obesity is linked to excessive growth and expansion of adipose tissue due to an imbalance between energy intake and expenditure [7].

AMP-activated protein kinase (AMPK) is a regulatory enzyme involved in lipid and energy metabolism [8]. Activation of AMPK regulates lipogenesis, fatty acid oxidation, and glucose transport [9]. Phosphorylation of AMPK inhibits lipid biosynthesis via inactivation of key metabolic enzymes involved in fatty acid and cholesterol synthesis including acetyl-CoA carboxylase (ACC) and hydroxy-3-methylglutaryl coenzyme A reductase (HMGCR) [10, 11] (Fig. 2). In addition, activation of AMPK leads to translocation of the glucose transporter 4 (GLUT4) into the cell membrane, which increases glucose uptake by cells [9].

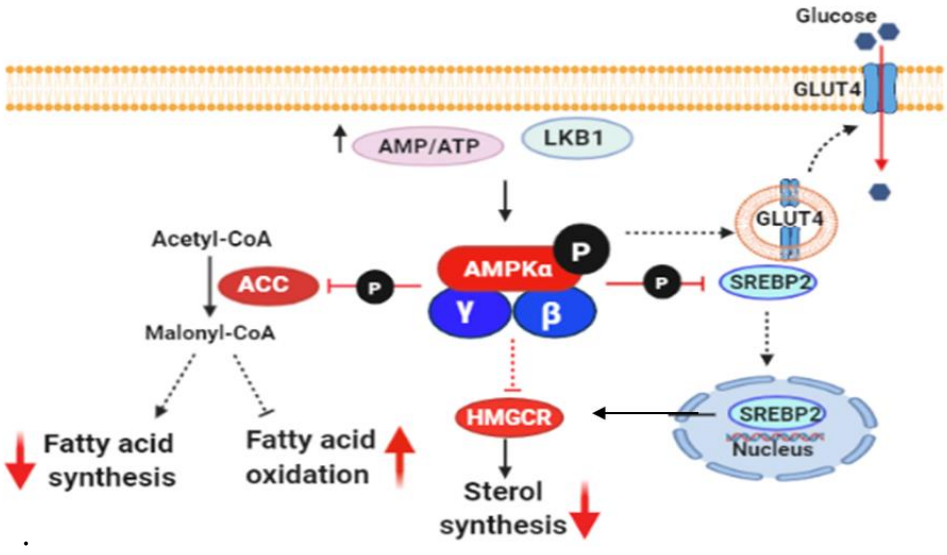

Fig. 2. Role of AMPK in the regulation of lipid and glucose metabolism.

Inflammation

Chronic low-grade inflammation and activation of the immune system lead to the pathogenesis of obesity-related insulin resistance and T2DM [6]. Increased concentrations of systemic inflammatory markers including TNF-α, IL-6, and IL-1β might interfere with insulin action by suppressing insulin signal transduction [12]. In particular, inflammation in adipose tissue and liver is associated with obesity [6].

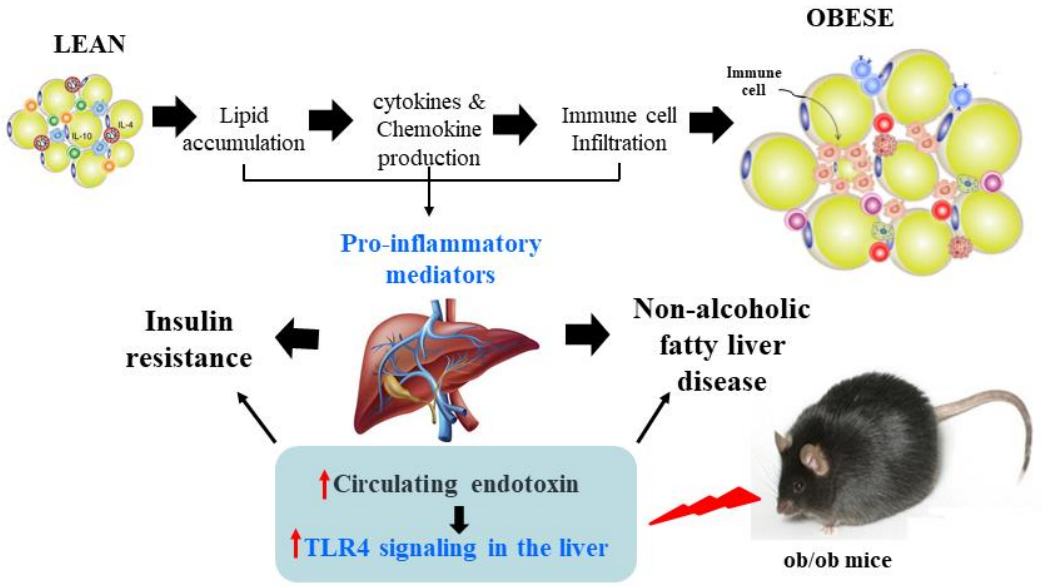

Fig. 3. Obesity-induce inflammation in the pathogenesis of the metabolic syndrome

The accumulation of lipids in adipose tissue leads to the initiation of an inflammatory cascade [6]. The release of chemokines and pro-inflammatory cytokines by adipocytes triggers immune cell infiltration into the adipose tissues resulting in systemic inflammation and peripheral insulin resistance [13]. Obese mice showed an increase in circulating endotoxins, which activate TLR4 signaling in the liver [14]. Liver inflammation stimulates insulin resistance and increases the risk of NAFLD [15] (Fig. 3).

Broccoli (Brassica oleracea var. italica)

Broccoli is a widely consumed green vegetable, which contains extensive amounts of GRN, SFN, antioxidants, vitamin C, carotenoids, and polyphenols [16]. Previous *in vitro* and *in vivo* studies have reported that consumption of young broccoli sprouts may improve IR in type 2 diabetic patients [17-19]. It was established that consumption of fresh broccoli sprouts leads to a significant decrease in insulin resistance and blood insulin concentration [17]. In addition, the treatment of broccoli sprouts reduced oxidative stress, serum triglycerides, and oxidized LDL/LDL-cholesterol ratio in diabetic conditions [18, 19]. Further, streptozotocin-induced diabetic rats showed significant low levels of blood glucose and liver glycogen after treatment with an aqueous extract of broccoli sprouts [16].

Suforaphane and Glucoraphanin

Glucoraphanin (GRN) is a naturally occurring glucosinolate found in broccoli [19]. GRN is converted to the bioactive isothiocyanate, sulforaphane (SFN), by the action of the enzyme myrosinase during the chopping or crushing of broccoli [19]. In both rodents and humans, GRN is hydrolyzed by gut microbiota-derived myrosinase into SFN before intestinal absorption [20] (Fig. 4).

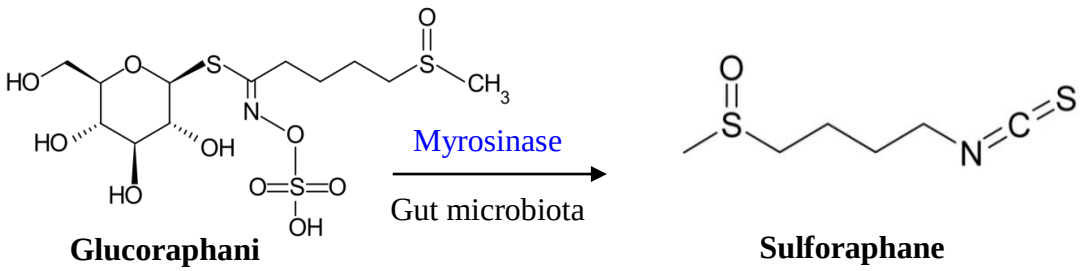

Glucoraphani **Sulforaphane**

Fig. 4. GRN convert into SFN by the action of the enzyme myrosinase

The anti-obesity mechanism of SFN was associated with regulation of AMPK pathway in obese mice [21]. SFN attenuates obesity by inhibiting adipogenesis and activating the AMPK pathway in obese mice fed with high-fat diet (HFD) [21]. SFN decreased the accumulation of lipid droplets and inhibited the elevation of triglycerides in adipocytes [22]. In addition, SFN treatment improved insulin sensitivity and hepatic glycogen production in the diabetic state [23]. SFN-treated obese mice showed increased levels of IRS1 protein, phosphorylated Akt, and enhanced GLUT4 translocation [24]. Furthermore, SFN suppressed glucose production and decreased gluconeogenesis in H4IIE cells [25].

GRN ameliorated obesity and insulin resistance via adipose tissue browning and reduction of metabolic endotoxemia in diet-induced obese mice [26]. GRN treatment increased UCP1 protein expression in white adipose depots and enhanced browning in beige adipocytes of obese mice [26].

Finally, these findings suggest that GRN and SFN exert anti-obesity and anti-diabetic effects, and represent potential therapeutic agents in the management of obesity and T2DM. Nevertheless, further studies are needed to corroborate these findings and test the efficacy of these agents in treating obese and diabetic patients.

Even though the anti-diabetic effects of broccoli sprouts in animal models have been documented, evidence is inadequate to support the benefits of broccoli by-products including leaves. The hydroalcoholic extract of broccoli leaves has hypoglycemic and hypolipidemic effects in diabetic rats [27]. However, the mechanism of broccoli leaf extract (BLE) in diabetes and obesity is poorly understood.

Differential gene expression

Differential gene expression profiling can be potentially used to elucidate the molecular mechanisms underlying biological pathways [28]. Disease signature is usually a list of genes within a specific tissue that are up- or down-regulated when compared with healthy controls, whereas a drug signature denotes differentially expressed genes between untreated and treated samples [29]. Investigation of the connection between gene expression profiles of disease and drug signatures is a potentially useful drug discovery strategy to facilitate the treatment of metabolic diseases [29]. Gene set enrichment analysis has been used to compare disease signatures with drug signatures and identify candidate drugs for diabetes, cancer, neurological, and gastrointestinal disorders [30-32]. However, the effects of SFN on the differential gene expression in diabetes, obesity, and inflammation have yet to be investigated in animal models.

Protein-protein interaction networks

Protein-protein interactions (PPIs) are the physical contacts of high specificity established between two or more protein molecules due to biochemical events [33]. PPIs play a crucial role in cellular function and biological events in all organisms [33]. The identification of protein interactions can lead to a better understanding of mechanisms and the development of therapeutic drugs [34]. In addition, previous studies have shown that highly connected network genes ("hub genes") are more likely to be involved in disease processes [35, 36]. The effect of SFN on the expressions of hub genes related to diabetes, obesity, and inflammation in an animal model of obesity is not discovered yet.

Hypothesis

The current study hypothesized that SFN content in BLE exerts anti-diabetic, anti-obesity, and anti-inflammatory effects by normalizing the expression of genes related to insulin signaling, lipid metabolism, and inflammation. In the present study, RNA sequencing analysis was performed to identify the effects of SFN and BLE on the differential gene expression profile related to diabetes, obesity, and inflammation.

The present study investigated whether or not SFN levels in BLE exert anti-diabetic, anti-obesity, and anti-inflammatory effects by restoring the disturbed gene expression profile related to insulin signaling, lipid metabolism, and inflammation to normal levels in obese mice (Fig. 5).

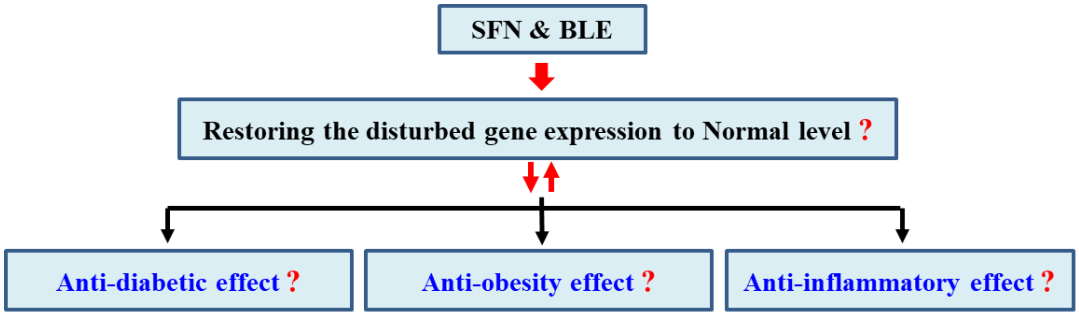

Fig. 5. Hypothetical model: SFN in BLE restores the disturbed gene expression related to diabetes, obesity, and inflammation to normal level

Objectives

This study was aimed to investigate the anti-diabetic, anti-obesity, and anti-inflammatory effects of SFN-enriched BLE, and its molecular mechanism by analyzing the differential gene expression related to insulin signaling, glucose metabolism, lipid metabolism, and inflammation.

The major objectives of the present study are:

1. To evaluate the anti-diabetic effect of SFN-enriched BLE and its molecular mechanism on HepG2 cells and ob/ob mice.
2. To investigate the anti-obesity effect of SFN-enriched BLE and its molecular mechanism on 3T3-L1 adipocytes and ob/ob mice.
3. To elucidate the anti-inflammatory effect of SFN-enriched BLE and its molecular mechanism on LPS-stimulated RAW 264.7 cells and ob/ob mice.

PART-I

Anti-diabetic effect of Sulforaphane in Broccoli leaf extract on HepG2 cells and ob/ob mice

1.1. Abstract

The present study evaluated the anti-diabetic activity of SFN enriched broccoli leaf extract (BLE) on HepG2 cells and ob/ob mice. The treatment of SFN and BLE significantly improved glucose uptake in high glucose treated HepG2 cells. Western blot analysis revealed that SFN and BLE increased phosphorylation levels of both Akt and GSK3β in high glucose treated HepG2 cells and ob/ob mice liver. SFN and BLE supplemented ob/ob mice showed significantly reduced ($P < 0.05$) serum insulin, blood glucose, and HOMA-IR values. Both insulin tolerance and glucose tolerance were significantly improved ($P < 0.05$) by SFN and BLE in ob/ob mice. Based on differential gene expression analysis, SFN and BLE normalized up-regulated 11 genes and down-regulated 11 genes related to insulin signaling and glucose metabolism in ob/ob mice liver. The protein-protein interaction network was evaluated through STRING analysis and revealed functional interaction between the normalized genes including *Atf4*, *Atf3*, *Myc*, *PGC-1α*, *Phkg1*, *Phka1*, *Pygm*, and *Gys*1 by SFN and BLE. Our findings suggest that SFN in BLE exerts a potent anti-diabetic effect by normalizing the expression of genes related to insulin signaling and glucose metabolism which are up- or down-regulated in ob/ob mice.

Keywords: Sulforaphane, Broccoli leaf extract, Anti-diabetic activity, HepG2 cells, ob/ob mice, Insulin signaling, Gene expression

1.2. Introduction

Dietary foods and food bioactive components have gained more attention in the prevention of diabetes and its complications [37, 38]. Broccoli (*Brassica oleracea var. italica*), a widely consumed green vegetable worldwide, contains high amounts of antioxidants, phenols, and glucosinolates [16]. Previous studies have reported the consumption of fresh broccoli sprouts reduced homeostasis model assessment of insulin resistance index (HOMA-IR) and serum insulin concentration [18, 17]. In addition, broccoli sprout reduces oxidative stress and improves both serum triglyceride and oxidized-LDL/LDL ratio in diabetes [39]. Broccoli sprouts have also shown a significant reduction of blood glucose and liver glycogen in streptozotocin-induced diabetic rats [16].

Broccoli, especially its sprouts, health benefits are predominantly attributed to its high content of bioactive compounds, such as glucosinolates and SFN [40]. GRN, the most abundant glucosinolate in broccoli [26], is converted to SFN by gut microbiota-derived myrosinase before intestinal absorption in both rodents and humans [41]. SFN has been shown to attenuate blood glucose levels in mice and diabetic patients [42] and protect against streptozotocin (STZ) induced type 1 diabetic [43]. Previously, the only well described SFN mechanism of action was through targeting Nrf2 pathway [26]. However, current evidence suggests that SFN might have additional target pathways [44, 45]. In recent studies, treatment with SFN was reported to have prevented hepatic insulin resistance by blocking ceramide biosynthesis in HepG2 cells [45], and SFN supplementation to obese mice improved

the insulin receptor signaling pathway [24]. While all these studies exist, the mechanism of SFN

in relation to insulin resistance, is not yet fully understood.

The present study investigated the possible mechanism underlying the anti-diabetic effect of SFN enriched BLE on insulin-resistant HepG2 cells and ob/ob mice. We observed the effect of SFN and BLE on the phosphorylation of essential proteins in the insulin signaling pathway and on the glucose uptake activity of high glucose treated HepG2 cells. In addition, the molecular mechanism underlining the anti-diabetic effect of SFN and BLE was explored by analyzing the differential gene expression profile related to insulin signaling and glucose metabolism (Fig. 6).

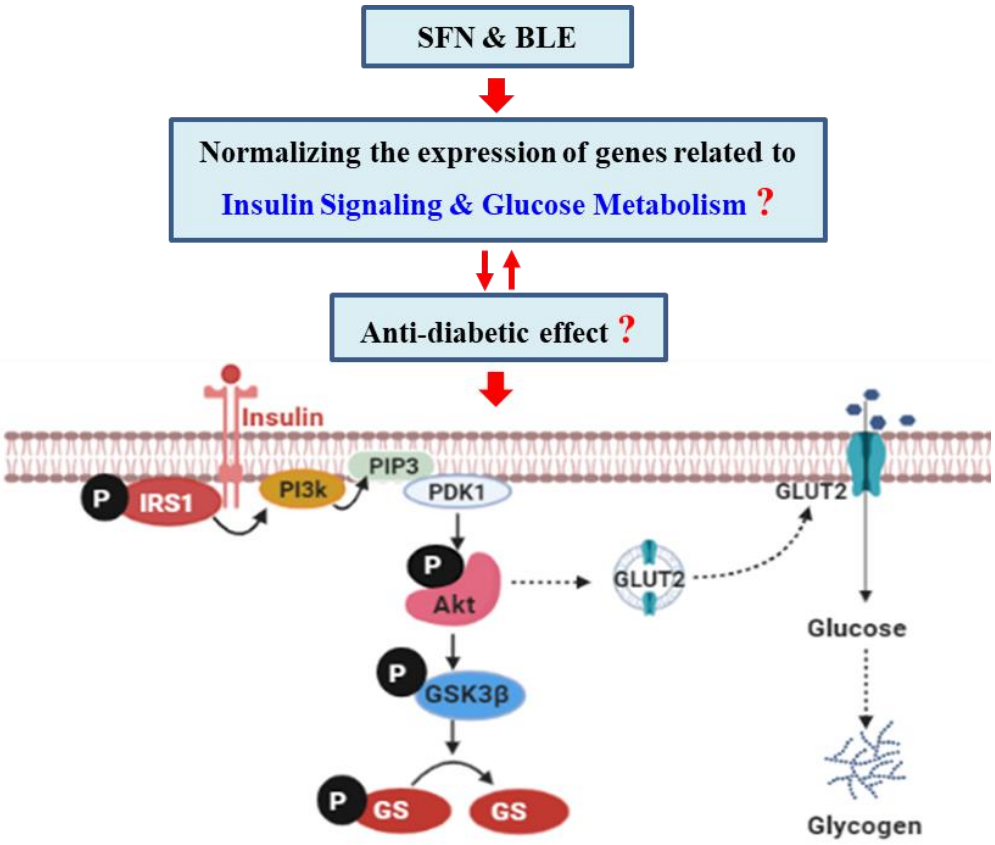

Fig. 6. Hypothetical model: anti-diabetic effect of SFN and BLE

1.3. Materials and Method

1.3.1. Materials and chemicals

Human insulin and SFN were purchased from Sigma Aldrich (USA) and GRN from Cayman Chemicals (USA). β-actin primary antibody was purchased from Thermofisher (USA), p-Akt (Ser473), p-GSK3β (Ser9), Akt, and GSK3β antibodies were purchased from Cell Signaling Technology (USA). The Human HepG2 cell line was purchased from American Type Culture Collection (ATCC® HB-8065™), (USA). Dulbecco's modified Eagle's medium (DMEM) from Life Technologies (USA), EZ-Western Lumi Pico and EZ-Cytox were from DoGenBio (Korea). Mouse Insulin ELISA kit was purchased from Crystal Chem (USA). All other reagents were purchased from commercial sources and were of the analytical grade.

1.3.2. Preparation of BLE

Broccoli leaves were minced into small pieces and were added 10× volume of distilled water. Pulsed electric field (PEF) treatment was performed using 5 kW PEF at 7 kJ of total energy for 5 sec (out voltage 60%, pulsed width 25 μs, frequency 100 Hz) (Fig. 7). The suspension was mixed with 10× volume of ethanol and was extracted for about 3 hrs at room temperature. The extract was lyophilized for 72 hrs using a lyophilizer, crushed to make a fine powder, and was stored at -80 °C until use.

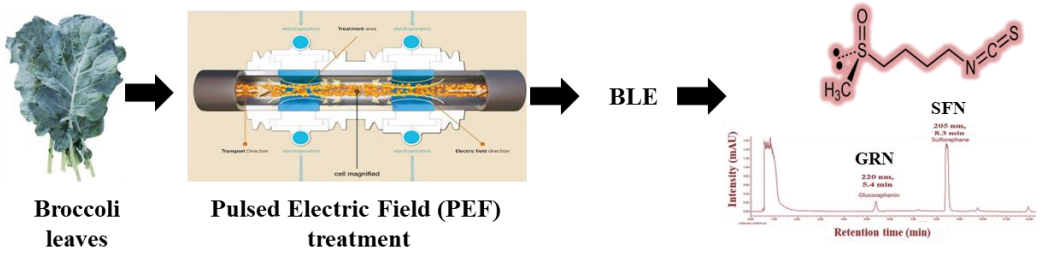

Fig. 7. Preparation of BLE by PEF treatment

1.3.3. Broccoli extract UPLC standardization

Ultra performance liquid chromatography (UPLC) analysis was performed to observe the SFN and GRN presence in the BLE. The chromatographic analysis was performed using an analytical ACQUITY UPLC™ BEH C18 column (2.1 × 100 mm) with a particle size of 1.7 µm (Waters Corporation, MA, USA). The column was installed in a column oven and maintained at 40 °C. The injection volume was 10 µL. The analysis was carried out isocratically at a flow rate of 0.5 mL/min, employing as the mobile phase a mixture of water containing 0.1% formic acid (solvent A) and acetonitrile containing 0.1% formic acid (solvent B). The gradient was 0.0 min, 2% B; 5 min, 7% B; 10 min, 20% B. SFN was detected at 205 nm and GRN was detected at 220 nm.

1.3.4. HepG2 cell culture and treatment

Human HepG2 cells were obtained from the ATCC. Cells were cultured in DMEM containing 5.5 mM D-glucose, 10% FBS, 1% penicillin, and streptomycin in a humidified atmosphere at 37 °C under 5% CO_2. After reaching about 80%

confluence, the cells were seeded in 96 well plates for the experiment. The insulin-resistant HepG2 cell model was established according to the reported method with slight modifications [46-48]. Briefly, after seeding in 96 well plates, cells were serum-starved for 12 hrs and incubated in serum-free DMEM containing either normal concentrations of glucose (5.5 mM D-glucose) or high concentrations of glucose (30 mM D-glucose) with or without the non-toxic concentration of samples (SFN; 5 μM, GRN; 5 μM, BLE; 20, 50, 100 μg/mL) for an additional 24 hrs. Cells treated with high glucose were used as insulin resistance models. Cells were treated with metformin (MET; 2 mM) used as the positive control. The cells were stimulated with or without 100 nM insulin for 30 min before harvesting.

1.3.5. Cell viability assay

The MTT assay was performed to determined cell viability using an EZ-cytox cell viability assay kit. HepG2 cells were cultured in 96-well plate at the cell density of 1×10^5 cells/well and then incubated with BLE (1-5,000 μg/mL) for 24 hrs. Cell culture media was removed and added fresh media containing 10% Ez-cytox into each well, according to the manufacturer's instructions. Plates were incubated for 3 hrs at 37 °C and 5% CO_2. Cell viability indicated by the production of formazan was measured with an ELISA microplate reader (Gordig, Austria) at 450 nm wavelength.

1.3.6. 2-NBDG glucose uptake assay in insulin resistance HepG2 cells

Cellular glucose uptake was determined by as previously reported 2-NBDG assay with slight modification [49]. HepG2 cells were cultured in 96-well plates.

After reaching confluence, the cells were serum-starved for 12 hrs and incubated in a serum-free medium containing either normal or high concentrations of glucose with or without samples (MET; 2 mM, SFN; 5 μM, GRN; 5 μM, BLE; 20, 50, 100 μg/mL) for an additional 24 hrs. The cells were incubated with 50 μM 2-NBDG with or without 100 nM insulin for 30 min. Cells were washed with ice-cold PBS for 3 times, and the fluorescence images were taken from IncuCyte® ZOOM Fluorescence Microscope (Essen BioScience, Inc. USA). The IncuCyte® ZOOM Fluorescence Processing Software was used to analyze the total fluorescent intensities of each well (Fig. 8).

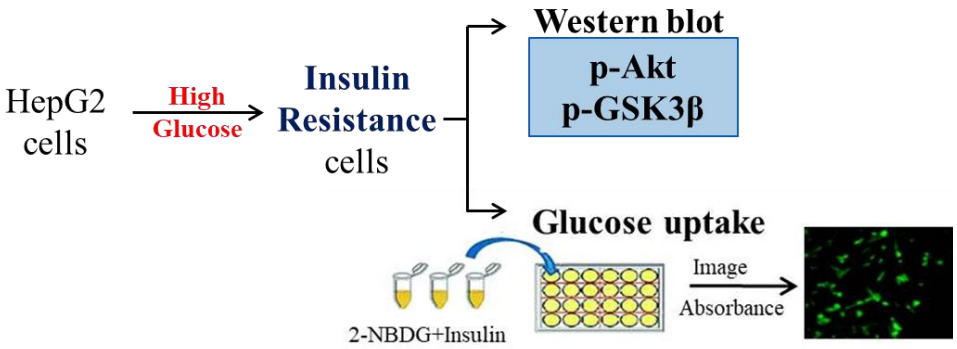

Fig. 8. HepG2 cell culture and experiments

1.3.7. Animals

Male C57BL/6J ob/ob mice (6 weeks old) were from Japan SLC Inc. (Japan). Mice were housed under conditions of controlled temperature (24 °C ± 1 °C) and 50-55% humidity with a 12 hrs light/12 hrs dark cycle. All experiments were carried out following the National Institute of Health Guide for the Care and Use of Laboratory

Animals and were approved by the Institutional Animal Care and Use Committee of Jeju National University (ACUCC; approval No. 2018-0051)

1.3.8. Sample treatment

The ob/ob mice were randomly allocated into six groups (n = 5): control ob/ob group and five samples treated groups were orally administrated MET; 100 mg/kg body weight, SFN; 0.5 mg/kg body weight, GRN; 2.5 mg/kg body weight and BLE in the dose of 50 and 500 mg/kg body weight every day in drinking water assuming that each mice drinks water 20 mL per day (Fig. 9). Normal C57BL/6 mice supplied by Orient Bio (Korea) were used as the non-obesity control group (n = 5). All the samples were diluted with distilled water, and mice were given ad libitum access to food and water. Samples were replaced with freshly prepared solutions every day to compensate for the degradative loss of active compounds. Sample treatment was continued for six weeks, and during the experiment period, food intake, water intake, and the bodyweight of the mice were monitored every day. At the end of the experiment, mice were fasted overnight, injected intraperitoneally with saline or insulin, (10 units/kg body weight) and sacrificed 15 min after injection. Tissues and blood were collected and stored at -80 °C for further analysis.

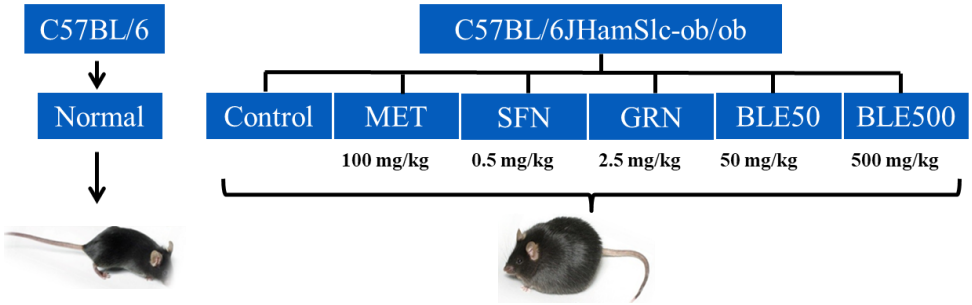

Fig. 9. Animal experiment: sample treatment

1.3.9. Insulin tolerance test (ITT)

At the end of week 4, mice were fasted for 6 hrs before administration of the insulin bolus. Human insulin (Sigma, USA) was injected to the mice intraperitoneally (IP) with 2 IU/kg body weight. Blood glucose concentrations were measured at time points 0, 30, 60, 90, and 120 min after the injection of insulin.

1.3.10. Glucose tolerance test (GTT)

At the end of week 4, mice were fasted for 14 hrs before administration of the glucose bolus. Glucose was administrated to the mice by gavage (20% glucose solution, 2 g/kg mice). Blood glucose levels were measured using a blood glucose monitor (Lipidpro, OSANG healthcare, Korea) from the tail vein at 0, 30, 60, 90, and 120 min after the injection.

1.3.11. Blood glucose, serum insulin, and HOMA-IR

After six weeks of treatment, mice were fasted 14 hrs, and blood glucose levels were measured using a blood glucose monitor (Lipidpro, OSANG healthcare, Korea). Fasting serum insulin levels were determined using an ELISA kit (Crystal Chem, USA) according to the manufacturer's instructions. HOMA-IR was calculated using fasting insulin and glucose values [(glucose mg/dL × insulin μU/mL)/405].

1.3.12. Western blot

Cells were washed with PBS and lysed with ice-cold RIPA buffer (20 mM Tris-HCl pH 7.5, 150 mM NaCl, 1 mM EGTA, 1 mM Na_2EDTA, 1% NP-40, 1% Sodium deoxycholate, 2.5 mM Sodium pyrophosphate, 1 mM $NaVO_4$, 1μg/mL leupeptin) containing protease and phosphatase inhibitor mixture. Liver tissues were homogenized with RIPA buffer and centrifuge at 12,000 rpm for 10 min. The supernatant was separated, and protein concentrations determined by Bradford assay. The equal amount of protein was mixed with 20% of loading buffer and separated by 10% SDS-PHAGE gel, and subjected to Western blot.

1.3.13. RNA isolation, library preparation, sequencing, and data analysis

Total RNA was isolated from liver tissues using an Easy-blue RNA extraction kit (iNtRON Biotechnology, Korea) according to the manufacturer's protocol (Fig. 10). The RNA quality was assessed by Agilent 2100 bioanalyzer using the RNA 6000 Nano Chip (Agilent Technologies, Netherlands). RNA quantification was performed using ND-2000 Spectrophotometer (Thermofisher, USA). Based on the manufacturer's instructions, a library for control and test RNAs was constructed using Quantseq 3'mRNA-Seq Library Prep Kit (Lexogen, Austria). In brief, each 500 ng total RNA were prepared, and an oligo-dT primer containing an Illumina-compatible sequence at its 5' end was hybridized to the RNA and reverse transcription was performed. Following degradation of the RNA template, complementary strand synthesis was started by random primer containing an Illumina-compatible linker sequence at its 5' end. Magnetic beads were used to

remove all reaction components. The library was amplified to add the complete adaptor sequences required for cluster generation. The completed library was purified from PCR components. High-throughput sequencing was performed as single-end 75 sequencings using NextSeq 500 (Illumina, USA). QuantSeq 3' mRNA-Seq reads were aligned using Bowtie2 version 2.1.0. Bowtie2 indices were either generated from genome assembly sequence or the representative transcript sequences for aligning to the genome and transcriptome. The alignment file was used for assembling transcripts, estimating their abundances and detecting differential expression of genes. Differentially expressed genes were determined based on counts from unique and multiple alignments using EdgeR within R version 3.2.2 using Bioconductor version 3.0 [50]. The RC (Read count) data were processed based on Quantile normalization method using the Genowiz^{TM} version 4.0.5.6 (Ocimum Biosolutions, India). The PPI network was analyzed using STRING application tool. Cytoscape (version 2.7), an open-source bioinformatics platform developed by the Institute of System Biology (Seattle, WA) was used to construct network diagrams. Gene classification was based on searches done by Medline database (National Centre for Biotechnology Information, USA)

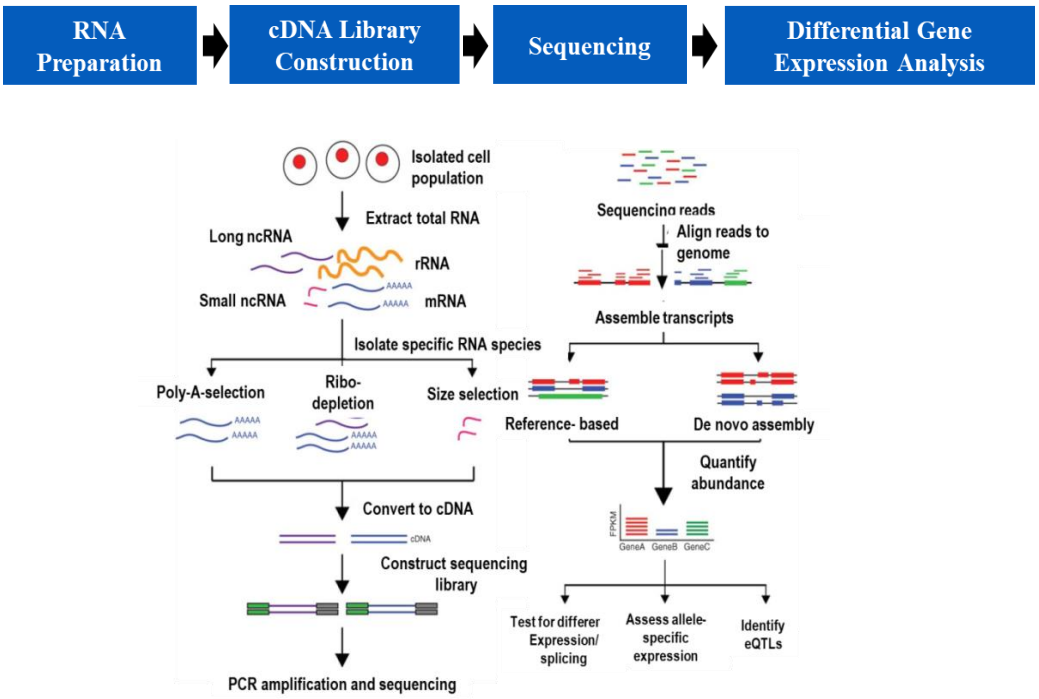

Fig. 10. Overview of RNA sequencing analysis

1.3.14. Statistical analysis

Values were expressed as means ± standard error of the mean (SEM) of three independent experiments. Data were statistically analyzed with IBM SPSS Statistics (Ver.17.0; USA). The statistical differences among groups were analyzed with one-way analysis (ANOVA) followed by Turkey's test. $P < 0.05$ indicates statistically significant differences from the control group.

1.4. Results

1.4.1. UPLC analysis of BLE

The UPLC analysis was performed to determine the presence of SFN and GRN in BLE. The retention time of SFN and GRN, isolated from the broccoli leaves were matched with the standard chromatogram (Fig. 11). The concentrations of SFN and GRN in the freeze-dried broccoli powder were 3.99 ± 0.09 µg/mg and 2.46 ± 0.2 µg/mg respectively. The results confirmed that BLE prepared by PEF treatment contained SFN and GRN.

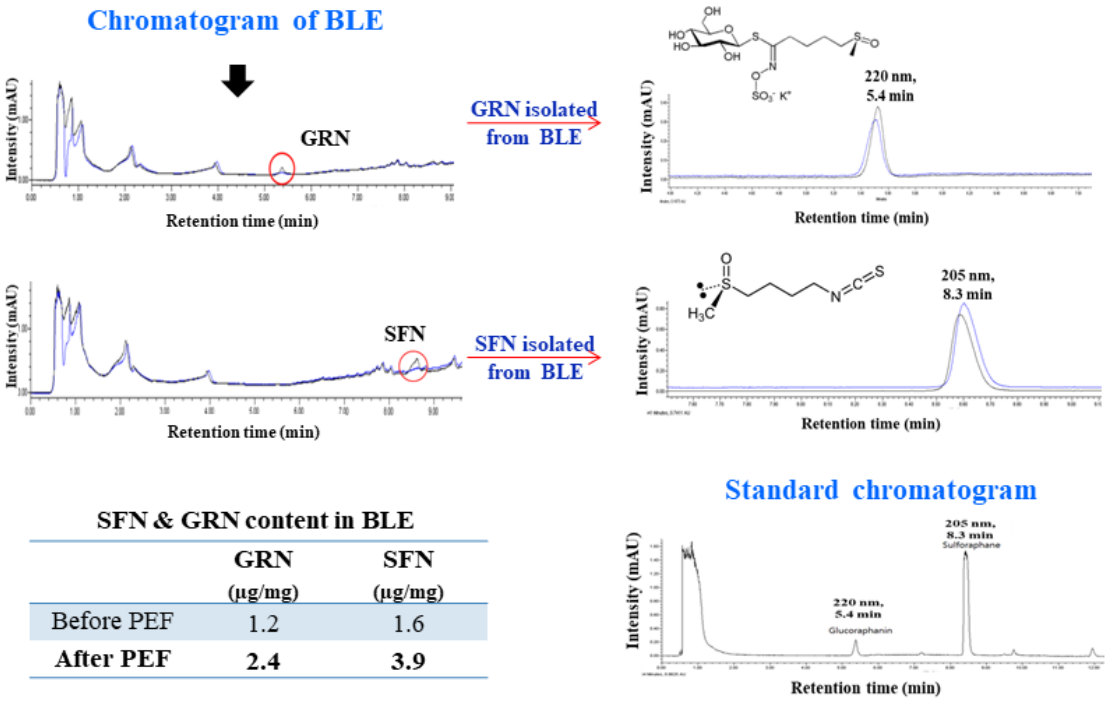

SFN & GRN content in BLE

	GRN (µg/mg)	SFN (µg/mg)
Before PEF	1.2	1.6
After PEF	**2.4**	**3.9**

Fig. 11. UPLC analysis of BLE

1.4.2. Cytotoxicity of BLE on HepG2 cells

Cytotoxicity of BLE on HepG2 cells was evaluated through MTT assay (Fig. 12). There was no significant cellular toxicity with up to 1,000 μg/mL concentration of BLE. Accordingly, further *in vitro* experiments were conducted with the non-toxic concentrations of BLE.

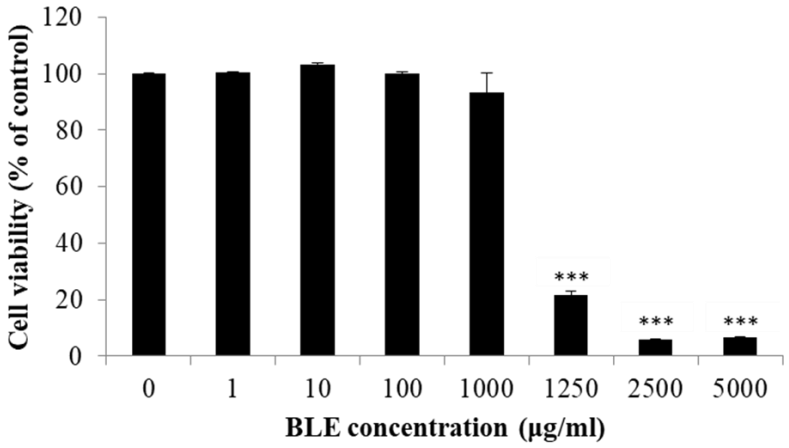

Fig. 12. Effect of BLE on HepG2 cell viability.
HepG2 cells were incubated with 0-5,000 μg/mL BLE for 24 hrs, and cell viability was measured by the MTT assay. All data are expressed as mean ± SEM (n = 3). ****P* < 0.0001 compared with the control.

1.4.3. Glucose uptake in high glucose treated HepG2 cells

The glucose uptake effect of SFN and BLE on high glucose treated HepG2 cells was evaluated through 2-NBDG uptake assay (Fig. 13). Glucose uptake was reduced in high glucose treated cells compared to the normal glucose treated cells. Both MET and SFN significantly improved glucose uptake, whereas with GRN treatment there was no significant change in glucose uptake effect in high glucose

treated HepG2 cells (Fig. 13A, 13B). Broccoli leaf extract significantly increased the glucose uptake by 2- 4-fold in a dose-dependent manner compared to the control, regardless of insulin stimulation (Fig. 13B). The results indicate that both SFN and BLE activated cellular glucose uptake pathways in high glucose treated HepG2 cells.

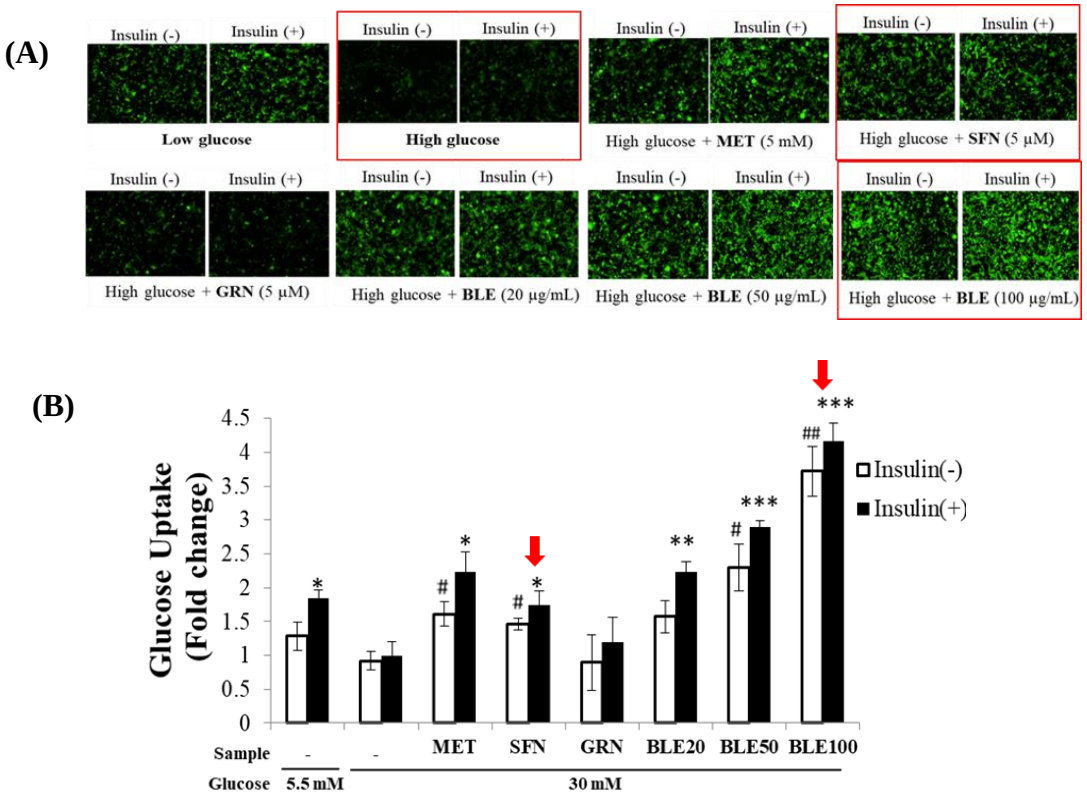

Fig. 13. Glucose uptake in high glucose treated HepG2 cells.

HepG2 cells were starved in serum-free medium for 12 hrs and incubated in serum-free medium containing either normal (5.5 mM) or high (30 mM) concentrations of glucose for an additional 24 hrs. Then they were incubated with or without insulin (100 nM) and the fluorescence D-glucose analogue, 2-NBDG (50 μM) for 30 min. Cells were washed with PBS, and the fluorescence was detected by IncuCyte® ZOOM at 20× magnification. The representative image was displayed from three independent experiments (A). Total fluorescence intensities were calculated using

IncuCyte® ZOOM fluorescence processing software (B). Values are mean ± SEM (n = 3). *P < 0.05, **P < 0.005, ***P < 0.0005 vs insulin-stimulated high glucose control and #P < 0.05, ##P < 0.005 vs without insulin-stimulated high glucose control.

1.4.4. The phosphorylation of Akt and GSK3β in high glucose treated HepG2 cells

Western blot was performed to examine the effect of SFN and BLE on phosphorylation of key enzymes in the insulin signaling (Fig. 14). The insulin-stimulated phosphorylation of Akt (Ser473) and GSK3β (Ser9) was significantly decreased in high glucose treated HepG2 cells as compared to those in normal glucose treated cells (Fig. 14A, 15B). Cells treated with MET and SFN showed a significant increase in p-Akt and p-GSK3β levels as compared to high glucose treated control cells, whereas GRN treated cells did not show significantly increased p-Akt and p-GSK3β levels. Treatment of HepG2 cells with BLE (20 and 100 μg/mL) significantly increased (P < 0.005) the insulin-stimulated phosphorylation of both Akt and GSK3β as compared to the high glucose treated control cells. These results suggest that SFN and BLE enhanced insulin sensitivity by improving the phosphorylation of both Akt (Ser473) and GSK3β (Ser9) in high glucose treated HepG2 cells.

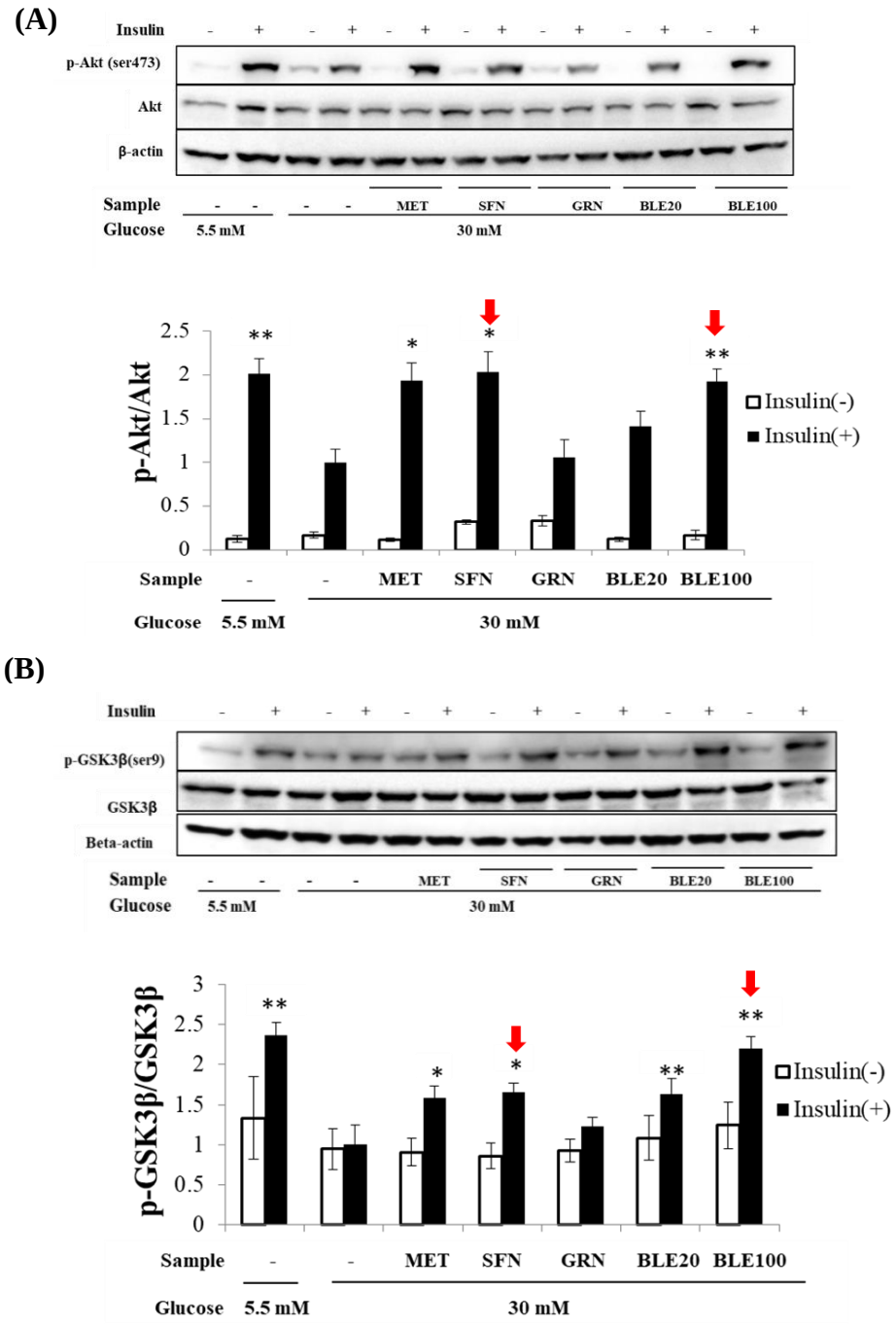

Fig. 14. Phosphorylation level of Akt and GSK3β in high glucose treated HepG2 cells.

HepG2 cells were starved in serum-free medium for 12 hrs and incubated in serum-free medium containing either normal (5.5 mM) or high (30 mM) concentrations of glucose with or without different samples for an additional 24 hrs. Before harvesting, the cells were stimulated with or without 100 nM insulin for 30 min. Total cell extract was subjected to Western blot, and band intensities were quantified using densitometry. The band intensities were expressed as p-Akt/Akt ratio (A), and p-GSK3β/GSK3β ratio (B). Values are the mean ± SEM, and that of control was set to 1. *$P < 0.05$, **$P < 0.05$ compared with high glucose control.

1.4.5. Insulin sensitivity in ob/ob mice

To evaluate the effect of SFN and BLE on insulin sensitivity in ob/ob mice, ITT was performed after four weeks of treatment with SFN or BLE (Fig. 15). Results of ITT indicated that normal mice maintained an expected physiological blood glucose level after the injection with insulin, whereas control ob/ob mice showed high blood glucose levels throughout the experiment (Fig. 15A). MET, SFN, and GRN treated mice showed higher rates of blood glucose disappearance and exhibited significantly reduced ($P < 0.05$) AUC values during ITT (Fig. 15A, 15B). Treating ob/ob mice with BLE 50 mg/kg and BLE 500 mg/kg showed significantly reduced ($P < 0.05$) blood glucose levels and AUC values compared to the control ob/ob mice. The results indicate that SFN and BLE significantly improved insulin sensitivity in ob/ob mice.

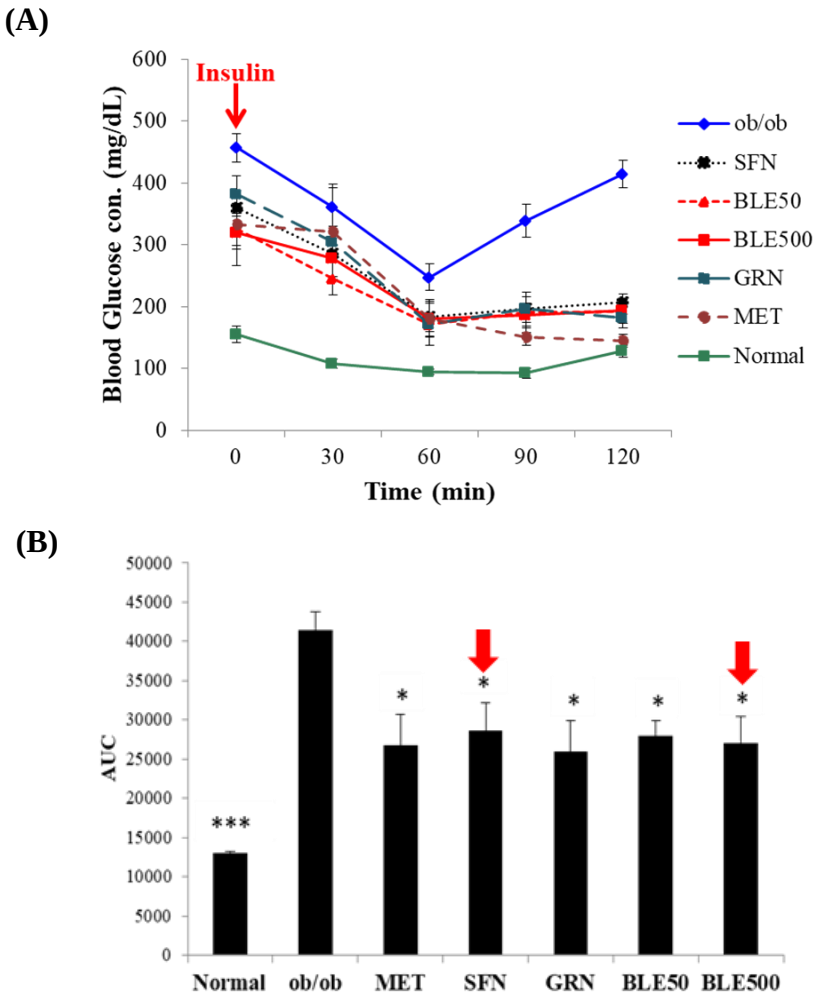

Fig. 15. Effect of SFN and BLE on the insulin tolerance in ob/ob mice.

ITT was performed after 4 weeks of samples administration to ob/ob mice. Mice were fasted for 6 hrs and insulin (2 U/kg) was injected intraperitoneally. Blood glucose values were measured at 0, 30, 60, 90, and 120 min after insulin injection. Blood glucose levels (A), AUCs (area under the curve) (B). Values are mean ± SEM (n = 4), ***$P < 0.005$ and *$P < 0.05$ vs control ob/ob group.

1.4.6. Glucose tolerance in ob/ob mice

To examine the effect of SFN and BLE on glucose tolerance, GTT was performed in ob/ob mice after four weeks of treatment with SFN or BLE (Fig. 16). After the administration of glucose, blood glucose levels in control ob/ob mice were high while normal mice maintained the basal glucose level (Fig. 16A). Treatment of ob/ob mice with MET, SFN, and GRN showed significantly reduced ($P < 0.05$) blood glucose levels and AUC values as compared to the control ob/ob group (Fig. 16A, 16B). BLE treated ob/ob mice showed significantly decreased blood glucose values (BLE 50 mg/kg; 284 ± 14 mg/dL and BLE 500 mg/kg; 261 ± 24 mg/dL) at the end of the test as compared to control ob/ob group (498 ± 42 mg/dL). The AUC values of the BLE treated ob/ob mice were also significantly lower ($P < 0.05$) than those of the control ob/ob mice throughout the experiment. The results demonstrate that SFN and BLE improved glucose tolerance in ob/ob mice.

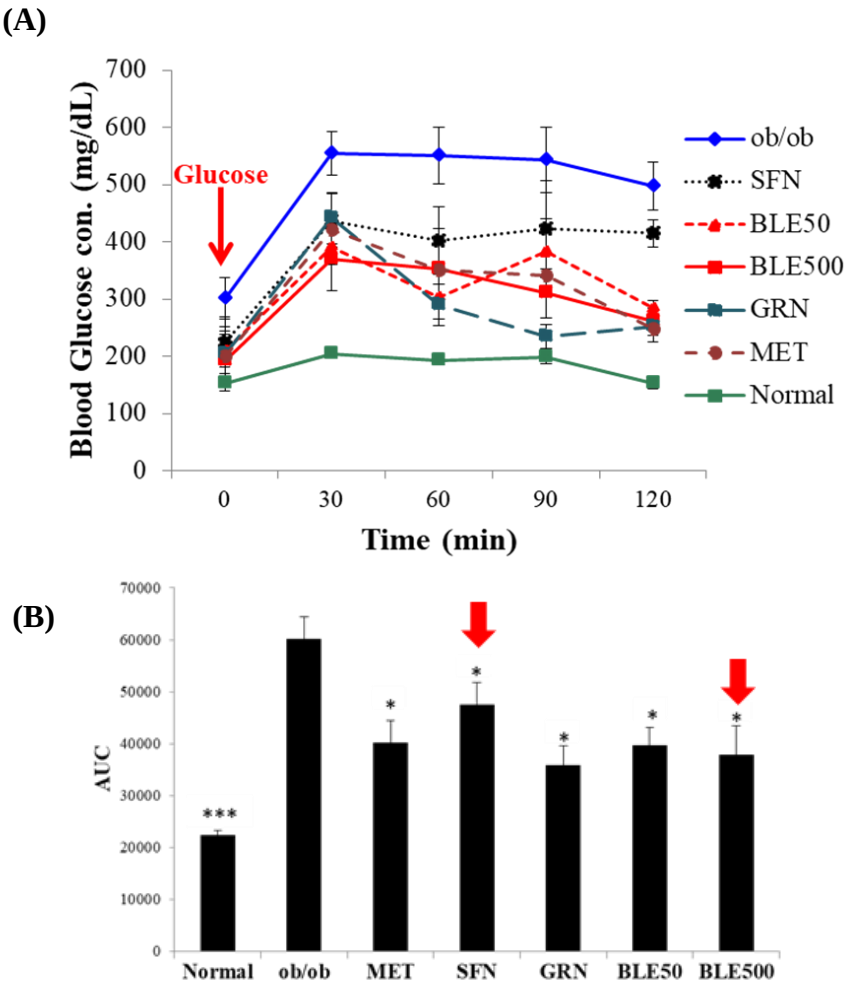

Fig. 16. Effect of SFN and BLE on the glucose tolerance in ob/ob mice.

GTT was performed after 4 weeks of samples administration to ob/ob mice. Mice were fasted for 14 hrs and blood glucose levels were measured at 0, 30, 60, 90, and 120 min after administration of glucose (2 g/kg BW). Blood glucose levels (A), AUCs (area under the curve) (B). Values are mean ± SEM (n = 4). ***$P < 0.005$ and *$P < 0.05$ vs control ob/ob group.

1.4.7. Serum parameters in ob/ob mice

To observe the effect of BLE on insulin resistance, both fasting glucose and insulin levels were measured, and the HOMA-IR index was calculated. The control ob/ob mice showed significantly higher ($P < 0.0005$) fasting blood glucose levels as compared to normal mice (Fig. 17A). Fasting serum insulin levels were also significantly higher ($P > 0.0005$) in control ob/ob mice as compared to normal mice (Fig. 17B). Treatment of ob/ob mice with MET, SFN, and GRN showed significantly decreased ($P < 0.05$) values of blood glucose, serum insulin and HOMA-IR index as compared to control ob/ob mice (Fig. 17A-17C). Broccoli leaf extract treatment significantly decreased ($P < 0.05$) blood glucose, serum insulin, and HOMA-IR values in ob/ob mice. These results indicate that the six weeks of SFN or BLE treatment improved insulin sensitivity in ob/ob mice.

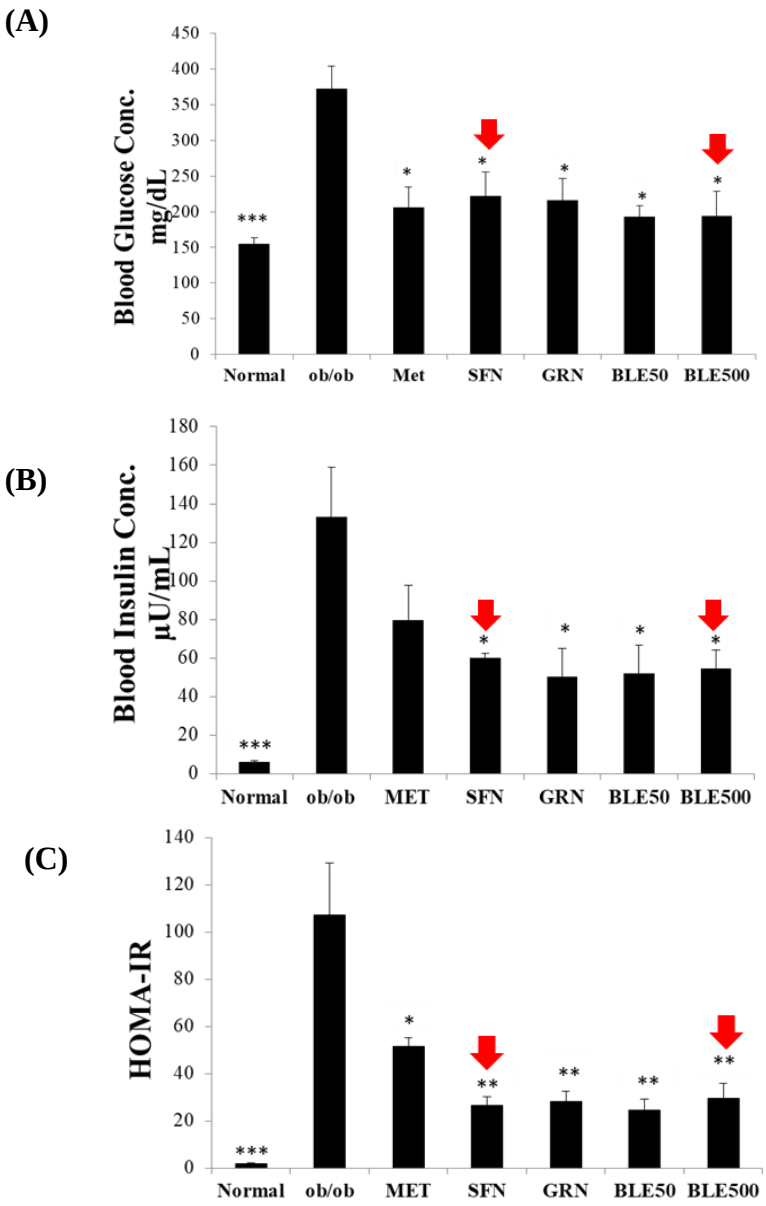

Fig. 17. Effect of SFN and BLE on the insulin resistance in ob/ob mice.

Fasting blood glucose (A), and serum insulin (B) were evaluated after 6 weeks of samples administration to ob/ob mice, and homeostasis model assessment (HOMA-IR) (C) was calculated according to the fasting glucose (mg/dL) × fasting insulin (μU/mL)/405. Values are mean ± SEM (n = 4). *P < 0.05 and **P < 0.005 vs control ob/ob group.

1.4.8. The phosphorylation levels of Akt and GSK3β in ob/ob mice liver

The effects of BLE on phosphorylation levels of Akt and GSK3β were further investigated in ob/ob mice liver (Fig. 18). The insulin-dependent phosphorylation of both Akt and GSK3β were decreased in the control ob/ob mice as compared to those in normal mice. Treatment with MET, SFN, and GRN significantly increased the phosphorylation levels of both Akt and GSK3β in ob/ob mice with insulin stimulation as compared to the control ob/ob mice. Broccoli leaf extract treated ob/ob mice showed restoration of both p-Akt and p-GSK3β to the normal levels with insulin stimulation (Fig. 18A, 18B). These findings indicate that SFN and BLE restored hepatic insulin signaling of ob/ob mice.

(A)

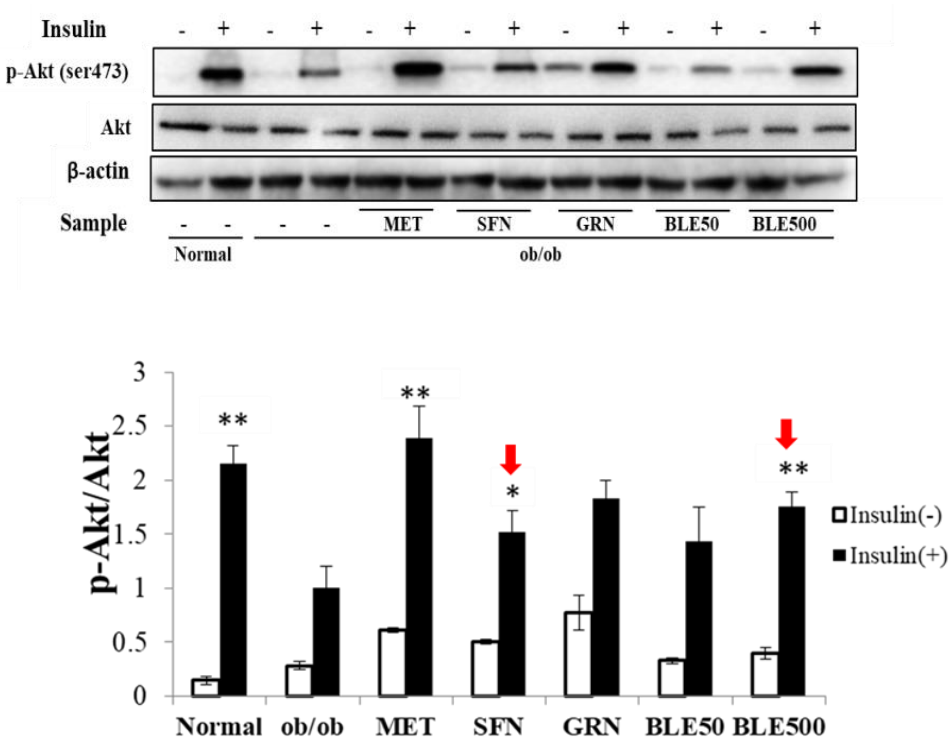

(B)

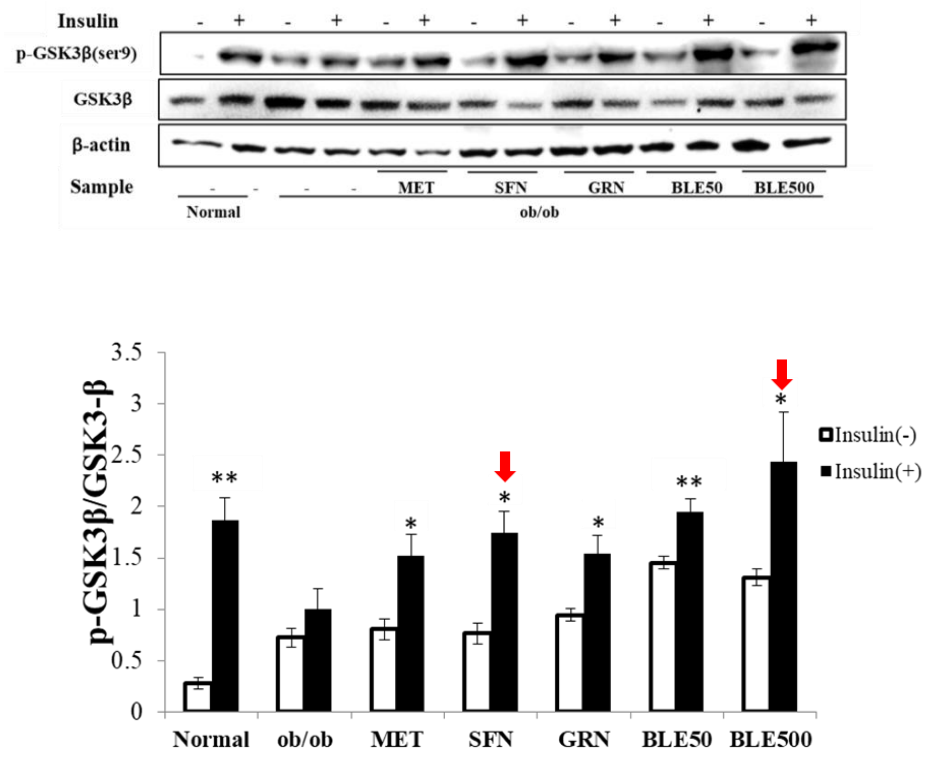

Fig. 18. The phosphorylation levels of Akt and GSK3β in ob/ob mice liver.

Samples were administrated to ob/ob mice for 6 weeks. Mice were injected intraperitoneally with or without insulin and were sacrificed 15 min after injection. Liver tissue lysate was subjected to Western blot, and band intensities were quantified using densitometry. The band intensities were expressed as p-Akt/Akt ratio (A), and p-GSK3β/GSK3β ratio (B). Values are the mean ± SEM that of control was set to 1. **P* < 0.05, ***P* < 0.05 compared with control ob/ob group.

1.4.9. Differential gene expression in ob/ob mice liver

RNA sequencing analysis was performed to observe the effect of BLE and SFN on the expression levels of genes in insulin signaling and glucose metabolism in ob/ob mice liver. The functional annotation of genes was performed through gene ontology (GO) analysis. As shown in Fig. 19, a large proportion of the genes in insulin signaling and glucose metabolism was changed in BLE treated ob/ob mice and control ob/ob mice as compared to normal mice. The up-regulated (higher than 1.5-fold) 11 genes including *Foxc2*, *Atf3*, *Atf4*, *Myc* and *Gapdhs*, and down-regulated (lower than 0.6-fold) 11 genes including *Pygm*, *Phkgi*, *Phka1*, *Gys1* and *Ppargc1a (Pgc-1α)* were normalized to control level by SFN and BLE in ob/ob mice liver (Table 1 and 2). To understand the relationship between normalized genes by SFN and BLE, the PPI network was constructed using STRING analysis and visualized as a set of nodes and edges (Fig. 19D). The normalized up-regulated genes including *Myc*, *Atf4*, and *Atf3* were closely located and interacted directly with each other within the PPI network. Normalized down-regulated genes including *Phka1*, *Pygm*, *Phkg1*, and *Gys1* were also closely located and formed a functional hub in the PPI network. RNA sequencing analysis revealed that SFN and BLE improved insulin sensitivity and glucose homeostasis by normalizing the gene expression in the insulin signaling pathway and glucose metabolism in ob/ob mice liver.

Table 1. Up-regulated genes related to insulin signaling & glucose metabolism in ob/ob mice liver which were normalized by SFN & BLE

Gene Symbol	ob/ob/ Normal	MET/ Normal	**SFN/ Normal**	GRN/ Normal	**BLE50/ Normal**	**BLE500/ Normal**
Atf3	5.053	1.260	**1.599**	0.982	**1.315**	**0.568**
Foxc2	4.506	0.957	**0.957**	0.960	**0.977**	**0.957**
Gapdhs	2.841	1.341	**1.028**	1.136	**1.298**	**1.363**
Myc	2.303	0.591	**1.236**	0.776	**1.064**	**1.153**
Pgk1	1.925	1.517	**1.330**	2.318	**1.623**	**1.435**
Ppp1r3e	1.922	1.203	**0.960**	2.759	**1.363**	**1.224**
Apod	1.904	0.990	1.910	1.988	0.995	0.990
Bcar1	1.831	1.972	2.777	2.028	0.597	1.020
Nampt	1.779	1.944	1.283	1.384	0.894	1.317
Fbn1	1.700	3.518	1.469	1.920	2.565	1.220
Atf4	1.589	1.228	1.258	0.913	1.566	1.107

Table 2. Down-regulated genes related to insulin signaling & glucose metabolism in ob/ob mice liver which were normalized by SFN & BLE

Gene Symbol	ob/ob/ Normal	MET/ Normal	**SFN/ Normal**	GRN/ Normal	**BLE50/ Normal**	**BLE500/ Normal**
Pygm	0.217	0.061	**0.974**	0.368	**1.566**	**1.002**
Phkg1	0.285	0.285	**1.051**	1.726	**0.615**	**1.945**
Gys1	0.314	1.576	**0.64**	0.479	**0.649**	**1.719**
Phka1	0.473	0.796	**0.712**	0.617	0.327	**0.772**
Ppargc1a	0.505	1.023	**0.743**	**0.823**	**1.007**	**0.987**
Pdk3	0.52	1.104	**1.058**	0.586	0.284	**0.873**
Brat1	0.531	0.939	0.987	0.802	0.544	**1.085**
Tnf	0.558	0.298	0.898	0.299	0.305	**0.875**

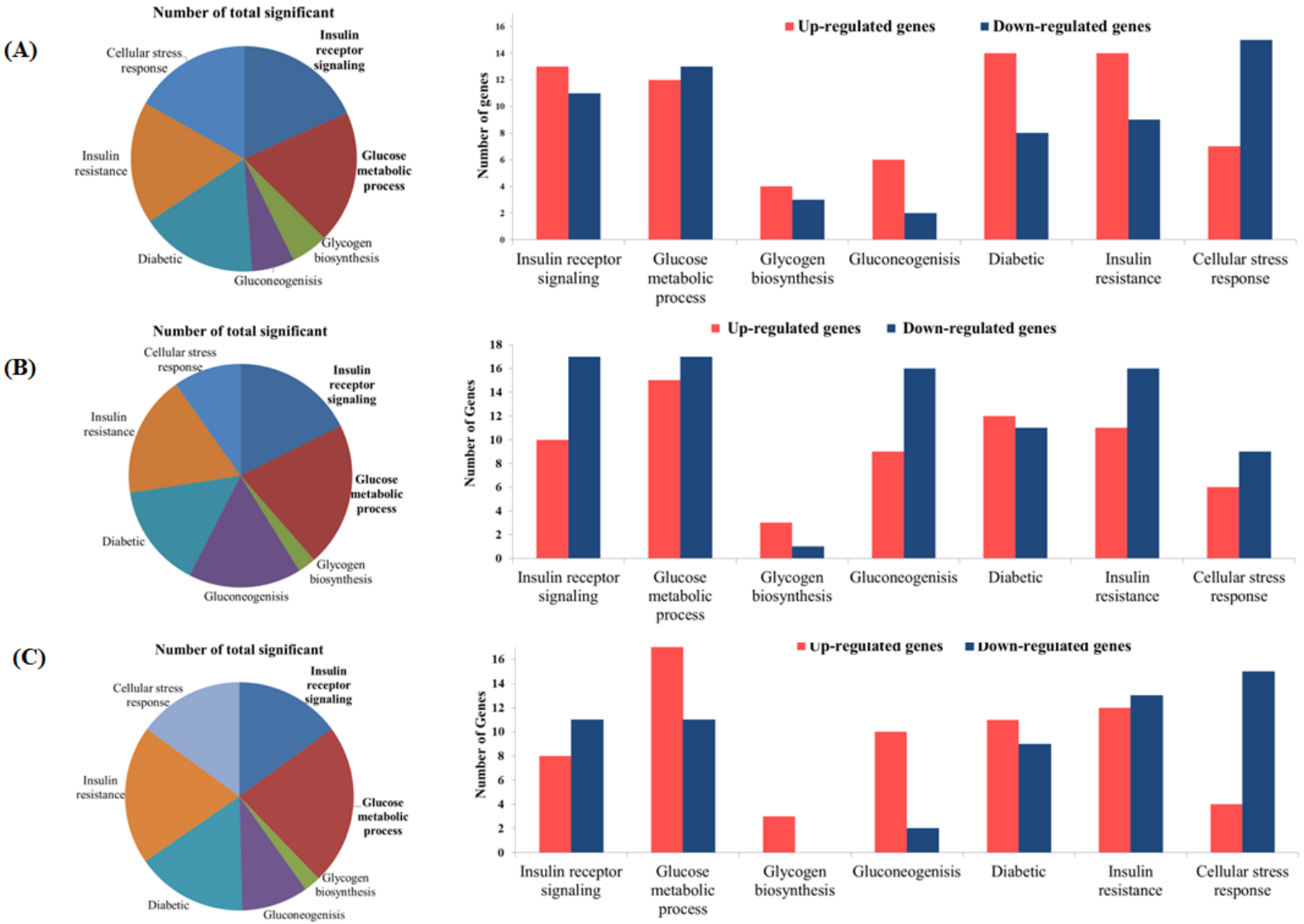

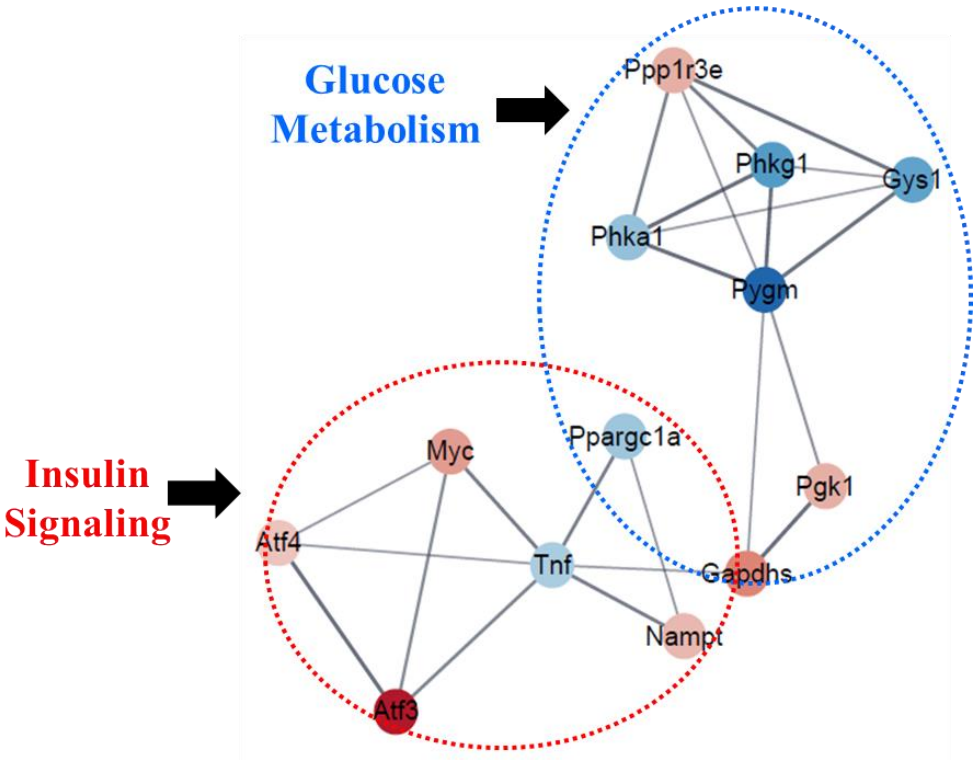

Fig. 19. Differential expression of genes in ob/ob mice liver.

GO analysis of control ob/ob mice compared to the normal mice (A), SFN treated ob/ob mice compared to the normal mice (B), 500 mg/mL of BLE treated ob/ob mice compared to the normal mice (C), (The pie chart indicates functional categorization of the differentially expressed genes in ob/ob mice liver, and the bar graph represents the number of genes up and down-regulated). PPI network of normalized genes related to insulin signaling pathway and glucose metabolic process in BLE treated ob/ob mice (D). Red circles represent up-regulated genes and blue circles represent down-regulated genes in control ob/ob mice.

1.5. Discussion

The present study investigated the possible mechanism underlying the anti-diabetic effect of SFN enriched BLE on insulin-resistant HepG2 cells and ob/ob mice. Our study results demonstrated that both SFN and BLE normalize the phosphorylation of Akt and GSK3β, and restore glucose uptake in high glucose treated HepG2 cells. In addition, our findings showed that SFN and BLE reduced both blood glucose and insulin levels, and improved both glucose tolerance and insulin sensitivity in ob/ob mice. RNA sequencing analysis revealed that both SFN and BLE normalized the insulin signaling and glucose metabolism genes including *Atf3*, *Atf4*, *Myc*, *Foxc2*, *Phkg1*, *Phka1*, *Pygm*, *Gys1*, and *Pgc-1α* in ob/ob mice.

The present study demonstrated that SFN and BLE significantly enhanced glucose uptake, regardless of insulin stimulation. Previous studies reported that SFN enhanced glucose uptake activity by activating the insulin signaling pathway in palmitic acid-induced insulin resistance HepG2 cells [45] and improved glucose uptake activity by increasing the expression of GLUT4 in 3T3-L1 adipocyte [44]. However, in another study SFN was reported to utilize a different pathway; activation of Nrf2 by SFN increased both glucose uptake and glucose utilization by activating the pentose phosphate pathway subsequently increasing the production of NADPH in mice fibroblasts [51]. These findings confirm that the glucose uptake ability of SFN, is not solely dependent on insulin-stimulated phosphorylation of Akt, but it may have an additional mechanism through Nrf2 activation. Similarly, results from our present study demonstrated that SFN enriched BLE activates the cellular glucose uptake pathway through an insulin-independent manner.

In the present study, insulin stimulated phosphorylation of both Akt and GSK3β were increased by SFN and BLE, which indicating that SFN and BLE could decrease the insulin resistance in high glucose treated HepG2 cells. Phosphorylation of Akt promotes the translocation of intracellular glucose transporters to the plasma membrane that leads to activate cellular glucose uptake [5]. Based on the previous study, SFN activates the insulin receptor substrate 1 (IRS-1)/protein kinase B (Akt) signaling pathway in palmitic acid-induced insulin-resistant HepG2 cells [45]. Similarly, our results demonstrated that SFN, increases phosphorylation of both Akt and GSK3β in high glucose treated HepG2 cells. The results indicate that SFN enriched BLE improves insulin sensitivity by increasing phosphorylation of both Akt and GSK3β in high glucose treated HepG2 cells.

The present study observed that both SFN and BLE exhibited its anti-diabetic efficacy through regulating the blood glucose level and improving the obesity-induced insulin resistance in ob/ob mice. Previous studies reported that SFN increases insulin sensitivity in streptozotocin-induced diabetic rats [23], and GRN increases both insulin and glucose tolerance in high-fat diet-fed C57BL/6 mice [52]. Previously, the glucose tolerance effect of SFN was reported to be via activation of the IRS1/Akt/GLUT4 pathway in obese mice [24]. Administration of GRN extracted from broccoli sprout to the obese mice significantly increased the insulin-stimulated phosphorylation of Akt in an Nrf2 dependent mechanism [26]. Our findings were consistent with the previous findings, and the results suggested that GRN and SFN present in BLE might be involved in the activation of hepatic insulin signaling

pathway by phosphorylation of the Akt and GSK3β, subsequently, increasing insulin sensitivity in ob/ob mice.

In the present study, RNA sequencing analysis was performed to investigate the molecular mechanism underlying the anti-diabetic effect of SFN and BLE in ob/ob mice. Our results showed that SFN and BLE normalized the up-regulated genes in insulin signaling and glucose metabolism, including *Atf3*, *Atf4*, *Foxc2*, and *Myc* in control ob/ob mice. *Atf3* a stress-inducible gene activates NF-kappa B, and Jun N-terminal kinase signaling pathways [53, 54]. The previous study reported that increased *Atf3* expression leads to hepatic steatosis and insulin resistance in diabetic rats and humans [53]. *Atf4* induces hepatic insulin resistance by inhibiting the activity of mTOR and downstream target S6K1 [54]. *Atf4* knockout mice showed enhanced insulin sensitivity and reduced hyperglycemia [54, 55]. *Foxc2* up-regulates the transcription of the regulatory subunit 1 of protein kinase A (PKA) to increase the β-adrenergic signaling pathway, leading to increased sensitivity to insulin [56]. The mRNA level of *Foxc2* is up-regulated by insulin resistance [56], and both *Foxc2* protein and mRNA levels are correlated with hyperglycaemia in T2DM patients [57]. Therefore, in the present study, up-regulation of *Foxc2* might be associated with increased blood glucose levels and insulin resistance in control ob/ob mice. Overexpression of *Myc* in β-cells of transgenic mice suppresses expression of the insulin gene, reduces GLUT2 expression, and leads to the development of diabetes [58]. Expectedly, the increased insulin sensitivity in our present study might be normalizing the expression of *Atf3*, *Atf4*, *Foxc2*, and *Myc* genes in ob/ob mice.

In the present study, we observed that SFN and BLE normalized the down-regulated genes in glucose metabolism, including *Phkg1*, *Phka1*, *Pygm*, *Gys1*, and *Pgc-1α* in control ob/ob mice. *Phka1* and *Phkg1* encode the alpha and gamma subunit of phosphorylase kinase (Phk) [59], which mediates the regulation of glycogenolysis [60]. *Pygm* is involved in the first step of glycogenolysis [61], and *Gys1* plays a role in glycogenesis [62]. Previous studies reported that dysregulation of *Phka1*, *Phkg1* [60], *Pygm* [63], and *Gys1* genes are associated with glycogen storage disease which is characterized by storage of excess glycogen in liver or muscle [64]. *Pgc-1α* regulates IRS1: IRS2 ratio expression, which is essential for the precise insulin signaling in hepatocytes [65]. Additionally, reduced *Pgc-1α* expression has previously been associated with increased insulin resistance in diabetes [66-69]. Based on these findings, it is evident that high blood glucose levels and glucose intolerance may be associated with dysregulation of *Phka1*, *Phkg1*, *Gygm*, *Gys1*, and *Pgc-1α* genes in the liver of ob/ob mice. Therefore, SFN and BLE protective effects against impaired glucose metabolism in ob/ob mice could be a result of the normalization of these genes.

In conclusion, we found that SFN enriched BLE exerted an insulin-sensitizing effect by phosphorylating both Akt and GSK3β in high glucose treated HepG2 cells and ob/ob mice. In addition, BLE and SFN increased glucose uptake in high glucose treated HepG2 cells. Furthermore, both SFN and BLE improved systemic insulin sensitivity and glucose metabolism through normalization of *Atf3*, *Atf4*, *Myc*, *Foxc2*, *Phkg1*, *Phka1*, *Pygm*, *Gys1*, and *Pgc-1α* genes expression in ob/ob mice (Fig. 20). However, further studies are needed to investigate the mechanism through which

BLE regulates gene expression and how the genes can be used as therapeutic targets for diabetes treatment. In our future study, we will evaluate the expression of those genes at the protein level. Overall results suggest that SFN enriched BLE is a promising therapeutic solution for glucose intolerance and impaired insulin resistance in patients with T2DM. Additionally, with high processing standards, BLE dietary supplement is a potential intervention for reducing diabetes prevalence.

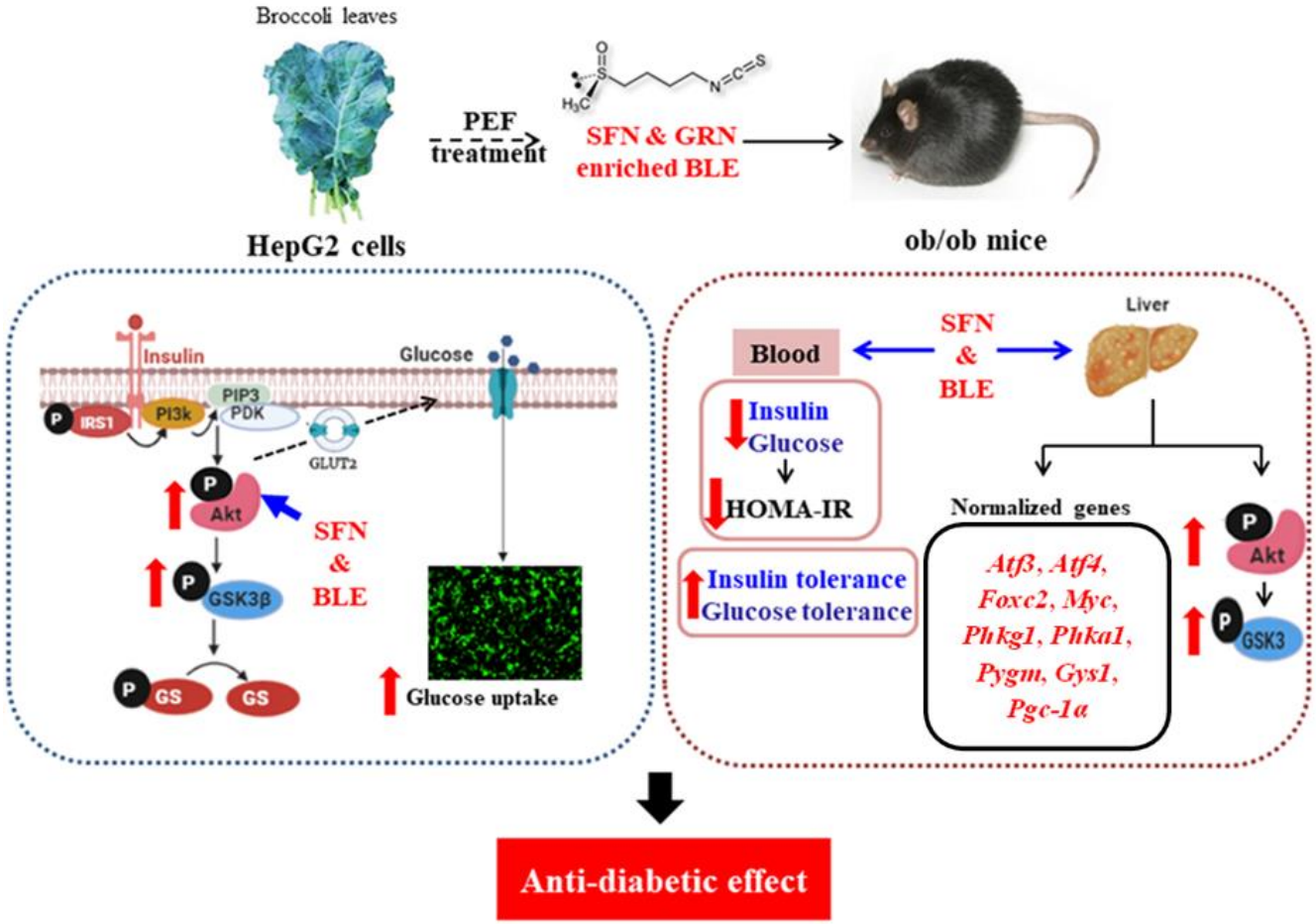

Fig. 20. Anti-diabetic effect of SFN and BLE

PART-II

Anti-obesity effect of Sulforaphane in Broccoli leaf extract on 3T3-L1 adipocyte and ob/ob mice

2.1. Abstract

The present study evaluated the anti-obesity effect of sulforaphane (SFN) and glucoraphanin (GRN)-enriched broccoli leaf extract (BLE) on 3T3-L1 adipocyte and ob/ob mice. Based on Oil Red O staining and triglyceride (TG) assay, SFN and BLE significantly reduced ($P < 0.05$) both lipid accumulation and TG content in the differentiated 3T3-L1 adipocytes. SFN and BLE increased 2-NBDG uptake by 3T3-L1 adipocytes in a dose-dependent manner. Western blot analysis confirmed that SFN and BLE increased the phosphorylation levels of both AMPK (Thr172) and ACC (Ser79) *in vitro* and *in vivo*. Both SFN and BLE significantly reduced the expression of HMGCR in liver and white adipose tissues of ob/ob mice. Histological analysis revealed that SFN and BLE ameliorated hepatic steatosis in ob/ob mice. Treatment with SFN and BLE significantly reduced ($P < 0.05$) the serum levels of TG, low-density lipoprotein cholesterol (LDL), total cholesterol (TC), and glucose in ob/ob mice. RNA sequencing analysis showed that up- or down-regulation of 32 genes related to lipid metabolism was restored to control level in both SFN-treated ob/ob mice group and BLE-treated group. A protein-protein interaction (PPI) network was constructed via STRING analysis, and *Srebf2*, *Pla2g2c*, *Elovl5*, *Elovl7*, *Plb1*, *Ctp1a*, *Lipin*, *Fgfr1*, *Plcg1*, and *Plcb4* were located in the functional hubs of the PPI network of lipid metabolism. Overall results suggest that the SFN content in BLE exerts a potential anti-obesity effect by normalizing the expression of genes related to lipid metabolism, which are up- or down-regulated in ob/ob mice.

Keywords: Sulforaphane, Broccoli, Anti-obesity, ob/ob mice, RNA sequencing analysis

2.2. Introduction

Obesity is defined as a state of excessive accumulation of body fat due to an imbalance between energy intake and energy expenditure [70]. In particular**,** obesity is associated with the development of metabolic disorders including type 2 diabetes, inflammation, and non-alcoholic fatty liver disease (NAFLD) [6]. NAFLD leads to non-alcoholic steatohepatitis (NASH), the most severe obese condition associated with increased mortality and morbidity [71].

AMP-activated protein kinase (AMPK) plays a key role in cellular homeostasis by regulating the imbalance between anabolic and catabolic mechanisms in response to metabolic stress [72]. Given the functional aspects of lipid metabolism, AMPK is considered as a major therapeutic target in the treatment of obesity [73]. Activation of AMPK by phosphorylation inhibits lipogenesis and increases fatty acid oxidation (FAO) [9]. In addition, AMPK inactivates key metabolic enzymes in fatty acid and cholesterol synthesis including acetyl-CoA carboxylase (ACC) and hydroxy-3-methylglutaryl coenzyme A reductase (HMGCR) [74, 75]. Metformin (MET) is used to treat obesity-related type 2 diabetes, and its mechanism of action is mainly attributed to the activation of AMPK [76, 77].

The use of herbal medicines to treat obesity and its complications is attractive because of fewer side effects than synthetic drugs [78, 79]. Broccoli (*Brassica oleracea var. italica*) is a cruciferous vegetable that contains high amounts of glucosinolates, including GRN and SFN [40]. GRN is converted to SFN by the action of myrosinase during chopping and chewing of broccoli or in the digestive

system of mammals [20]. SFN is the key bioactive isothiocyanate found in broccoli sprouts that is responsible for the anti-obesity properties [19]. SFN has been shown to attenuate obesity by inhibiting adipogenesis and activating the AMPK pathway in mice fed with the high-fat diet (HFD) [21]. In addition, SFN is known to enhance lipid decomposition via browning of adipose tissue in 3T3-L1 adipocytes [44]. Despite the potential effects of SFN and GRN in broccoli, the detailed mechanisms underlining the anti-obesity effect are poorly understood.

The present study hypothesized that SFN enriched BLE exerts anti-obesity effects on 3T3-L1 adipocytes and ob/ob mice. Thus, the effects of SFN and BLE on lipid accumulation and glucose uptake were evaluated in 3T3-L1 adipocytes. The phosphorylation levels of AMPK, ACC, and expression of HMGCR was monitored to determine whether SFN and BLE act on the AMPK pathway. In addition, the effect of SFN and BLE on hepatic lipid accumulation and serum lipid profile was evaluated in ob/ob mice. In particular, the differential gene expression profile in ob/ob mice liver was analyzed to investigate the molecular mechanism underlining the anti-obesity effect of SFN and BLE.

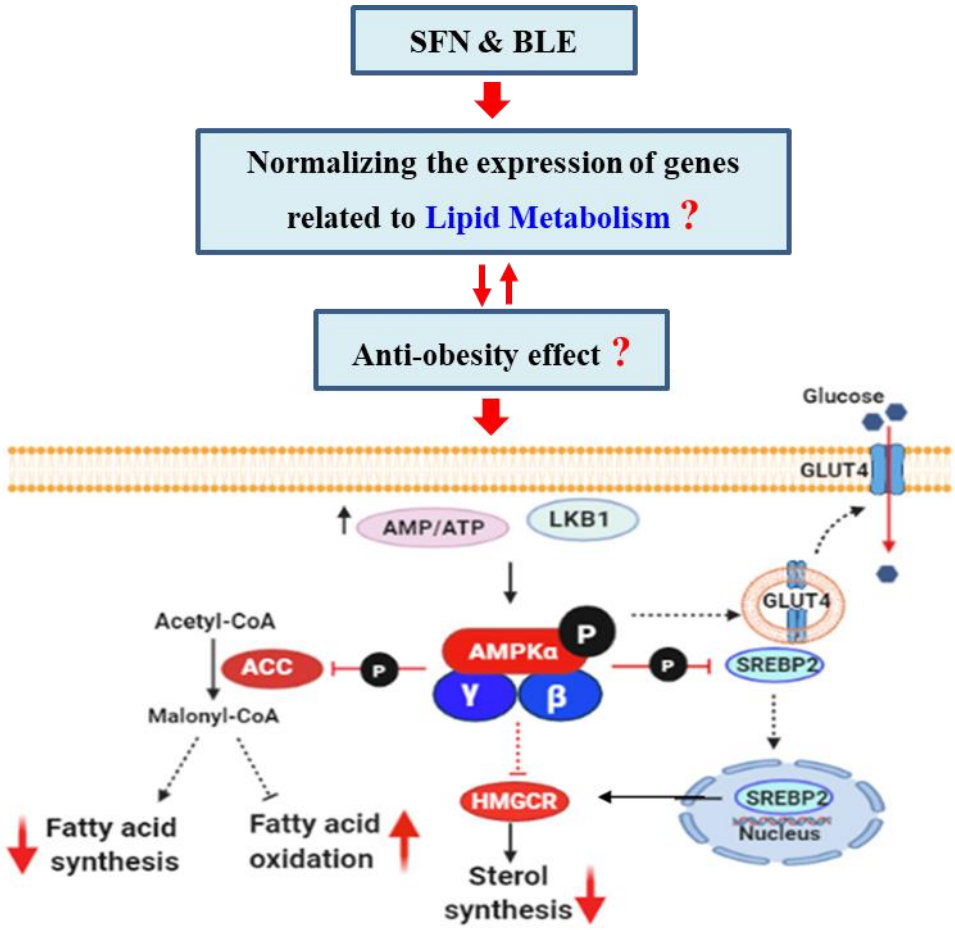

Fig. 21. Hypothetical model: anti-obesity effect of SFN and BLE

Because AMPK is considered as the master regulator of lipid metabolism, the present study evaluated whether or not SFN in BLE exhibits anti-obesity effects by activating AMPK. In addition, the present study investigated the molecular mechanism underlining the anti-obesity effect of SFN and BLE by analyzing differential gene expression profiles related to lipid metabolism (Fig. 21).

2.3. Materials and methods

2.3.1. Material and Chemicals

Dulbecco's-modified Eagle medium (DMEM), fetal bovine serum (FBS), and bovine calf serum (BS) were obtained from Thermo Fisher Scientific (USA). Dexamethasone (Dex), isobutyl-1-methylxanthine (IBMX), human insulin, MET, bovine serum albumin (BSA), and SFN were purchased from Sigma Aldrich (USA). 2-[N-(7-Nitrobenz-2-oxa-1,3-diazol-4-yl)amino]-2-deoxy-d-glucose (2-NBDG) and HMGCR antibody were purchased from Invitrogen (CA, USA). GRN was purchased from Cayman Chemicals (USA). 3T3-L1 mouse preadipocyte (KCLB 10092.1) cell line was obtained from the Korean Cell Line Bank (KCLB, South Korea). p-AMPK, AMPK, p-ACC, and ACC antibodies were purchased from Cell Signaling Technology (USA). EZ-Western Lumi Pico and EZ-Cytox from DoGenBio (South Korea). All other reagents were purchased from commercial sources and were of the analytical grade or better.

2.3.2. Preparation of broccoli leaf extract

Broccoli leaves were minced into small pieces and were added 10× volume of distilled water. Pulsed electric field (PEF) treatment was performed using 5 kW PEF at 7 kJ of total energy for 5 sec (out voltage 60%, pulsed width 25 μs, frequency 100 Hz). The suspension was mixed with 10× volume of ethanol and was extracted for about 3 hrs at room temperature. The extract was lyophilized for 72 hrs using a lyophilizer, crushed to make a fine powder and was stored at -80 °C until use.

2.3.3. Broccoli extract UPLC standardization.

Ultra performance liquid chromatography (UPLC) analysis was performed to observe the SFN and GRN presence in the BLE. The chromatographic analysis was performed using an analytical ACQUITY UPLC™ BEH C18 column (2.1 × 100 mm) with a particle size of 1.7 μm (Waters Corporation, MA, USA). The column was installed in a column oven and maintained at 40 °C. The injection volume was 10 μL. The analysis was carried out isocratically at a flow rate of 0.5 mL/min, employing as the mobile phase a mixture of water containing 0.1% formic acid (solvent A) and acetonitrile containing 0.1% formic acid (solvent B). The gradient was 0.0 min, 2% B; 5 min, 7% B; 10 min, 20% B. SFN was detected at 205 nm and GRN was detected at 220 nm.

2.3.4. Cell culture and differentiation

Murine 3T3- L1 preadipocyte were maintained in a complete medium consisting of DMEM, 10% BS and 1% penicillin-streptomycin (PS) at 37 °C in a humidified incubator containing 5% CO_2 and 95% air. After cells reached about 80% confluence, they were seeded in experimental plates in order to induce the differentiation process. Adipocyte differentiation was induced at two days post-confluence (designated as day 0) by adding differentiation initiation media (DIM) containing DMEM, 1% PS, 10% FBS, 0.5 mM IBMX, 0.5 μM Dex, and 10 μg/mL insulin for 48 hrs, and then the cell medium was changed to a normal medium (DMEM containing 1% PS and 10% FBS) containing 10 μg/mL insulin. The media were changed to normal growth media after 48 hrs and every 2 days thereafter until

differentiation to mature adipocytes. To examine effects of test samples on the lipid accumulation, cells were cultured with DIM medium with or without test samples; MET (5 mM), SFN (5 μM), GRN (5 μM), and BLE (20, 50, 100 μg/mL) until differentiation to mature adipocytes. At day 10-12, completely differentiated adipocytes were used to observe the lipid accumulation through Oil Red O staining and Western blot analysis (Fig. 22).

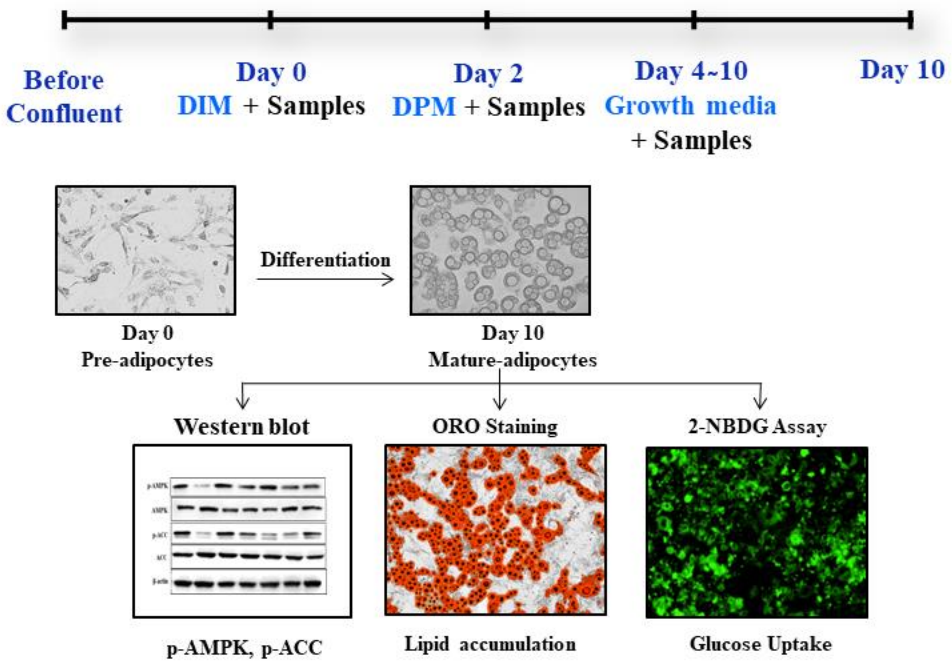

Fig. 22. 3T3-L1 cell culture and treatment.

2.3.5. Cytotoxicity assay

Cytotoxicity of BLE against 3T3-L1 preadipocytes was evaluated by colourimetric MTT assay using an EZ-cytox cell viability assay kit. Briefly, 3T3-L1 preadipocytes grown in 96-well plates were treated with or without different concentrations (0 - 5,000 μg/mL) of BLE for 48 hrs**.** Cell media was removed by

using a suction valve and added new media containing 10% Ez-cytox into each well. Plates were incubated for 3 hrs at 37 ℃ and 5% CO_2. Cell viability indicated by the production of formazan was measured with an ELISA microplate reader at 450 nm wavelength.

2.3.6. Oil Red O staining

After adipocyte differentiation, on day 10, cells were stained with Oil Red O according to the previous method [80] with slight modifications**.** Briefly, cells were washed with PBS, fixed with 10% buffered formalin for 30 min at room temperature, and stained with Oil Red O solution (0.5 g in 100 mL isopropanol) for 1 hr**.** After removing the staining solution, the cells were washed twice with distilled water. Images were acquired using the IncuCyte ZOOM® fluorescence microscope at 20× and 4× magnifications. The total integrated red intensity (CU × μm2 /Image) of the whole wells was calculated using IncuCyte® ZOOM fluorescence processing software.

2.3.7. Measurement of triglyceride (TG) content in 3T3-L1 adipocytes

Cellular triglyceride contents were quantified using a commercially available TG colourimetric assay kit (BioAssay Systems, USA). Briefly, the differentiated 3T3-L1 cells were washed with PBS and harvested to cell lysis buffer containing 5% Triton X-100. Cells were homogenized and centrifuged at 3000 × g for 5 min to remove the fat layer. The TG and protein contents of the diluted supernatants were

measured according to the manufacturer's instructions. The protein concentration of each sample was measured using Bio-Rad DC protein assay (Bio-Rad Laboratories, USA). Triglycerides contents were normalized with the respective protein concentration, employing BSA as the calibration standard.

2.3.8. 2-NBDG uptake assay

Glucose uptake was monitored by 2-NBDG as a fluorescent probe. Briefly, 3T3-L1 preadipocytes were seeded into the 96-well culture plate and were then induced to differentiate into mature adipocytes. Mature 3T3-L1 adipocytes were incubated with different samples for 48 hrs, followed by incubation with 2-NBDG (40 μM) for 30 min. Cells were washed with PBS, and images were acquired using IncuCyte ZOOM® fluorescence microscope at 20× magnification. The fluorescence intensity in each image was calculated using IncuCyte® ZOOM florescence processing software.

2.3.9. Animals

Male leptin-deficient six weeks old ob/ob mice (C57BL/6JHamSlc-ob) were purchased from Japan SLC Inc. (Japan). The mice strain was originated from Jackson Laboratory (USA) and was developed to C57BL/6JHamSlc-ob in Japan SLC Inc. (Japan) [81]. Mice were housed at 24 ± 1 ˚C with 50-55% humidity under a 12 hrs light/12 hrs dark cycle and maintained on a standard chow diet. All experiments were carried out in accordance with the National Institute of Health Guide for the Care and Use of Laboratory Animals and were approved by the Institutional Animal

Care and Use Committee of Jeju National University (ACUCC; approval No. 2018-0051).

2.3.10. Sample treatment

The ob/ob mice were randomly allocated into 6 groups (n = 5), control ob/ob and five groups in which ob/ob mice were given by MET (100 mg/kg body weight), SFN (0.5 mg/kg body weight), GRN (2.5 mg/kg body weight), and BLE in a dose of 50 and 500 mg/kg body weight every day with drinking water. Aged matched C57BL/6 mice were supplied by Orient Bio (Korea) were used as the normal control group (n = 5). All the samples were diluted with distilled water, and mice were given *ad libitum* access to food and water. Control groups (ob/ob control mice and normal mice) were treated with drinking water. Samples were administered orally for 6 weeks. At the end of the experiment, mice were fasted overnight and were sacrificed, their blood and tissues (liver tissues and peritoneal white adipose tissues; pWAT) were collected and stored at -80 ˚C for further analysis.

2.3.11. Blood glucose

Blood glucose levels were measured at 0, 2, 4, and 6 weeks of sample treatment in blood taken from the tail of 6 hrs fasted mice. The concentrations of blood glucose were determined using a blood glucose monitor (Lipidpro, OSANG healthcare, Korea).

2.3.12. Serum parameters in ob/ob mice

Serum was separated from the collected blood by the centrifugation at 3500 × g for 10 min at 4 ˚C. Colourimetric quantification of LDL, TC, and TG was determined in serum using the EnzyChrom AF HDL, LDL/VLDL, and TG assay kit (BioAssay Systems) according to the manufacturer's instructions. Briefly, the cell lysate was centrifuged with 1:1 precipitating reagent solution. The LDL/VLDL fraction was separated by the dissolution of the collected pellet in PBS. For TC assay, diluted serum was mixed with assay buffer. Cholesterol standard was prepared according to the instruction given by the manufacture. Transferred 50 µL prepared samples into a transparent flat-bottom 96 well plate. Fifty microliters of a dye reagent-enzyme mix were added into each well, and the plate was incubated at room temperature for 30 min. Absorbance was measured at 570 nm using ELISA microplate reader. For TG analysis, serum samples were diluted 5-fold and assayed directly using a colourimetric assay kit (BioAssay Systems, USA). TG concentrations were determined by comparison with a standard curve.

2.3.13. Tissue processing and hematoxylin & eosin (H&E) staining

Mice liver tissues were fixed in 10% neutral buffered formalin immediately after sacrifice. Fixed tissues were embedded in paraffin wax and sliced into 3 µM thickness sections. Tissue sections were mounted on glass slides and stained with H&E (Sigma-Aldrich). Stained sections were observed under the microscope, and images of representative section areas were obtained using Olympus DP-72 microscope camera (Olympus, Tokyo, Japan).

2.3.14. Western blot analysis

Liver tissue lysate, white adipose tissue lysate, and harvested cell pellets were homogenized in RIPA lysis buffer (20 mM Tris-HCl pH 7.5, 150 mM NaCl, 1 mM EGTA, 1 mM Na_2EDTA, 1% NP-40, 1% Sodium deoxycholate, 2.5 mM Sodium pyrophosphate, 1 mM $NaVO_4$, and 1 μg/mL leupeptin). The supernatant was collected after centrifugation for 10 min at 13,000 × g at 4 ˚C. The protein concentration was determined using a Bradford assay kit (Bio-Rad Lab, USA) with BSA as the standard. The total proteins were separated by 10% sodium dodecyl sulfate-polyacrylamide gel electrophoresis (SDS-PAGE) and subjected to Western blot.

2.3.15. RNA sequencing analysis

Total RNA was isolated from liver tissues using an Easy-blue RNA extraction kit (iNtRON Biotechnology, Korea) according to the manufacturer's protocol. The RNA quality was assessed by Agilent 2100 bioanalyzer using the RNA 6000 Nano Chip (Agilent Technologies, Netherlands). RNA quantification was performed using ND-2000 spectrophotometer (Thermofisher, USA). Based on the manufacturer's instructions, a library for control and test RNAs was constructed using Quantseq 3'mRNA-Seq Library Prep Kit (Lexogen, Austria). In brief, each 500 ng total RNA was prepared, and an oligo-dT primer containing an Illumina-compatible sequence at its 5' end was hybridized to the RNA and reverse transcription was performed. Following degradation of the RNA template, complementary strand synthesis was started by random primer containing an Illumina-compatible linker sequence at its 5' end. Magnetic beads were used to

remove all reaction components. The library was amplified to add the complete adaptor sequences required for cluster generation. The completed library was purified from PCR components. High-throughput sequencing was performed as single-end 75 sequencings using NextSeq 500 (Illumina, USA). QuantSeq 3' mRNA-Seq reads were aligned using Bowtie2 version 2.1.0 [82]. Bowtie2 indices were either generated from genome assembly sequence or the representative transcript sequences for aligning to the genome and transcriptome. The alignment file was used for assembling transcripts, estimating their abundances and detecting differential expression of genes. Differentially expressed genes were determined based on counts from unique and multiple alignments using EdgeR within R version 3.2.2 using Bioconductor version 3.0 [50]. The RC (Read count) data were processed based on Quantile normalization method using the Genowiz^{TM} version 4.0.5.6 (Ocimum Biosolutions, India). The PPI network was analyzed using STRING application tool. Cytoscape (version 2.7), an open-source bioinformatics platform developed by the Institute of System Biology (Seattle, WA) was used to construct network diagrams. Gene classification was based on searches done by the Medline database (National Centre for Biotechnology Information, USA).

2.3.16. Statistical analysis

Results are expressed as the mean ± standard error of the mean (SEM). One-way analysis of variance (ANOVA) was performed, followed by Turkey's test (SPSS 17.0, USA) to determine the significant differences between groups. $P < 0.05$ indicates statistically significant differences from the control group.

2.4. Results

2.4.1. UPLC analysis of BLE

UPLC analysis was performed to determine the concentration of SFN and GRN available in BLE. The retention times of SFN and GRN isolated from the broccoli leaves were matched with the standard chromatograms (data not shown). The SFN and GRN levels in the freeze-dried broccoli powder were 3.9 ± 0.09 μg/mg and 2.4 ± 0.2 μg/mg, respectively. The results confirmed the presence of both SFN and GRN in BLE obtained via PEF treatment.

2.4.2. Cytotoxicity of BLE in 3T3-L1 cells

The cytotoxicity of BLE to 3T3-L1 cells was measured via MTT assay. There was no significant cellular toxicity up to 1,000 μg/mL of BLE (Fig. 23). In this study, up to 200 μg/mL of BLE was used for further experiments.

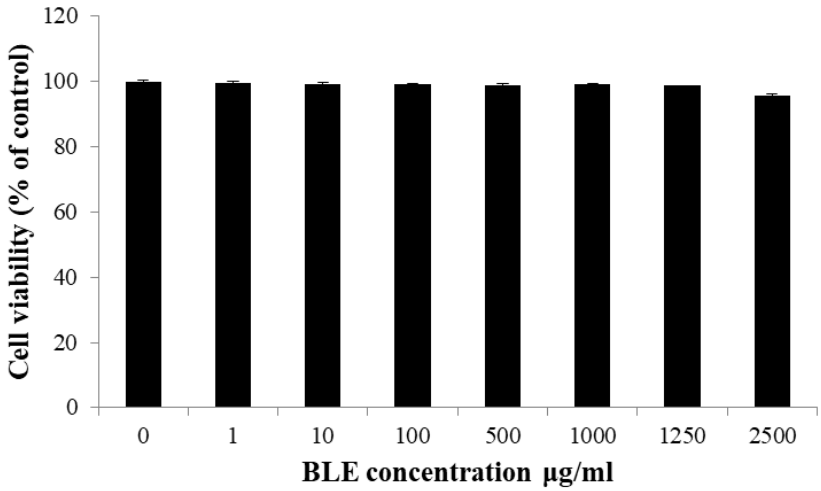

Fig. 23. Effect of BLE on 3T3-L1 cell viability.

3T3 cells were incubated with 0-2,500 μg/mL BLE for 24 hrs, and the MTT assay was used to measure cell viability. Values represent mean ± SEM (n = 3). $^{**}P < 0.001$, $^{***}P < 0.0001$ compared with the control.

2.4.3. Lipid accumulation and TG content in 3T3-L1 adipocytes

The effects of BLE and its major compounds SFN and GRN on intracellular lipid accumulation and TG content of 3T3-L1 adipocytes were observed via Oil Red O staining and TG assay (Fig. 24). Differentiated 3T3-L1 adipocytes showed a significantly increase ($P < 0.0005$) in lipid accumulation and TG content when compared with undifferentiated adipocytes (Fig. 24A, 24B). However, treatment with MET and SFN significantly decreased lipid accumulation ($P < 0.0005$) and TG content ($P < 0.05$) in differentiated 3T3-L1 adipocytes, whereas GRN treatment showed no significant change in lipid accumulation or TG content compared with the differentiated control adipocytes. In particular, exposure to BLE significantly inhibited both lipid accumulation ($P < 0.0005$) and TG level ($P < 0.05$) in differentiated 3T3-L1 adipocytes in a dose-dependent manner. Thus, both SFN and BLE suppressed lipid accumulation and TG content in differentiated 3T3-L1 adipocytes.

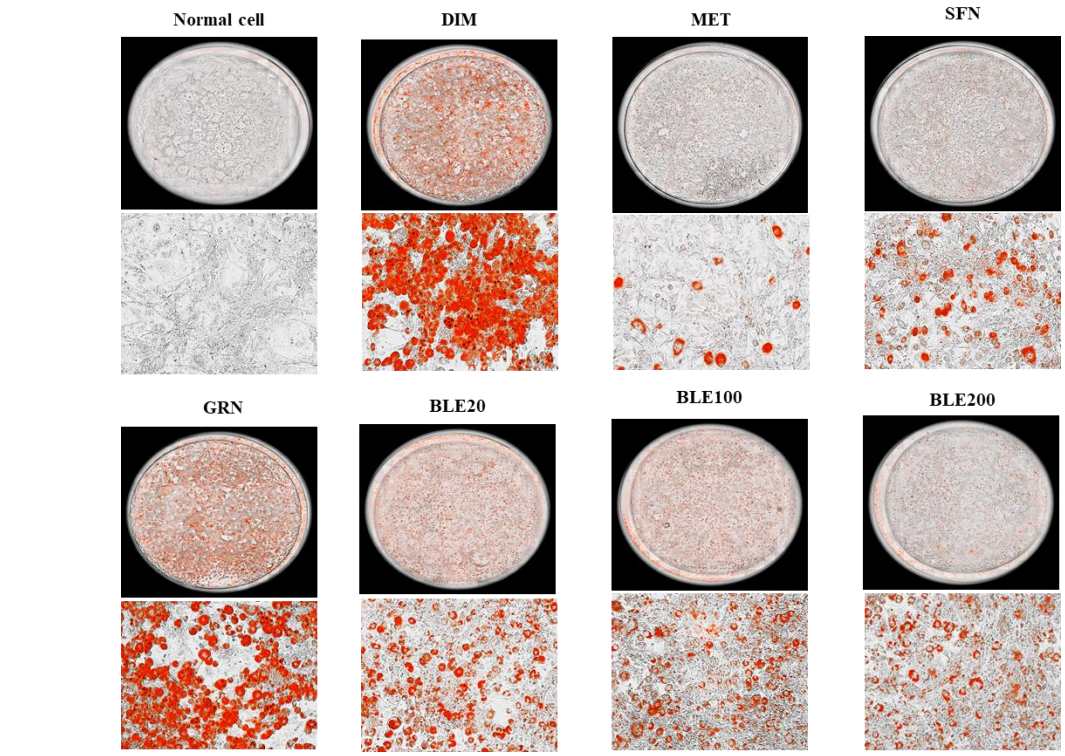

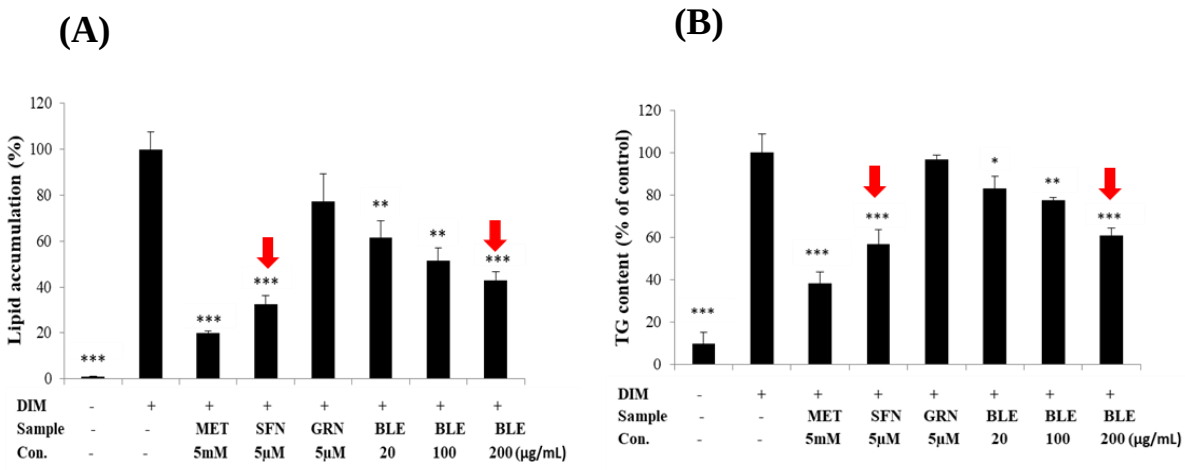

Fig. 24. Lipid accumulation and TG content of 3T3-L1 adipocytes

The 3T3-L1 cells were treated with differentiation initiation media (DIM) with or without samples for 48 hrs, and then the cell medium was changed to a normal

medium containing 10 μg/mL insulin in different samples. The media were changed to normal growth media after 48 hrs and every 2 days thereafter until differentiation to mature adipocytes. Cells were stained with Oil red O on day 10, and images were acquired using the IncuCyte ZOOM® fluorescence microscope at 20× and 4× magnifications (A). Quantitative analysis of lipid accumulation in 3T3-L1 adipocytes calculated with IncuCyte ZOOM® fluorescence processing software (B). TG accumulation in 3T3-L1 adipocytes (C). Values represent mean ± SEM (n = 3). *P < 0.05, **P < 0.005, and ***P < 0.0005 vs. the differentiated control.

2.4.4. Glucose uptake in 3T3-L1 adipocytes

The glucose uptake effects of BLE, SFN, and GRN on 3T3-L1 adipocytes were analyzed via 2-NBDG uptake assay (Fig. 25). Differentiated 3T3-L1 adipocytes showed increased glucose uptake when compared with undifferentiated adipocytes. Both MET and SFN significantly increased (P < 0.05) glucose uptake, whereas GRN had no significant effect on glucose uptake in differentiated 3T3-L1 adipocytes compared with the differentiated control adipocytes. Treatment of differentiated 3T3-L1 adipocytes with BLE significantly increased (P < 0.0005) glucose uptake in a dose-dependent manner. These results indicate that both SFN and BLE stimulated the cellular glucose uptake in differentiated 3T3-L1 adipocytes.

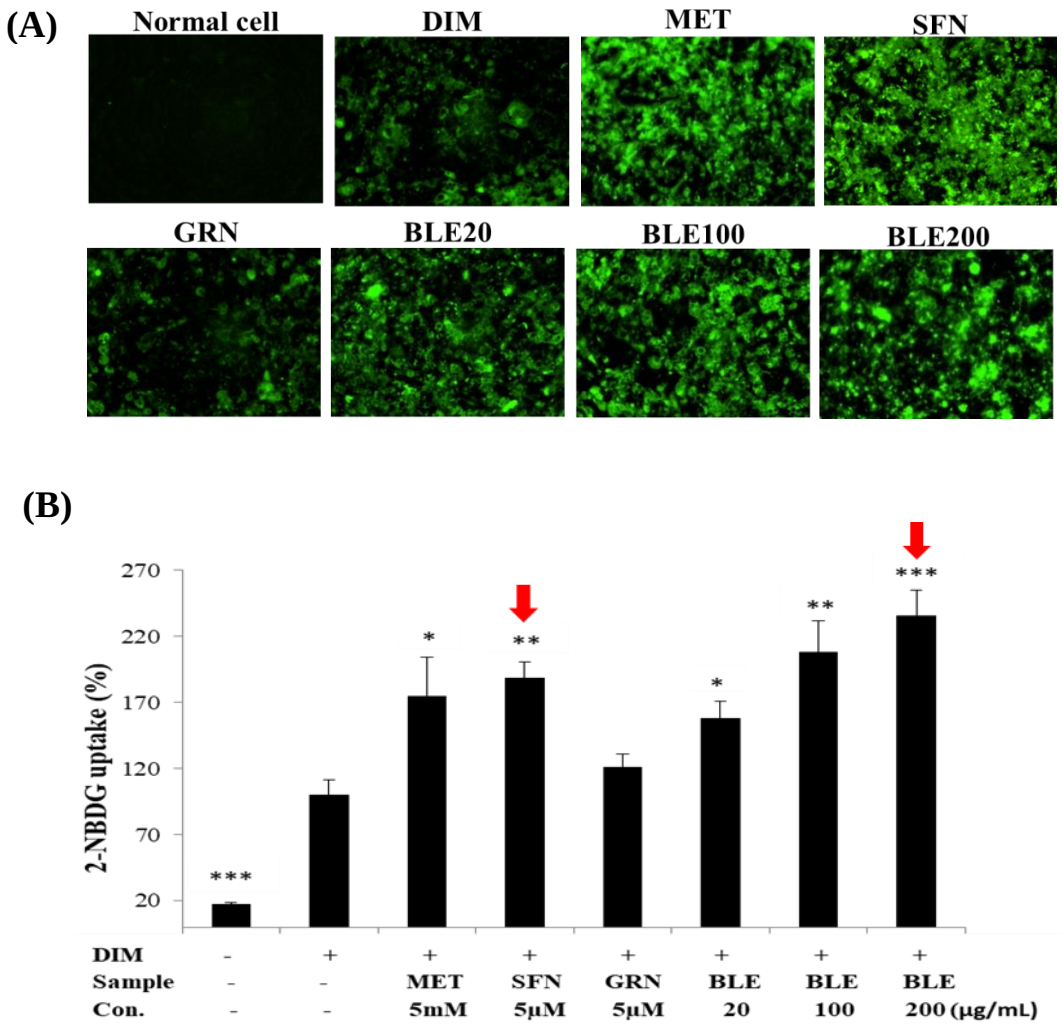

Fig. 25. Glucose uptake in the 3T3-L1 adipocytes.

Glucose uptake was monitored by 2-NBDG as a fluorescent probe. Mature 3T3-L1 cells were incubated with different samples for 48 hrs, followed by incubation with 2-NBDG (40 μM) for 30 min. Cells were washed with PBS, and images were acquired using IncuCyte ZOOM® fluorescence microscope at 20× magnification (A). Total fluorescent intensity was calculated using IncuCyte ZOOM® florescent processing software (B). Values are mean ± SEM (n = 3). **P* < 0.05, ***P* < 0.005, and ****P* < 0.0005 vs. the differentiated control.

2.4.5. Phosphorylation of AMPK and ACC in 3T3-L1 adipocytes

Western blot analysis was performed to analyze the effects of BLE, SFN, and GRN on the phosphorylation of key enzymes in the AMPK signaling pathway (Fig. 26). Differentiated 3T3-L1 adipocytes showed a significant decrease ($P < 0.05$) in the phosphorylation levels of both AMPK (Thr172) and ACC (Ser79) compared with undifferentiated adipocytes. Both MET and SFN treatment significantly increased ($P < 0.05$) the phosphorylation levels of AMPK (Thr172) and ACC (Ser79), whereas GRN treatment did not show a significant effect on the phosphorylation of either AMPK (Thr172) or ACC (Ser79) in differentiated 3T3-L1 adipocytes compared with differentiated control adipocytes. In particular, the treatment with BLE (100 μg/mL) significantly increased ($P < 0.05$) the phosphorylation levels of both AMPK (Thr172) and ACC (Ser79) in differentiated 3T3-L1 adipocytes compared with the differentiated control adipocytes. These results suggest that both SFN and BLE activated AMPK signaling pathway in 3T3-L1 adipocytes.

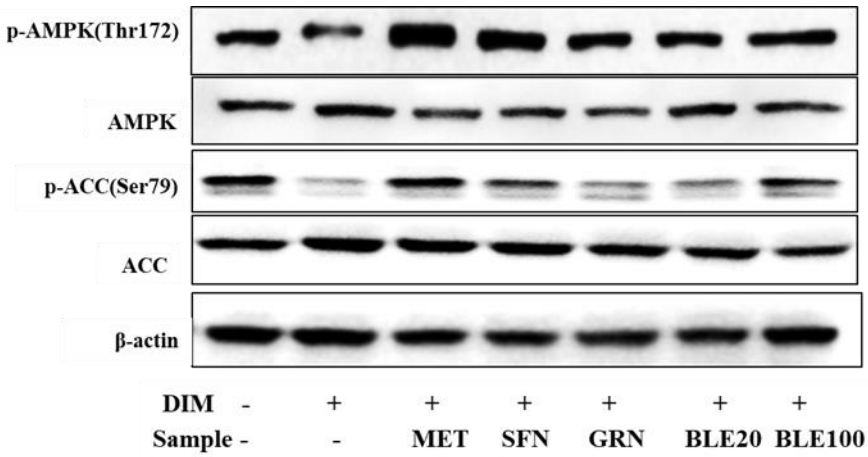

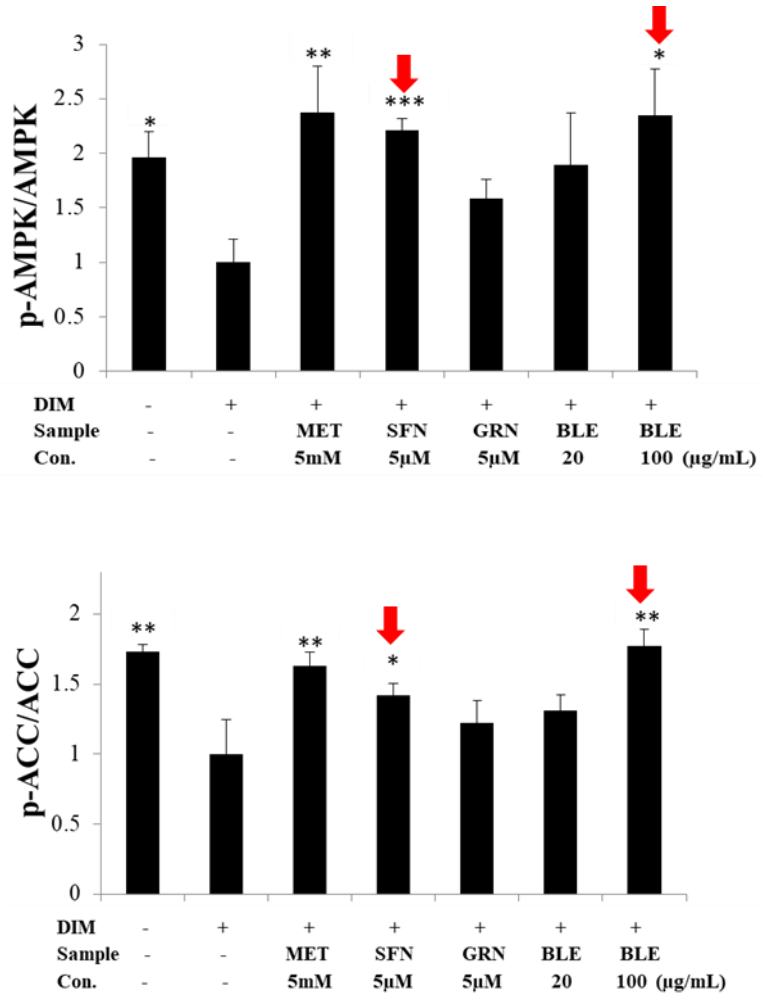

Fig. 26. Phosphorylation of AMPK pathway molecules in 3T3-L1 adipocytes. 3T3-L1 preadipocytes were treated with samples until differentiation. Cells were harvested on day 10, and subjected to Western blot analysis of p-AMPK and p-ACC. Protein band intensities were quantified and presented as mean ± SEM (n = 3). **P* < 0.05, ***P* < 0.005, and ****P* < 0.005 vs. the differentiated control group.

2.4.6. Hepatic lipid accumulation in ob/ob mouse liver

H & E staining of hepatic tissues was conducted in ob/ob mice to investigate the effects of BLE, SFN, and GRN on hepatic lipid accumulation (Fig. 27). Histological analysis revealed that the livers of ob/ob mice showed higher lipid accumulation when compared with those of the normal mice (Fig. 27A). However, ob/ob mice treated with MET, SFN, and GRN showed decreased hepatic lipid accumulation compared with the livers of control ob/ob mice. In particular, ob/ob mice treated with BLE showed reduced lipid accumulation compared with the liver of control ob/ob mice. The reduction in hepatic lipid accumulation was accompanied by increased phosphorylation levels of AMPK (Thr172) and ACC (Ser79), and reduced expression levels of HMGCR in ob/ob mice treated with MET, SFN, GRN, and BLE (Fig. 27B). These results suggest that SFN and BLE reduced hepatic lipid accumulation and activated AMPK pathway in ob/ob mice.

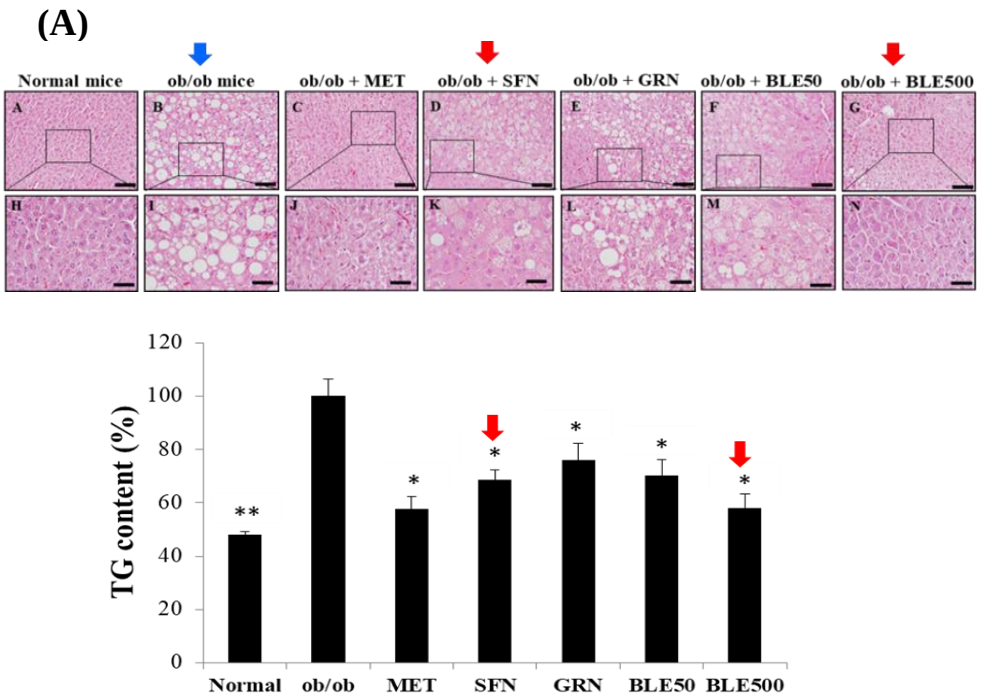

(B)

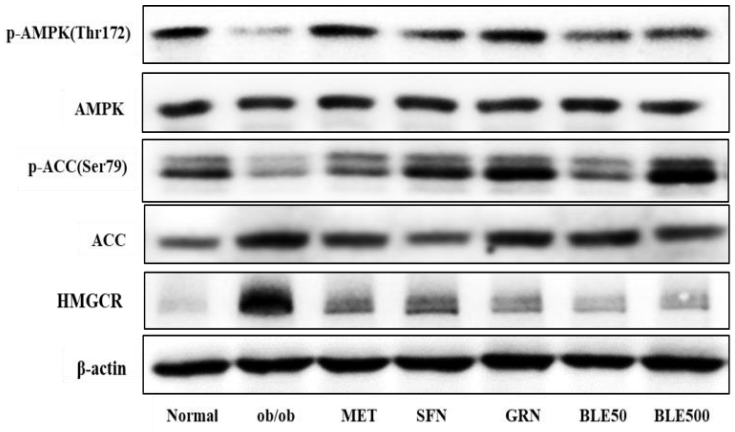

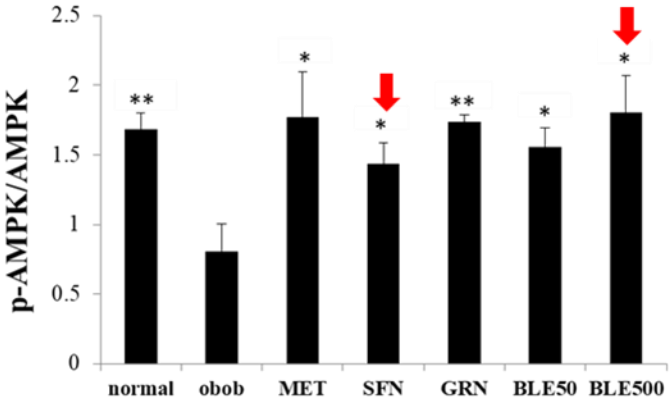

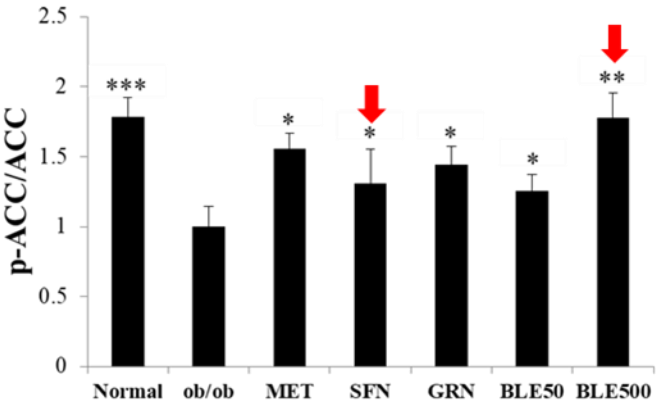

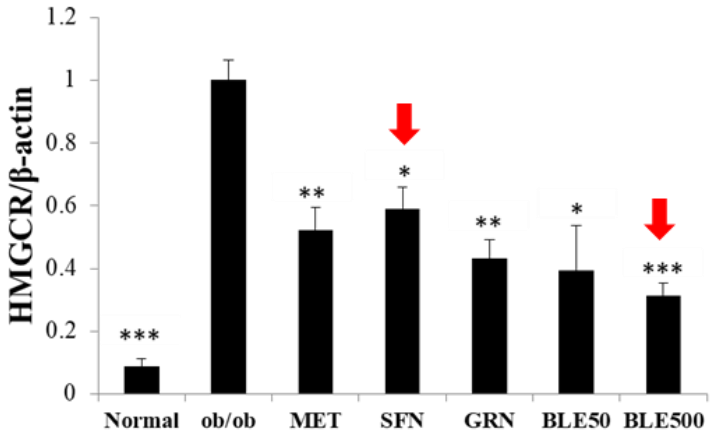

Fig. 27. Hepatic lipid accumulation in ob/ob mice.

Histological analysis (H&E staining) and TG content of liver tissues in ob/ob mice treated with vehicle or samples (A). The most representative observations are shown. Scale bars of (A)–(G) =100 μm; scale bars of (H)–(N) = 25 μm. Western blot analysis of phosphorylation of AMPK and ACC, and expression of HMGCR in ob/ob mice liver (B). Protein band intensities were quantified and presented as mean ± SEM (n = 5). *P < 0.05, **P < 0.005, and ***P < 0.0005.

2.4.7. AMPK signaling pathway in white adipose tissue of ob/ob mice

The effects of BLE, SFN, and GRN on phosphorylation of AMPK (Thr172) and its downstream targets ACC (Thr172) and HMGCR were analyzed by Western blot of pWAT in ob/ob mice (Fig. 28). Results showed that control ob/ob mice carry decreased phosphorylation levels of both AMPK (Thr172) and ACC (Ser79), and increased expression of HMGCR compared with normal mice. However, exposure to MET, SFN, and GRN significantly enhanced ($P < 0.05$) the phosphorylation of both AMPK (Thr172) and ACC (Ser79), and significantly reduced ($P < 0.05$) the expression of HMGCR in pWAT of ob/ob mice. In particular, BLE-treated ob/ob mice showed significantly increased ($P < 0.05$) levels of phosphorylation involving both AMPK (Thr172) and ACC (Ser79), and significantly decreased ($P < 0.05$) the expression of HMGCR compared with the control ob/ob mice. These results suggest that SFN and BLE activated the AMPK pathway in the white adipose tissues of ob/ob mice.

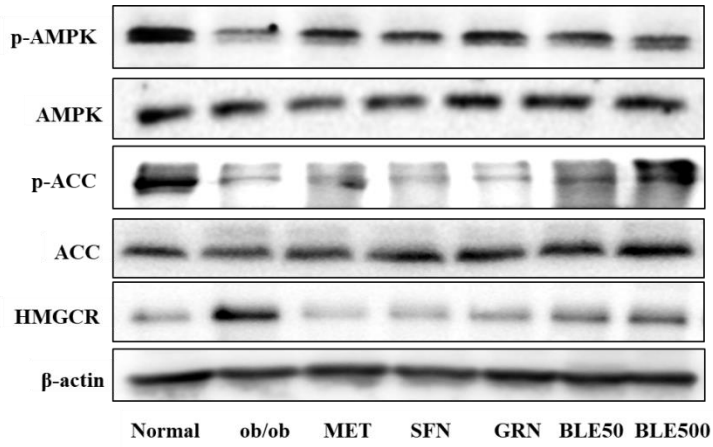

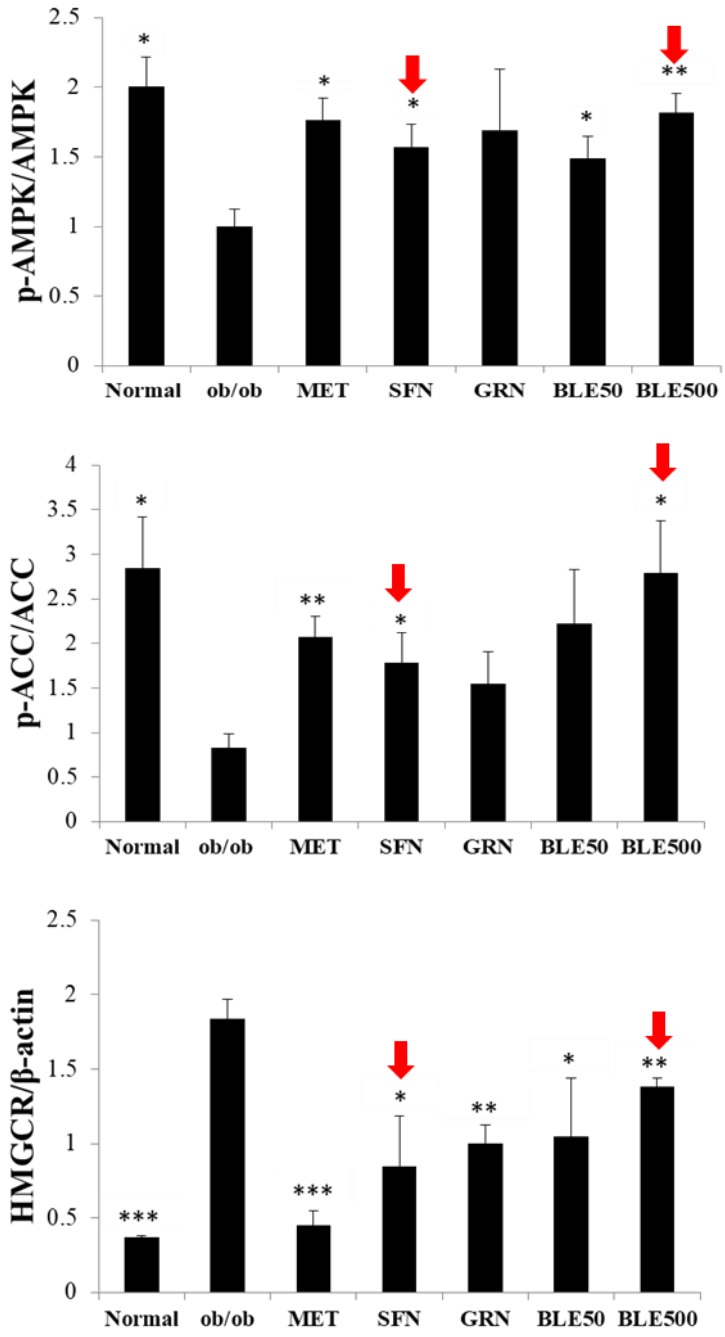

Fig. 28. Phosphorylation of AMPK, ACC, and the expression of HMGCR in white adipose tissue of ob/ob mice.

Mice exposed to the indicated diet for 6 weeks were sacrificed. pWAT lysate was analyzed by Western blot to determine the phosphorylation levels of AMPK and

ACC, and the expression of HMGCR. Protein band intensities were quantified and presented as mean ± SEM (n = 5). *P < 0.05, **P < 0.005, and ***P < 0.0005 vs. the control ob/ob group.

2.4.8. Serum parameters of ob/ob mice

The effects of BLE, SFN, and GRN on serum parameters were monitored by analyzing TG, LDL, and TC levels in ob/ob mice (Fig. 29). The serum levels of TG, LDL, and TC were significantly increased (P < 0.0005) in control ob/ob mice compared with those of normal mice (Fig. 29A-29C). In contrast, the treatment of ob/ob mice with MET, SFN, GRN showed a significantly decrease (P < 0.05) in the serum levels of TG, LDL, and TC when compared with the control ob/ob mice. Particularly, the treatment of ob/ob mice with BLE (50 mg/kg and 500 mg/kg) significantly reduced (P < 0.05) serum levels of TG, LDL, and TC when compared with control ob/ob mice. Thus, both SFN and BLE reduced serum lipid levels in ob/ob mice.

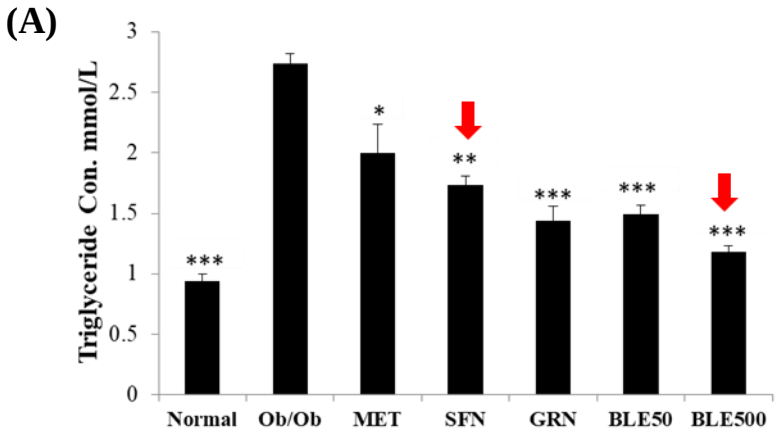

(B)

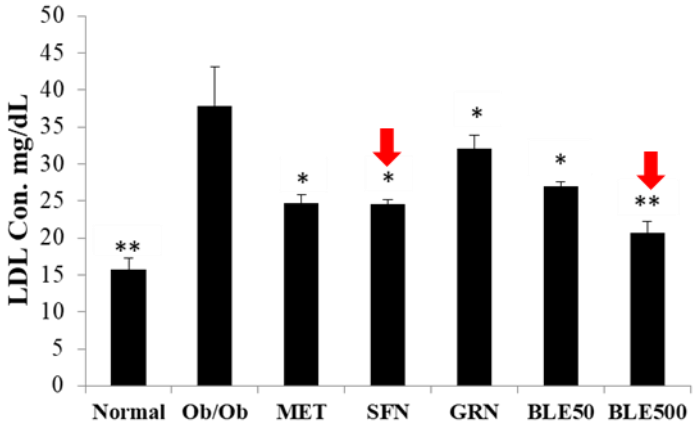

(C)

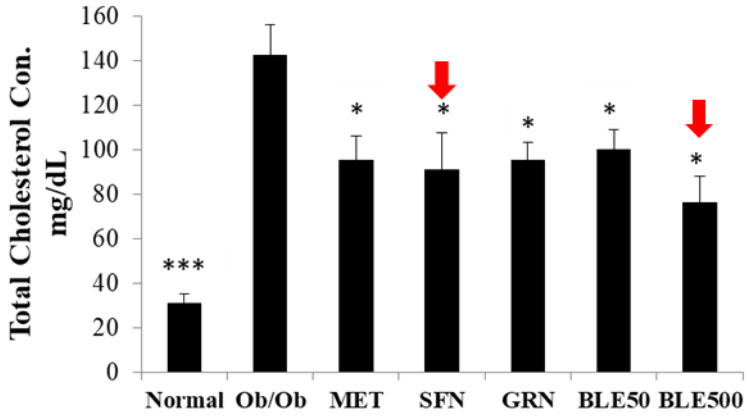

Fig. 29. Serum parameters in ob/ob mice.

At the end of the study, blood was collected from the fasted mice and serum was separated by centrifugation. The serum levels of TG (A), LDL (B), and TC (C) levels were measured. Values represent mean ± SEM (n = 5). *P < 0.05, **P < 0.005 and ***P < 0.0005 vs. the control ob/ob group.

2.4.9. Blood glucose concentrations of ob/ob mice

The effects of BLE, SFN, and GRN on blood glucose concentrations were measured at 0, 2, 4, and 6 weeks of treatment in ob/ob mice (Fig. 30). The control ob/ob mice showed significantly elevated blood glucose concentration (440 ± 14 mg/dL) at the beginning when compared with the normal mice (166 ± 13 mg/dL). The ob/ob mice treated with MET showed the lowest blood glucose level (227 ± 12.6 mg/dL) after four weeks of treatment. In addition, the groups treated with SFN, GRN, and BLE showed a gradual decline in blood glucose levels with time and significantly reduced ($P < 0.05$) blood glucose levels after six weeks of treatment when compared with the control ob/ob mice. In particular, BLE-treated groups showed a significantly decrease ($P < 0.05$) in blood glucose concentrations (255 ± 41.5 mg/dL and 232.5 ± 17.5 mg/dL at the dose of 50 mg/kg and 500 mg/kg, respectively) after six weeks of treatment when compared with control ob/ob mice (460.5 ± 31 mg/dL). Results suggest that six weeks of treatment with SFN and BLE significantly reduced the blood glucose levels in ob/ob mice.

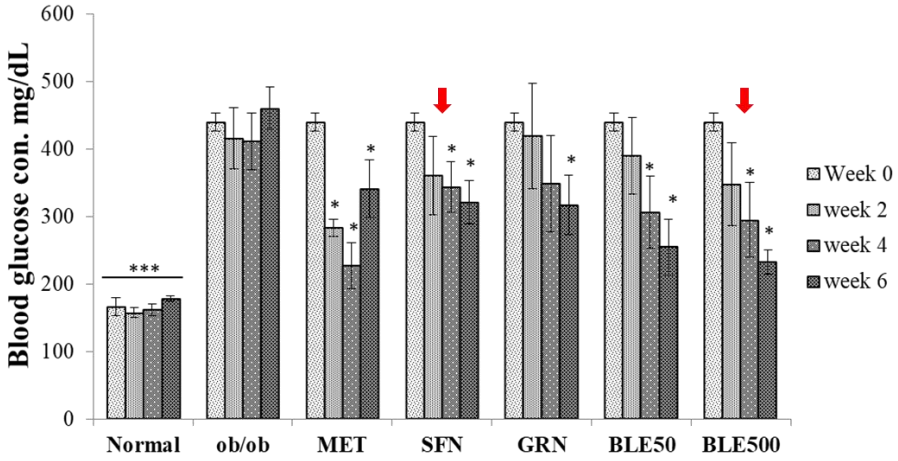

Fig. 30. Blood glucose concentration of ob/ob mice.

Glucose levels were measured in blood taken from the tail at 0, 2, 4, and 6 weeks of sample treatment in ob/ob mice. Values represent mean ± SEM (n = 5). *$P < 0.05$ and ***$P < 0.005$ vs. the control ob/ob group.

2.4.10. Hepatic gene expression analysis

RNA sequencing was performed to analyze the effects of BLE and SFN on the expression of genes related to hepatic lipid accumulation in ob/ob mice (Fig. 31). Based on Gene Ontology (GO) analysis, a large proportion of the genes involved in lipid metabolism were changed in ob/ob mice when compared with normal mice (Fig. 31A-31C). The results showed that 21 up-regulated (higher than 1.8-fold) genes and 8 down-regulated (less than 0.6-fold) genes related to lipid metabolism were restored to normal level by BLE and SFN in the livers of ob/ob mice (Table 1, 2). STRING analysis was performed to identify protein-protein interactions among the normalized genes induced by both SFN and BLE, and visualize as a set of nodes and edges (Fig. 31D). The proteins related to lipogenesis and FAO (*Srebf2*, *Elov5*, *Mboat1*, *Lpinl*, *Cpt1c*, and *Cpt1a*) formed a functional cluster in the network of lipid metabolism. In addition, fatty acid metabolism-related proteins including *Pla2g2c*, *Plb1*, *Cyp2c55*, and *Cyp2c39* also showed a functional association by forming a small cluster within the PPI network. Furthermore, another separate cluster was identified in the PPI network, which consisted of six nodes including *Fgf23*, *Fgfr1*, *Plcg1*, *Plcb4*, and *Pik3cd*. The six nodes are related to lipolysis and intracellular signaling. These results suggest that both SFN and BLE regulate the expression of genes related to lipid metabolism in ob/ob mice.

Table 3. Up-regulated genes related to lipid metabolism in ob/ob mice liver which were normalized by SFN & BLE

Gene symbol	ob/ob/ Normal	MET/ Normal	**SFN/ Normal**	GRN/ Normal	**BLE50/ Normal**	**BLE500/ Normal**
Fut7	7.358	0.968	0.968	0.969	0.983	0.968
Cpt1c	6.983	4.505	**3.488**	1.882	**0.965**	**0.934**
Mboat1	6.367	1.256	**2.271**	1.171	**1.616**	**1.165**
Rbp7	5.529	0.970	0.970	2.926	2.027	0.970
Elovl7	4.957	0.886	**0.562**	0.630	0.058	**1.607**
Ip6k3	4.736	0.987	**0.987**	0.988	**0.993**	**0.987**
Slc35c1	3.507	0.942	0.942	4.740	0.969	0.942
Elovl5	3.417	1.790	**1.193**	2.357	**1.274**	**1.407**
Srebf2	3.068	1.231	**1.042**	1.164	**1.063**	**1.898**
Oc90	2.869	0.993	0.993	0.994	0.997	0.993
Pla2g2c	2.806	2.875	**0.981**	0.982	**0.990**	**0.981**
Ephx3	2.765	2.842	0.973	0.974	0.986	0.973
Fgf23	2.765	1.895	0.973	0.974	0.986	0.973
Hmgcr	2.684	1.545	1.654	1.958	1.640	1.707
Plp1	2.293	1.275	1.287	0.303	0.167	1.299
Cyp2c55	2.162	0.591	0.999	1.266	0.741	1.487
Alg12	1.969	0.950	1.662	0.656	1.094	1.310
Mt3	1.927	0.997	0.997	0.997	0.998	0.997
Plb1	1.915	0.993	**0.993**	0.994	**0.997**	**0.993**
Cyp2c39	1.913	1.393	1.351	1.525	1.080	0.858
Galr2	1.883	0.984	2.832	0.985	0.992	0.984

Table 4. Down-regulated genes related to lipid metabolism in ob/ob mice liver which were normalized by SFN & BLE

Gene symbol	Ob/ob/ Normal	MET/ Normal	**SFN/ Normal**	GRN/ Normal	**BLE50/ Normal**	**BLE500/ Normal**
Fgfr1	0.411	1.031	**1.095**	0.867	**0.758**	**1.241**
Plcg1	0.445	2.639	**0.849**	0.896	**0.906**	**1.232**
Plcb4	0.445	0.909	**0.900**	0.038	**0.726**	**1.219**
Pik3cd	0.477	0.983	**0.875**	0.357	**0.977**	**1.407**
Acer2	0.565	0.490	0.896	0.937	0.999	0.865
Cpt1a	0.575	0.923	**1.078**	1.388	**1.554**	**1.038**
Lpin1	0.579	1.499	**1.055**	0.861	**1.040**	**1.276**
Prkab2	0.628	0.240	1.362	1.353	0.385	1.109

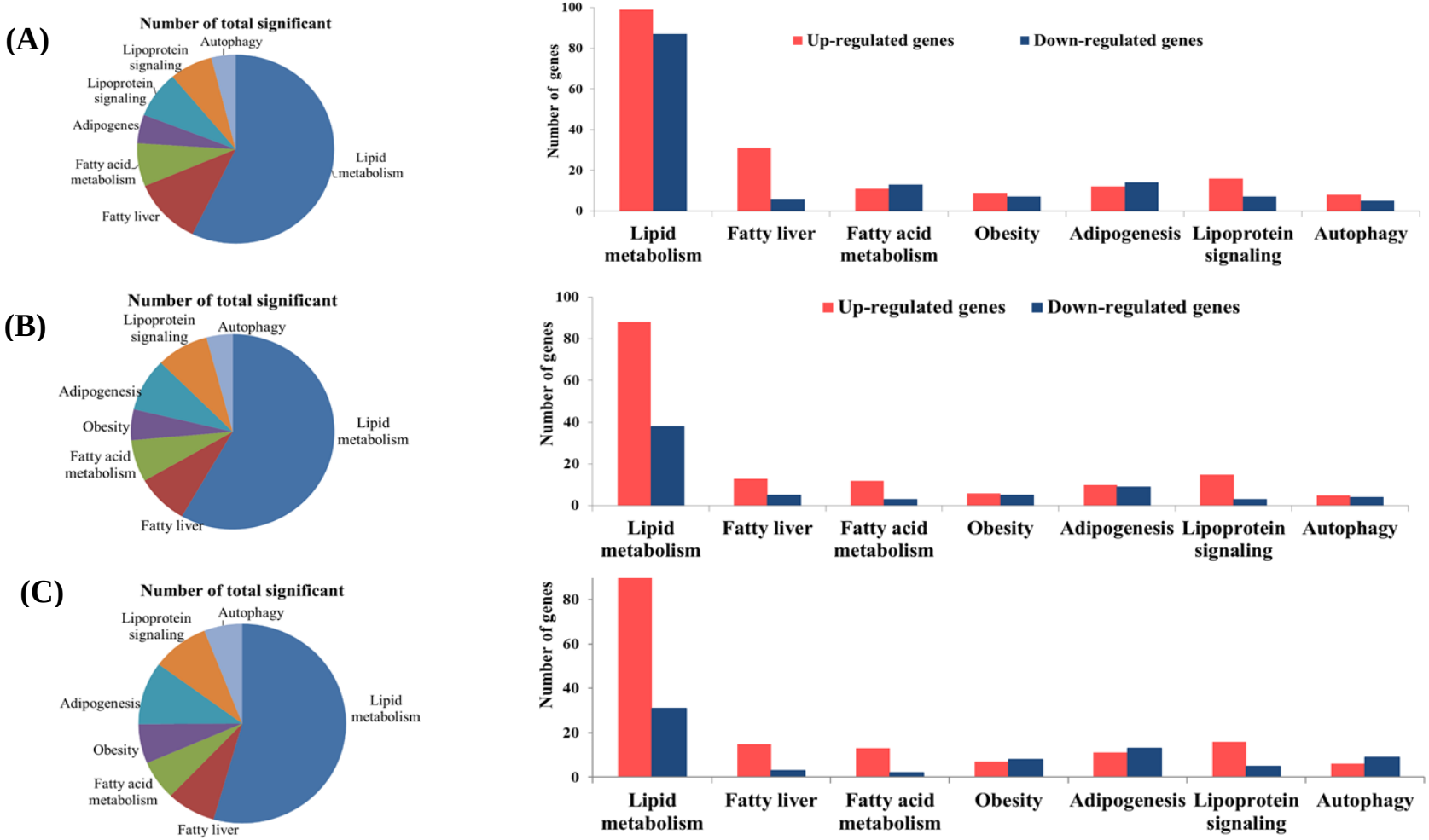

(D)

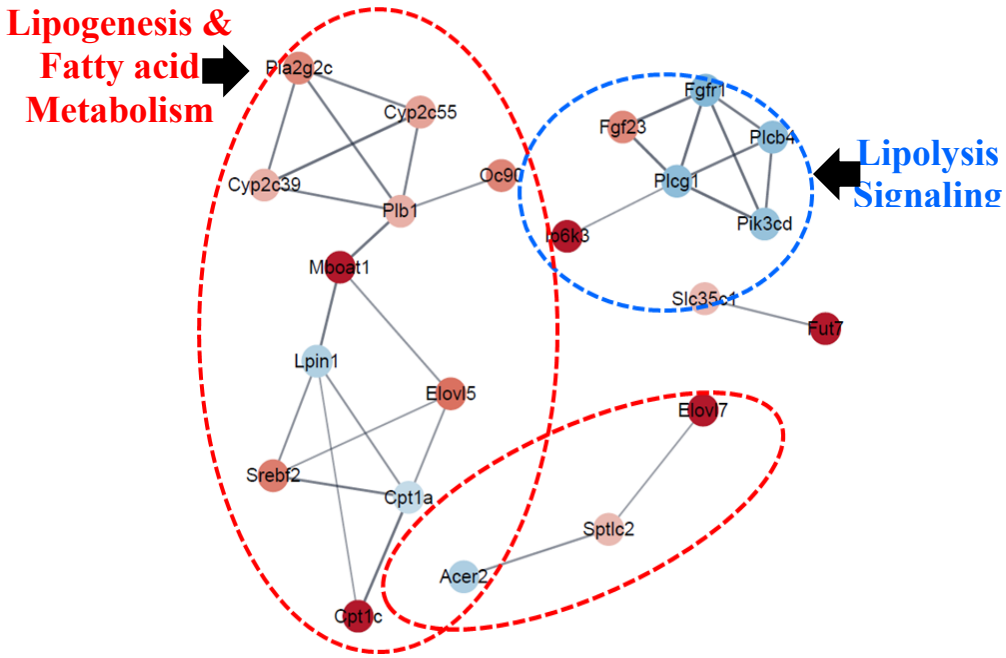

Fig. 31. Differential gene expression analysis in ob/ob mice liver.

GO analysis of ob/ob control mice compared to the normal mice (A), SFN treated ob/ob compared to the normal mice (B), BLE (500 mg/kg) treated ob/ob mice compared to the normal mice (C), (The pie chart indicates functional categorization of the differentially expressed genes in ob/ob mice liver, and the bar graph represents the number of up and down-regulated genes). PPI network of normalized genes related to lipid metabolism in BLE treated ob/ob mice (D). Red circles represent up-regulated genes, and blue circles represent down-regulated genes in control ob/ob mice compared to the normal mice.

2.5. Discussion

The present study elucidated the possible mechanism underlying the anti-obesity effect of SFN enriched BLE on 3T3-L1 adipocytes and ob/ob mice. The results demonstrate that SFN and BLE reduce lipid accumulation and increase glucose uptake in 3T3-L1 adipocytes. SFN and BLE increased phosphorylation of AMPK and ACC in both 3T3-L1 adipocytes and ob/ob mice. In addition, SFN and BLE reduced the expression of HMGCR in the liver and white adipose tissue of ob/ob mice. Furthermore, both SFN and BLE decreased the serum lipid profiles (TG, LDL, and TC) and blood glucose levels of ob/ob mice. RNA sequencing analysis revealed that both SFN and BLE exhibit an anti-obesity effect by normalizing the genes related to lipid metabolism including *Srebf2*, *Pla2g2c*, *Plb1*, *Ip6k3*, *Elovl5*, *Elovl7*, *Slc27a3*, *Fgfr1*, *plcb4*, *Plcg1*, *Ctp1a*, and *Lipin1* in ob/ob mice liver.

The present findings suggest that BLE and its active compound SFN inhibited lipid accumulation and reduced TG content in 3T3-L1 adipocytes. Previous studies reported that SFN inhibited the early stage of adipogenesis [83], and reduced lipid accumulation by suppressing the mRNA levels of C/EBPα and PPARγ in 3T3-L1 cells [84]. In addition, SFN reduced TG synthesis by decreasing the DGAT-1 expression in 3T3-L1 adipocytes [44]. Furthermore, SFN inhibited lipid accumulation via lipolysis by increasing the phosphorylation of HSL at Ser-563 and Ser-660 in 3T3-L1 adipocytes [44]. These results suggest that the SFN content in BLE plays a significant role in the inhibition of lipid accumulation and TG synthesis in differentiated 3T3-L1 adipocytes.

The present study confirmed that both BLE and SFN significantly increased glucose uptake in 3T3-L1 adipocytes. A recent study reported that SFN increased the glucose uptake by enhancing the expression of GLUT4, and utilization of glucose via glycolysis and tricarboxylic acid cycle in 3T3-L1 adipocytes [44]. In addition, SFN increased glucose uptake in primary human muscle cells [85] and HepG2 cells [45]. These findings suggest that SFN contained in BLE increased cellular glucose uptake that might affect glucose metabolism in differentiated 3T3-L1 adipocytes.

The present findings suggest that BLE and SFN increased the phosphorylation levels of both AMPK and ACC in 3T3-L1 adipocytes and ob/ob mice. In addition, the activation of AMPK by BLE and SFN might reduce cholesterol synthesis in ob/ob mice by inhibiting HMGCR protein expression. A previous study reported that SFN increases p-AMPK and p-ACC levels, and reduces HMGCR level in epididymal adipose tissues of obese mice [21]. Oral administration of SFN prevented high-fat diet-induced NAFLD via activation of the AMPK related autophagy in the liver [86]. Furthermore, the activation of AMPK reduced the blood glucose level by increasing cellular glucose uptake, and decreased the plasma TG level in ob/ob mice [27, 28]. The current results demonstrate that BLE reduced blood glucose and serum levels of TG, LDL, and TC in ob/ob mice, which are consistent with previous studies reporting GRN-induced decrease in serum levels of TG, LDL, and TC in obese rats [87]. A broccoli diet rich in GRN reduced plasma LDL level in obese mice [88]. The previous and the present findings suggest that SFN-enriched BLE regulates lipid metabolism by activating AMPK pathway in both 3T3-L1 adipocytes and ob/ob mice, which potentially contributes to ameliorate the metabolic dysfunction in obesity.

The present study demonstrated that BLE and SFN reduced hepatic lipid accumulation in ob/ob mice. Previously, the administration of GRN reduced hepatic lipid accumulation by suppressing fatty acid synthesis related genes including *Srebp1*, *Fasn*, and *Pparγ* [26]. In addition, SFN increased the expression of FAO associated genes including *Pparα*, *Acox*, and *Cpt1a* in obese mice [87]. Furthermore, SFN treatment prevented NAFLD in the high-fat diet-fed mice [86]. Therefore, it is evident that the presence of both SFN and GRN in BLE play a significant role in reducing hepatic lipid accumulation in ob/ob mice liver.

In the present study, RNA sequencing analysis was performed to investigate the molecular mechanism underlying BLE- and SFN-induced reduction in hepatic lipid accumulation. The findings also suggest that up-regulated genes including *Srebf2*, *Pla2g2c*, *Plb1*, *Ip6k3*, *Elovl5*, *Elovl7*, and *Slc27a3* in ob/ob mice liver were normalized by treatment with BLE and SFN. Srebf2 regulates the expression of genes involved in cholesterol homeostasis including Hmgcr in the liver [89]. Previous studies reported that the expression of *Srebf2* was increased in obese mice [89]. Both *Pla2g2c* and *Plb1* show phospholipase A2 (PLA2) activity [90]. PLA2 are a group of enzymes that hydrolyzes phospholipids into fatty acids and other lipophilic molecules including arachidonic acid [90]. *Ip6k3* generates inositol pyrophosphates (IPPs) which inactivates Akt [91], AMPK [92], and LKB1 [93] signaling pathways. *Ip6k3* knockout mice showed reduced body weight and increased glucose tolerance [94]. Both *Elovl5* and *Elovl7* catalyze the elongation of long-chain fatty acids (LCFA) by adding 2 carbons to the chain of fatty acids [95]. In addition, *Slc27a3* is involved in cellular uptake and metabolic activation of LCFA [96]. As expected, the present study showed reduced lipid accumulation following

treatment with SFN and BLE by normalizing the expression of *Srebf2*, *Pla2g2c*, *Plb1*, *Ip6k3*, *Elovl5*, *Elovl7*, and *Slc27a3* genes in ob/ob mice.

In addition, the down-regulated *Fgfr1*, *Pik3cd*, *plcb4*, and *Plcg1* genes in ob/ob mice liver were normalized following treatment with SFN and BLE. *Fgfr1* is crucial for liver homeostasis and regeneration [97]. Activation of *Fgfr1* signaling improved hepatic lipid accumulation, inflammation, and liver damage in mice [98-100]. Both *Plcg1* and *plcb4* hydrolyze phosphatidylinositol 4,5-bisphosphate into diacylglycerol (DAG) which increases intracellular calcium signaling in liver [101]. Therefore, BLE and SFN restore the lipid metabolism to the normal level by normalizing the expression of *Fgfr1*, *Pik3cd*, *plcb4*, and *Plcg1* genes in ob/ob mice.

The present study observed that BLE and SFN normalized down-regulated *Ctp1a* and *Lipin1*, which are FAO related genes in ob/ob mice liver. The carnitine palmitoyltransferase 1 (Ctp1) family of proteins catalyze the FAO by converting acyl-CoAs into acylcarnitines [102]. *Lipin1* is a transcriptional co-activator that regulates the expression of genes involved in FAO [103, 104]. Decreased FAO in ob/ob mice liver resulted in NAFLD [105]. Particularly, GRN treatment increased *Ctp1* expression and reduced lipid accumulation in the liver of obese mice [87]. In this regard, normalizing the expression of *Ctp1a* and *Lipin1* genes by BLE and SFN restore FAO process to normal level in ob/ob mice.

In conclusion, the present study provides evidence suggesting that SFN-enriched BLE plays a significant role in reducing lipid accumulation by increasing AMPK and ACC phosphorylation in 3T3-L1 adipocytes. Both SFN and BLE affect glucose metabolism by increasing glucose uptake in 3T3-L1 adipocytes. In addition,

SFN and BLE reduced serum lipids (TG, LDL, and TC), blood glucose, and hepatic lipid accumulation probably by increasing the phosphorylation levels of AMPK and ACC, and by decreasing the expression level of HMGCR in ob/ob mice. In particular, RNA sequencing analysis revealed that both SFN and BLE have an anti-obesity effect by normalizing the expression of *Srebf2*, *Pla2g2c*, *Plb1*, *Ip6k3*, *Elovl5*, *Elovl7*, *Slc27a3*, *Plcg1*, *Fgfr1*, *Pik3cd*, *plcb4*, *Ctp1a*, and *Lipin1* genes in ob/ob mice (Fig. 32). Further studies are needed to delineate the role of these genes as therapeutic targets in obesity. The overall results suggest that SFN content in BLE has a potent anti-obesity effect by normalizing the expression of genes related to lipid metabolism, which are up- and down-regulated in ob/ob mice.

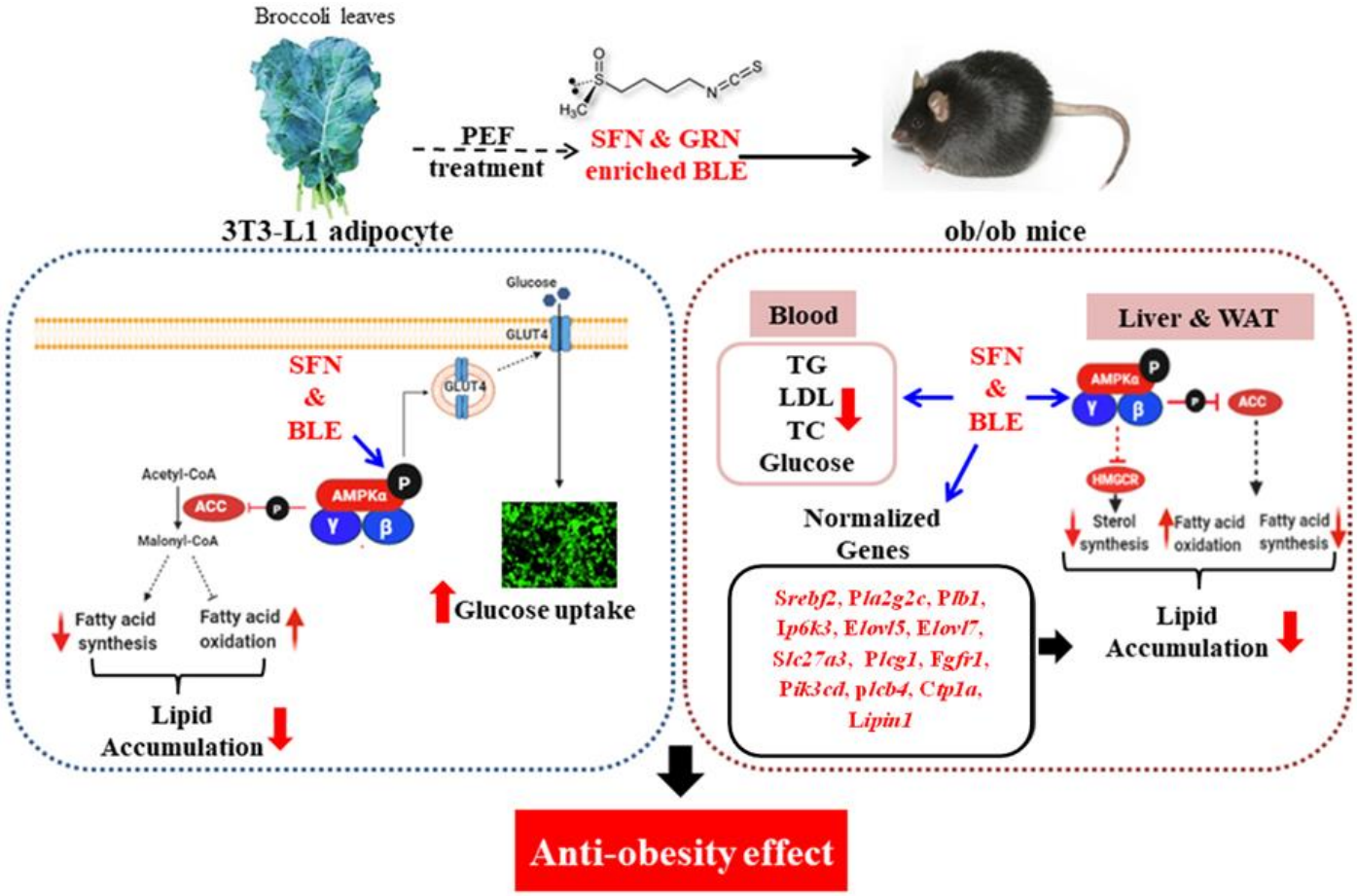

Fig. 32. Anti-obesity effects of SFN and BLE

PART-III

Anti-inflammatory effects of Sulforaphane in Broccoli leaf extract on LPS-stimulated RAW 264.7 cells and ob/ob mice

3.1. Abstract

This study examined the relationship between the anti-inflammatory effects of sulforaphane (SFN) in broccoli leaf extract (BLE) and the differential gene expression pattern in SFN and BLE treated ob/ob mice. Both SFN and BLE showed anti-oxidant activity by increasing the DPPH radical scavenging ability in a dose-dependent manner. Production of nitric oxide (NO), and pro-inflammatory cytokines including tumor necrosis factor-α (TNF-α), interleukin-1β (IL-1β) and interleukin-6 (IL-6), were decreased by SFN and BLE in LPS stimulated RAW 264.7 cells. Based on the western blot analysis, both SFN and BLE reduced the expression of both cyclooxygenase-2 (COX-2) and inducible nitric oxide (iNOS) protein levels in LPS stimulated RAW 264.7 cells. RNA sequencing analysis showed that the expression levels of 28 genes related to inflammation were up-regulated (> 2-fold), and six genes were down-regulated (< 0.6-fold) in the control ob/ob mice compared to normal mice. In contrast, the gene expression levels were restored to the normal level by SFN and BLE. The protein-protein interaction (PPI) network showed that chemokine ligand (*Cxcl14*, *Ccl1*, *Ccl3*, *Ccl4*, *Ccl17*) and chemokine receptor (*Ccr3*, *Cxcr1*, *Ccr10*) were located in close proximity and formed a "functional cluster" in the middle of the network. The overall results suggest that SFN in BLE exerts a potent anti-inflammatory effect by normalizing the expression of genes related to inflammation that were perturbed in ob/ob mice.

Key words: Sulforaphane, Broccoli leaf extract, Anti-inflammatory activity, RAW 264.7 macrophage, RNA sequencing analysis, ob/ob mice

3.2. Introduction

Inflammation is the most commonly identified condition in the clinical field, which involves protecting the body from infection and tissue damage [106]. Macrophages are one of the major groups of the immune system, which perform a critical role in response to injury and infection [107]. Nuclear factor-κB (NF-κB) is a key regulatory element in macrophages [108]. The activation of NF-κB is essential for the expression of NO, iNOS, COX-2, and pro-inflammatory cytokines, including TNF-α, IL-6, and IL-1β [109]. Cytokines released from the inflammatory tissue disturb the metabolic functions of many organs, including the liver [110]. In particular, chronic inflammation is closely related to the progression of many metabolic diseases, including obesity and insulin resistance [111].

Obesity is associated with low-grade inflammation that causes oxidative stress, which leads to insulin resistance and non-alcoholic fatty liver disease (NAFLD) [112]. In the present study, ob/ob mice were selected as the appropriate *in vivo* model because they exhibit severe disturbances of the immune functions [14]. In particular, ob/ob mice have high levels of circulating endotoxin, which contributes to the development of inflammation by activating toll-like receptor 4 (TLR4) signaling in the liver [14]. The inflammatory state of obesity is the augmented infiltration of T cells and macrophages into the metabolic tissues, including the liver [113]. In addition, ob/ob mice display hepatic lipid accumulation that induces inflammation, leading to NAFLD development [114]. Therefore, the liver of ob/ob mice was used to observe the effects of SFN on inflammatory gene expression.

SFN is an isothiocyanate present in cruciferous vegetables, such as cabbage, cauliflower, and broccoli [115]. GRN, one of the main glucosinolates in cruciferous vegetables, is converted to SFN by the gut microbiota-derived myrosinase in both rodents and humans [41]. A previous study found that GRN ameliorates obesity-induced inflammation in high-fat diet-treated obese mice [116]. In addition, bioactivated GRN with myrosinase reduced pro-inflammatory signaling related to a spinal cord injury in an experimental mouse model [117]. The supplementation of GRN-rich broccoli sprout extract reduced inflammatory reactions in endothelial cells [118]. Furthermore, synthetic GRN exhibited anti-inflammatory activity by reducing TNF-α secretion in lipopolysaccharide (LPS)-stimulated THP-1 cells [119]. Because GRN has an anti-inflammatory effect *in vivo* and *in vitro*, the present study used it as a control to compare the anti-inflammatory effect with SFN on both RAW 264.7 cells and ob/ob mice. SFN shows high chemical reactivity because of the electrophilicity of its isothiocyanate group [120]. Previous studies reported that SFN prevents oxidative stress-induced inflammation [121]. Furthermore, the SFN treatment prevented nod-like receptor protein 3 (NLRP3) inflammasome-induced NAFLD in obese mice [86]. Despite the anti-inflammatory and antioxidant effects of SFN, its exact mechanism related to the inflammatory genes is not completely understood.

The present study examined the anti-inflammatory activity of SFN enriched BLE on LPS-stimulated RAW 264.7 cells and ob/ob mice. The effects of SFN and BLE on the expression levels of pro-inflammatory mediators, such as NO, COX-2, iNOS, TNF-α, IL-6, and IL-1β, were analyzed in LPS-stimulated RAW 264.7 cells. In addition, the effects of SFN and BLE on obesity-related inflammation were

identified from the expression levels of genes related to inflammation in ob/ob mouse livers.

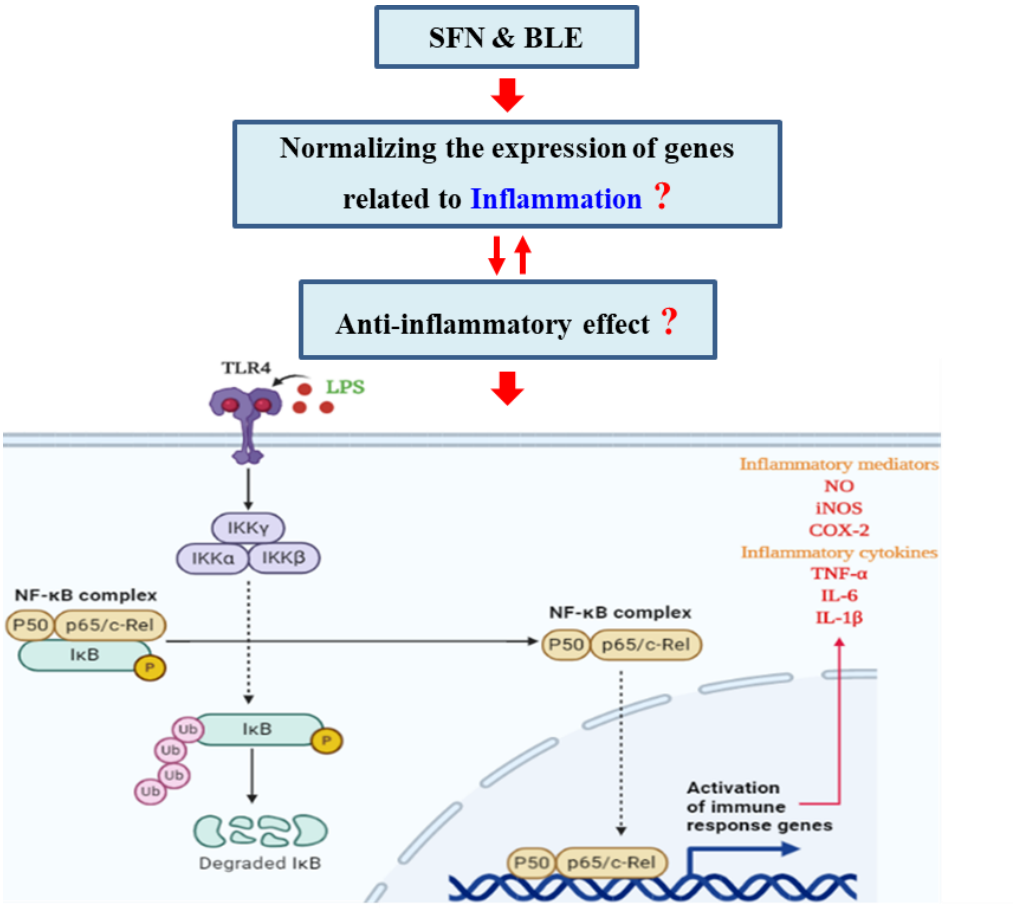

Fig. 33. Hypothetical model: anti-inflammatory effect of SFN and BLE

It is recognized that inflammation is involved in the pathogenesis of obesity-related insulin resistance and T2DM. Therefore, the present study aimed to observed how SFN in BLE improves obesity-induced inflammation by regulating differential gene expression related to inflammation (Fig. 33)

3.3. Materials and Methods

3.3.1. Materials

2,2-diphenyl-1-picrylhydrazyl (DPPH), Lipopolysaccharides, SFN, iNOS, and COX-2 primary antibodies were obtained from Sigma-Aldrich (USA). β-actin primary antibody was purchased from Thermofisher (USA). Griess reagent system was purchased from Promega (USA). Mouse IL-2, mouse IL-1β, mouse IL-6 ELISA complete kits, and Tris-Glycine-PAG non-SDS Precast Gels (10%) were purchased from Koma biotech (Korea). RAW 264.7 macrophage cells were purchased from the Korean Cell Line Bank (Korea). Dulbecco's modified Eagle's medium (DMEM) were purchased from Life Technologies (USA). EZ-Western Lumi Pico and EZ-Cytox were purchased from DogenBio (Korea). All other reagents were purchased from commercial sources and were of the analytical grade.

3.3.2. Preparation of broccoli leaf extract

Broccoli leaves were minced into small pieces and were added 10× volume of distilled water. Pulsed electric field (PEF) treatment was performed using 5 kW PEF at 7 kJ of total energy for 5 sec (out voltage 60%, pulsed width 25 μs, frequency 100 Hz). The suspension was mixed with 10× volume of ethanol and was extracted for about 3 hrs at room temperature. The extract was lyophilized for 72 hrs using a lyophilizer, crushed to make a fine powder, and was stored at -80 °C until use.

3.3.3. DPPH radical scavenging activity

The antioxidant activity of the SFN and BLE was evaluated using stable free radical 2,2-diphenyl-1-picrylhydrazyl (DPPH) according to a slight modification of a previously described method [122]. Various concentrations of SFN (Sigma, USA), BLE, and GRN (Cayman Chemicals, USA) were diluted in dimethyl sulfoxide (DMSO) (Sigma) and incubated with ethanolic 0.1 mM DPPH (Sigma) at 37 ºC for 30 min. The absorbance was measured at 517 nm using a UV spectrophotometer (Mecasys, Korea). The blanks were prepared by replacing the sample volumes with DMSO. The results were calculated as percentages of the control (100%), and the concentration of extracts required to decrease the initial DPPH concentration by 50% was expressed as the IC_{50} value. The radical scavenging ability (%) of the samples was calculated as % inhibition = $[(A_{Blank} - A_{sample})/A_{Blank}] \times 100$, where A_{Blank} = absorbance of the DPPH without the sample and A_{sample} = absorbance of the SFN or GRN. The antioxidant activity of the SFN is expressed as the ascorbic acid (AA) equivalent antioxidant capacity (AEAC) as AA/100 g dry weight (DW) using the equation, $AEAC = IC_{50\ (Ascorbic\ acid)}/IC_{50\ (Sample)} \times 10^5$.

3.3.4. RAW 264.7 cell culture and treatment

The murine macrophage RAW 264.7 cells were obtained from Korean Cell Line Bank and cultured in DMEM supplemented with 10% FBS, 1% penicillin-streptomycin and incubated in a humidified atmosphere at 37 °C under 5% CO2. After reaching 70%-80% confluence, cells were sub-cultured within two days intervals.

3.3.5. Cell viability assay

The MTT assay was performed to determined cell viability using an EZ-cytox cell viability assay kit. RAW 264.7 macrophage cells were cultured in 96-well plate at cell density of 1×10^5 cells/well for 24 hrs and then cells were pretreated with different concentrations of BLE for 1 hr, and then stimulated with LPS for 24 hrs. Normal cells that were not treated with the compounds and not activated with LPS were used as the control group. Cell media was removed by using a suction valve and added new media containing 10% Ez-cytox into each well. Plates were incubated for 3 hrs at 37 °C and 5% CO2. Cell viability indicated by the production of formazan, was measured with an ELISA microplate reader (Gordig, Austria) at 450 nm wavelength.

3.3.6. Measurement of NO production

After reaching 70–80% confluence, the RAW 264.7 macrophage cells were cultured in 96 well plates. After 24 h incubation, the cells were pretreated with samples for 1 hr, and then stimulated with LPS (Escherichia coli 0111:B4; Sigma-Aldrich, USA) for 24 hrs. The concentration (5 μM) of SFN was determined according to a previous study [123], and the same concentration (5 μM) of GRN was used to compare its activity with SFN. The level of NO production by LPS-stimulated RAW 264.7 macrophage cells was determined by measuring the nitrite level in the culture media using Griess reagent (Promega, USA). Briefly, the 50 μL of culture media from each well was mixed with 50 μL of N-(1-naphthyl) ethylenediamine dihydrochloride (NED) and 50 μL of a sulfanilamide solution. After incubating the mixture for 10 min at room temperature, the absorbance was read at

550 nm in an enzyme-linked immunosorbent assay (ELISA) microplate reader (TECAN, Austria).

3.3.7. Enzyme-linked immunosorbent assay (ELISA)

RAW 264.7 macrophage cells were cultured in 96 well plates (1×10^5 cells/well) in DMEM, 10% FBS, and 1% penicillin-streptomycin. After 24 hrs of incubation, the cells were pretreated with samples and then stimulated with LPS for 24 hrs. The concentrations of TNF-α, IL-6, and IL-β in the culture media were measured using commercially available ELISA kits (Koma Biotech, Korea) according to the manufacture instructions.

.

3.3.8. Measurement of COX-2 and iNOS protein expression

RAW 264.7 macrophage cells were cultured in six-well plates (1×10^6 cells/well) in DMEM, 10% FBS, and 1% penicillin-streptomycin. After 24 hrs incubation, the cells were pretreated with samples for 1 hr and then stimulated with LPS for 24 hrs. The expression levels of the COX-2 and iNOS proteins were observed by Western blot analysis. The cells were lysed with RIPA buffer containing a protease inhibitor mixture. The supernatant was separated, and the protein concentrations were evaluated using the Bradford assay (Bio-Rad Laboratories, USA). The equal amount of protein was mixed with 20% of loading buffer and separated by Tris-Glycine-Polyacrylamide, non-sodium dodecyl sulfate precast gel (10%, Koma Biotech) and subjected to Western blot with COX-2 (Sigma), iNOS (Sigma), and β-actin (Thermofisher, USA) antibodies. A Chemi-luminescence

Bioimaging Instrument (NeoScience Co., Korea) was used to detect the proteins of interest.

3.3.9. Animals experiments

Male ob/ob mice (6 weeks old) were purchased from Japan SLC Inc. (Japan). The mouse strain was originated from Jackson Laboratory (USA) [81], and was developed to C57BL/6JHamSlc-ob in Japan SLC Inc. (Japan). Male C57BL/6 mice (6 weeks old) supplied by Orient Bio (Korea) were used as the non-obesity control group. The mice were housed at a controlled temperature (24 °C ± 1 °C) and 50-55% humidity with a 12 hrs light/12 hrs dark cycle. All experiments were carried out according to the National Institute of Health Guide for the Care and Use of Laboratory Animals and were approved by the Institutional Animal Care and Use Committee of Jeju National University (ACUCC; approval No. 2018-0051)

3.3.10. Sample treatment

The ob/ob mice were allocated randomly into five groups (n = 5): control ob/ob group and 4 sample-treated groups were orally administrated SFN (0.5 mg/kg body weight), GRN (2.5 mg/kg body weight), and BLE (50 mg/kg and 500 mg/kg) every day in their drinking water assuming that each mouse drinks 20 mL of water per day. The concentrations of SFN and GRN were selected based on previous studies [124]. The samples were diluted with distilled water, and the mice were given access to water and food ad libitum. The samples were replaced with freshly prepared solutions every day to compensate for the degradative loss of the active

compounds. After 6 weeks of sample treatment, the mice were fasted overnight and sacrificed. The liver tissues were collected and stored at −80 °C for further experiments.

3.3.11. Total RNA isolation, library preparation, sequencing, and data analysis

The total RNA was purified from liver tissues using an Easy-blue RNA extraction kit (iNtRON Biotechnology, Korea) according to the manufacturer's protocol. The RNA quality and quantity were analyzed on an Agilent 2100 bioanalyzer using the RNA 6000 Nano Chip (Agilent Technologies, Netherlands) and ND-2000 Spectrophotometer (Thermofisher), respectively. The control and test RNA libraries were constructed using Quantseq 3′ mRNA-Seq Library Prep Kit (Lexogen, Austria). Briefly, 500 ng of the total RNA was prepared, and an oligo-dT primer containing an Illumina-compatible sequence at its 5′ end was hybridized to the RNA. Reverse transcription was then performed. Following degradation of the RNA template, complementary strand synthesis was initiated by a random primer containing an Illumina-compatible linker sequence at its 5′ end. Magnetic beads were used to eliminate all the reaction components. The library was amplified to add the complete adaptor sequences required for cluster generation. The constructed library was purified from the polymerase chain reaction mixture. High-throughput sequencing was performed as single-end 75 sequencings using Illumina NextSeq 500 (Illumina, USA). The QuantSeq 3′ mRNA-Seq reads were aligned using Bowtie2 version 2.1.0. The Bowtie2 indices were either generated from representative transcript sequences or the genome assembly sequence to align with the transcriptome and genome. The alignments were used to assemble transcripts,

estimating their abundances, and detecting differential expression of genes. The differentially expressed genes were determined based on the counts from unique and multiple alignments using R version 3.2.2 and Bioconductor version 3.0. The Read count (RC) data were analyzed based on the Quantile normalization method using the Genowiz™ version 4.0.5.6 (Ocimum Biosolutions, India). The PPI network was analyzed using the STRING application tool. Cytoscape (version 2.7), a bioinformatics platform at the Institute of System Biology, USA, was used to construct the network diagrams. Gene classification was performed using the Medline database (National Center for Biotechnology Information, USA)

3.3.12. Statistical analysis

Values are expressed as the means ± SEM of three independent experiments. The data were statistically analyzed using IBM SPSS Statistics (Ver.17.0; USA). The statistical differences between the groups were observed with one-way analysis of variance (ANOVA) followed by a Turkey's test. The $P < 0.05$, $P < 0.005$, and $P < 0.0005$ indicate statistically significant differences from the control group.

3.4. Results

3.4.1. DPPH radical scavenging activity

The anti-oxidant activity of the SFN and BLE was determined based on the DPPH radical scavenging activity. According to the results, the DPPH free radical scavenging activity was increased by BLE and SFN (Fig. 34). In contrast, GRN did not exhibit any free radical scavenging activity compared to the control. SFN showed up to 58% radical scavenging activity with 500 µg/mL. The radical scavenging ability of BLE was increased by 20%, 40%, and 43% with 1,000 µg/mL, 2,000 µg/mL, and 2,500 µg/mL concentrations respectively. The calculated IC_{50} values of SFN, BLE, and GRN were 405.79 ± 14.6, 740.18 ± 6.85, and 4,163.5 ± 167 µg/mL, respectively. In addition, the AEAC of SFN, BLE, and GRN were 2,557.97 ± 89.08, 1,402.36 ± 31.06, and 249.309 ± 8.22 mg AA/100g, respectively (Table 5). These results indicate that both SFN and BLE showed antioxidant potential through the free radical scavenging.

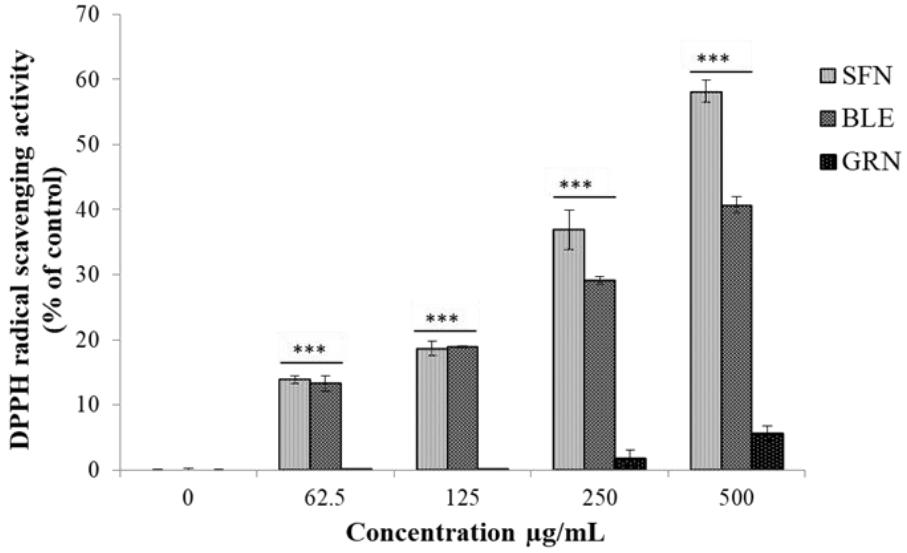

Fig. 34. DPPH radical scavenging activity of SFN and BLE.

The results are the means of ± SEM for three independent experiments. DPPH, 2,2-diphenyl-1-picrylhydrazyl; SFN, sulforaphane; GRN, glucoraphanin. $^{***}P < 0.0005$ compared to the control.

Table 5. Antioxidant activity of samples expressed as IC^{50} and AEAC values

Sample	IC^{50} Values (μg/mL)	AEAC Values
SFN	405.79 ± 14.6	2,557.97 ± 89.08
BLE	740.18 ± 6.85	1,402.36 ± 31.06
GRN	4,163.5 ± 167	249.309 ± 8.22
Ascorbic acid	10.38 ± 0.12	-

Values represent as mean ± SE. IC_{50}, the concentration at which 50% of free radical scavenged; AEAC, AA equivalent antioxidant capacity expressed as AA/100 g dry weight; AA, ascorbic acid; SFN, sulforaphane; GRN, glucoraphanin.

3.4.2. Effects of BLE on cell viability in RAW 264.7 cells

Cytotoxicity of BLE on RAW 264.7 cells was evaluated through MTT assay. The results indicated that BLE did not reduce the viability of RAW 264.7 cells up to 1,500 μg/mL concentration (Fig. 35). Accordingly, further *in vitro* experiments were conducted with the non-toxic concentrations of BLE.

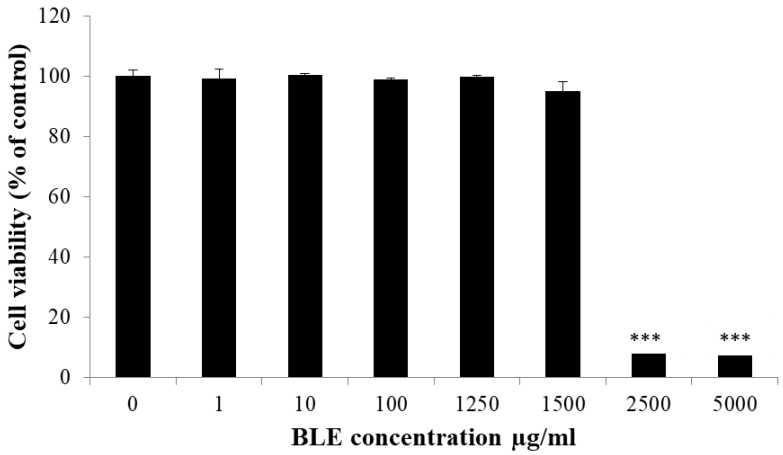

Fig. 35. Effects of BLE on RAW 264.7 cell viability.

Cells were pretreated with different concentrations of BLE for 1 hr, and then stimulated with LPS for 24 hrs. Cell viability was measured by MTT assay. All data are expressed as mean ± SEM (n = 3). ***$P < 0.0001$ compared with the control.

3.4.3. Inhibition of LPS-stimulated NO production in RAW 264.7 cells

To examine the effects of SFN and BLE on LPS-stimulated NO production in RAW 264.7 cells, the amount of NO released from the cells was determined using a Griess assay. In addition, the cell morphology was observed to ensure the experiments were performed under the right conditions. As shown in Fig. 36A, the morphologies of the RAW 264.7 cells were not changed after treating the SFN and GRN with LPS compared to the control cells. The results suggested that both SFN and GRN used in this study do not alter the RAW 264.7 cell morphology. Based on the Griess assay results, NO production was increased significantly after the LPS treatment in RAW 264.7 cells compared to the normal cells (Fig. 36). The treatment of SFN and BLE inhibited LPS-stimulated NO production in a concentration-dependent manner, whereas the GRN treatment showed no significant change in NO

production. The inhibition level of LPS-stimulated NO production was decreased significantly to 78% and 80% at 5 μM of SFN and 1,000 μg/mL of BLE compared to the LPS-treated control cells. The result confirmed that SFN and BLE inhibited NO production in LPS-stimulated RAW 264.7 cells.

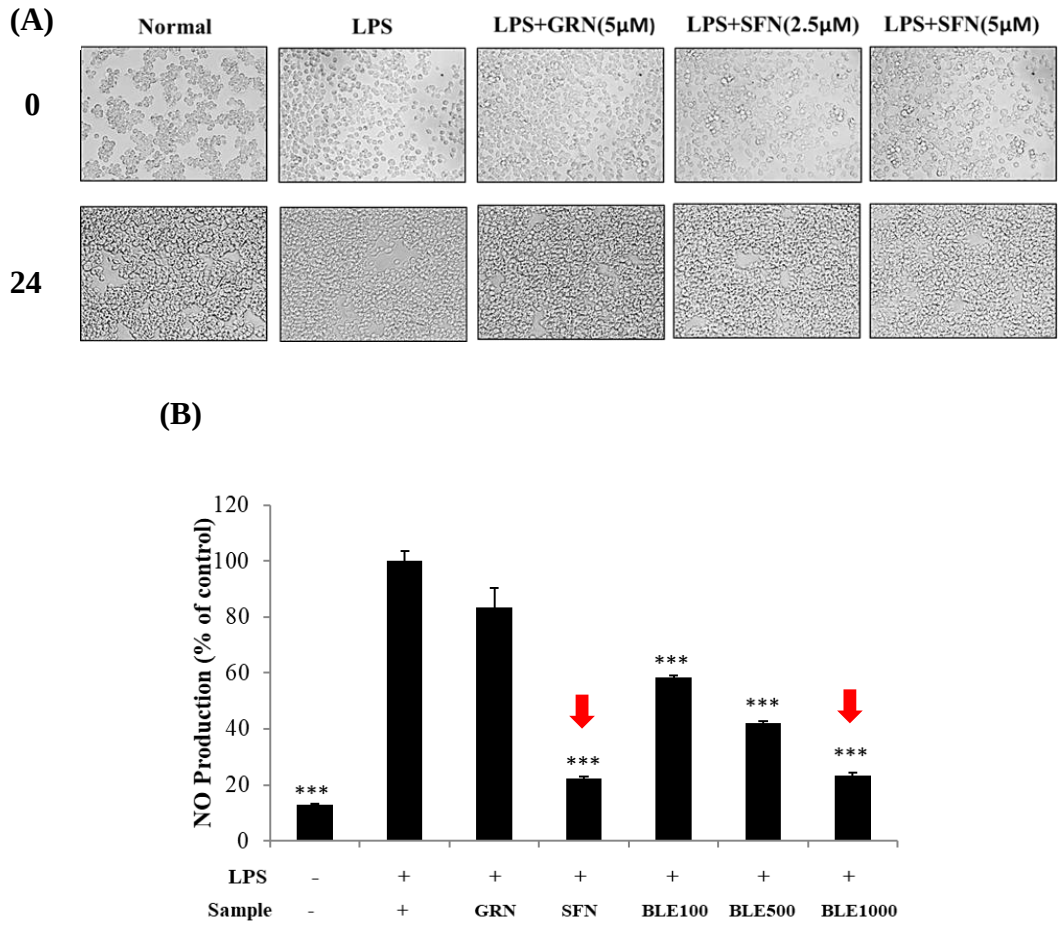

Fig. 36. Cell morphology and NO production in LPS-induced RAW 264.7 cells. Phase-contrast microscopy (20×) showing the morphology of RAW 264.7 cells before and after incubation with samples for 24 hrs (A). NO production by LPS-stimulated RAW 264.7 cells treated with or without SFN and GRN (B). All data are expressed as the mean ± SEM. ****P* < 0.0001 compared to the control.

3.4.4. Inhibition of LPS-stimulated COX-2 and iNOS production in RAW 264.7 cells

The inhibitory effect of SFN and BLE on the expression levels of the COX-2 and iNOS proteins in LPS-stimulated RAW 264.7 cells were investigated by western blot analysis (Fig. 37). The results demonstrated that un-stimulated RAW 264.7 cells did not express iNOS and COX-2 proteins, but LPS treatment significantly increased iNOS and COX-2 expression. Cells treated with SFN showed a significant decrease in COX-2 and iNOS levels as compared to LPS treated control cells, whereas GRN treated cells did not show significantly decreased COX-2 and iNOS levels. BLE treated cells showed a significant inhibitory effect of expression of iNOS and COX-2 in a concentration-dependent manner (Fig. 37). These results indicated that SFN and BLE regulate the inflammation by inhibiting the iNOS and COX-2 in LPS-stimulated RAW 264.7 cells.

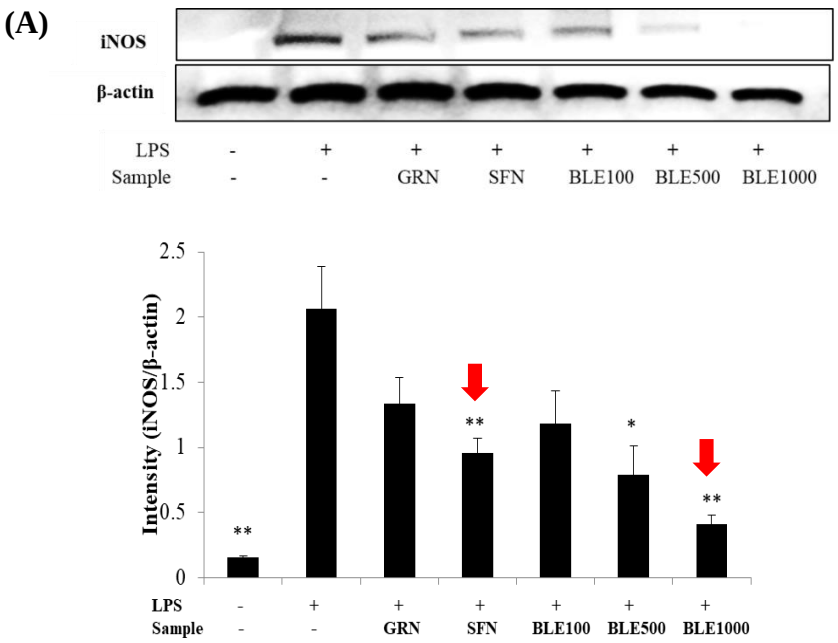

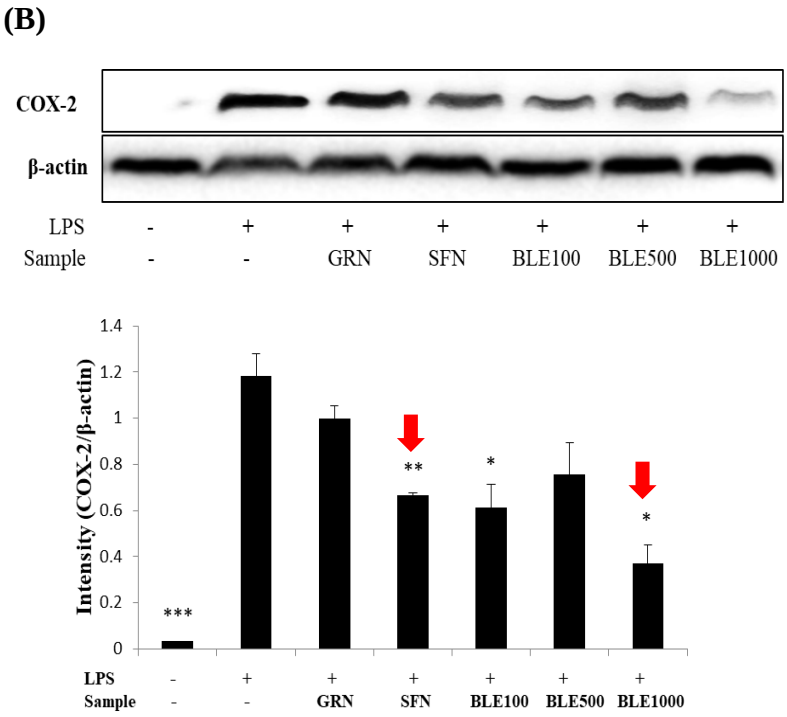

Fig. 37. Effects of SFN and BLE on iNOS and COX-2 expressions

Cells were incubated with or without samples and LPS for 24 hrs. The iNOS and COX-2 protein expression levels were determined by Western blotting, and the relative levels of iNOS (A) and COX-2 (B) proteins were normalized to β-actin. All data are expressed as mean ± SEM (n = 3). *P < 0.01, **P < 0.001, ***P < 0.0001 compared with the control.

3.4.5. Inhibitory effect of SFN and BLE on TNF-α, IL-6, and IL-1β production

The effects of SFN and BLE on the LPS-stimulated pro-inflammatory cytokines, TNF-α, IL-6, and IL-1β production were investigated in RAW 264.7 cells (Fig. 38). Treatment of SFN showed significant inhibition of TNF-α, IL-6, and IL-1β production. In contrast, GRN did not significantly affect the production of those

cytokines in LPS-stimulated RAW 264.7 cells. SFN inhibited the LPS-stimulated TNF- α, IL-6, and IL-1β production by 32%, 31%, and 53%, respectively, at 5 μM compared to the control. BLE inhibited the production of TNF-α by 14%, 25%, and 31% with 100 μg/mL, 500 μg/mL, and 1,000 μg/mL sample concentrations respectively compared to the control. IL-6 production was inhibited by 24%, 35%, and 44% with 100 μg/mL, 500 μg/mL, and 1,000 μg/mL BLE concentrations respectively. IL-1β production was inhibited by 19%, 28%, and 34% with 100 μg/mL, 500 μg /mL, and 1,000 μg/mL BLE concentrations respectively compared to the control. Results confirme that SFN and BLE inhibited the pro-inflammatory cytokines in LPS-stimulated RAW 264.7 cells.

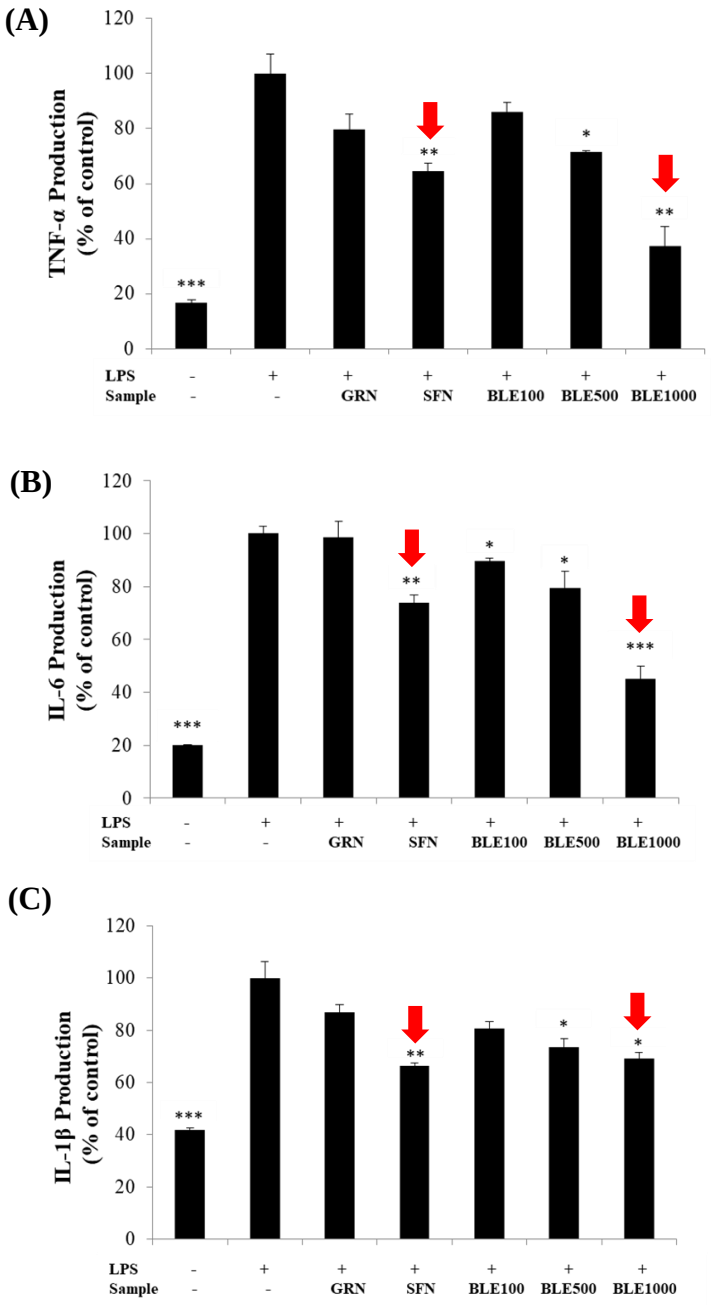

Fig. 38. Effects of SFN and BLE on the productions of pro-inflammatory cytokines in LPS-stimulated RAW 264.7 cells.

Cells were incubated with or without samples and LPS for 24 hrs. The levels of IL-1β, IL-6, and TNF-α released by LPS-stimulated RAW 264.7 cells into the culture

supernatants were measured by ELISA assay kit. Production of TNF-α (A), production of IL-6 (B), and production of IL-1β (C) by LPS-stimulated RAW 264.7 cells. All data are expressed as mean ± SEM (n = 3). *P< 0.01, **P < 0.001, ***P < 0.0001 compared with the control.

3.4.6. Differential gene expression analysis of ob/ob mice liver

RNA sequencing analysis was performed to observe the effects of SFN and BLE on the expression levels of the genes related to inflammation in ob/ob mice. The functional annotation of the genes was evaluated by Gene Ontology (GO) analysis. As shown in Fig. 39, a large portion of the genes related to inflammation was up- or down-regulated in the SFN and BLE-treated ob/ob mice and control ob/ob mice compared to normal mice. The up-regulated (> 2-fold) 28 genes, including *Ccl1*, *Ccl4*, *Cxcr1*, *Ccr3*, and *Ifng*, and 6 down-regulated (lower than 0.6-fold) genes, including *Fn1*, *Itgb2l*, *Pik3cd*, and *Adora2a*, were normalized to the control level by the SFN and BLE (Tables 6 and 7). The PPI network was constructed using the STRING analysis to understand the relationship between normalized genes by SFN and BLE. The PPI network was visualized as nodes (genes) and edges (interactions between the genes), as shown in Fig. 39D. Among the proteins related to inflammation, the chemokine ligands (*Ccl1*, *Ccl4*, *Ccl3*, and *Ccl17*) and chemokine receptors (*Cxcr1*, *Ccr3*, and *Ccr10*) were closely associated and formed a large "functional cluster" in the middle of the network (Fig. 39D). The present results confirmed that SFN and BLE restored the expression levels of the genes related to inflammation to the normal level, which were up or down-regulated in ob/ob mice.

Table 6. Up-regulated genes related to inflammation in ob/ob mice liver which were normalized by SFN & BLE

Gene symbol	obob/ Normal	**SFN/ Normal**	GRN/ Normal	**BLE50/ Normal**	**BLE500/ Normal**
Gpx2	16.245	0.951	0.954	0.974	0.951
Alox5	10.686	0.944	0.947	0.970	0.944
Cst7	7.909	1.750	1.889	5.936	0.937
Fut7	7.358	0.968	0.969	0.983	0.968
Zfr2	7.220	0.955	0.958	0.976	0.955
Nqo1	6.633	2.785	3.459	2.435	1.198
Dcst1	6.488	0.973	1.956	0.986	0.973
Eomes	4.736	0.987	0.988	0.993	0.987
Ccl17	**4.091**	**0.896**	0.902	**4.808**	**1.363**
Ifng	3.785	0.987	0.988	0.993	0.987
Ifng	3.785	0.987	0.988	0.993	0.987
Pdgfb	3.729	2.094	1.991	0.722	1.109
Ccl1	**3.728**	**1.872**	0.980	**0.989**	**0.978**
Ccl1	**3.631**	**0.98**	0.991	**0.984**	**0.978**
Trem1	3.572	3.592	0.956	0.975	0.953
Trem1	3.572	3.592	0.956	0.975	0.953
Npy	3.561	6.299	0.954	0.974	0.951
Cxcl14	3.231	1.448	1.255	3.102	1.279
Lgals3	3.008	1.661	0.811	1.082	1.096
Tnfrsf14	2.852	0.990	0.991	0.995	0.990
Relb	2.769	2.023	0.658	0.652	1.118
Ccl4	2.710	**1.814**	1.672	**0.799**	**0.983**
Cxcr1	2.704	**1.814**	1.931	**0.97**	**0.96**
Tlr13	2.690	0.926	0.727	1.122	1.089
Ccr10	2.589	**0.933**	1.881	**1.713**	**0.933**
Cd46	2.568	**1.724**	0.932	**0.961**	**0.928**
Ccr3	2.403	**0.216**	0.217	**0.925**	**1.255**
Myc	2.303	1.236	0.776	0.064	1.153
Plp1	2.293	1.287	0.303	0.167	1.299
P2ry14	2.237	1.280	2.261	1.054	1.038
Sqstm1	2.168	1.28	1.039	1.247	1.181
Ccl3	2.046	**0.141**	0.313	**2.608**	**0.876**
Ikbke	1.996	0.961	0.733	0.768	0.932

Table 7. Down-regulated genes related to inflammation in ob/ob mice liver which were normalized by SFN & BLE

Gene symbol	Ob/ob/ Normal	**SFN/ Normal**	GRN/ Normal	**BLE50/ Normal**	**BLE500/ Normal**
Tspan2	0.415	1.101	0.376	0.952	1.440
Fn1	0.508	0.818	0.622	0.866	0.730
Ticam1	0.533	1.181	0.698	1.429	1.206
Pik3cd	0.544	0.807	0.352	0.855	1.176
Tcirg1	0.566	0.636	0.556	1.104	0.935
Itgb2l	0.568	0.962	1.488	0.812	0.815
Adora2a	0.595	0.688	0.761	0.846	1.005

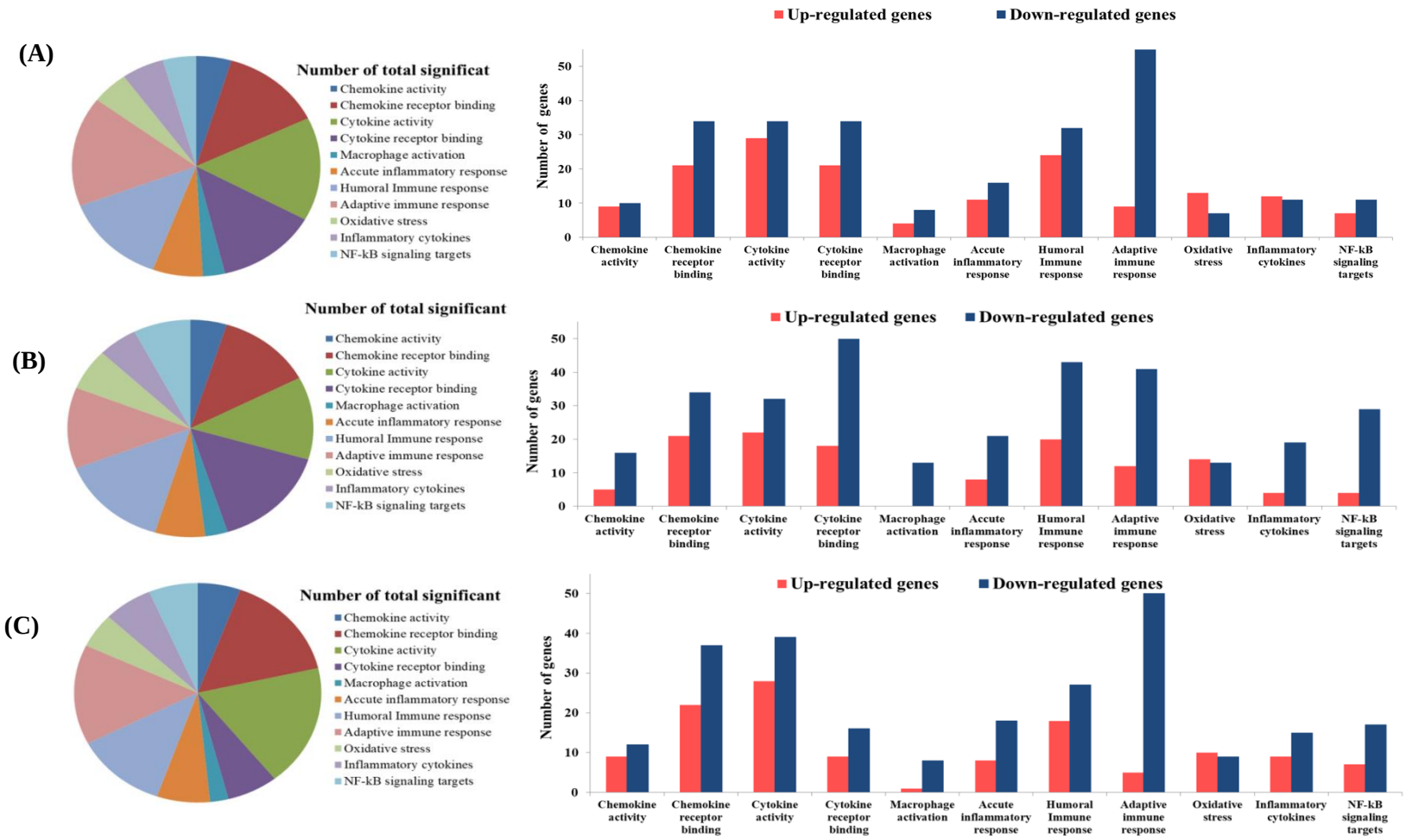

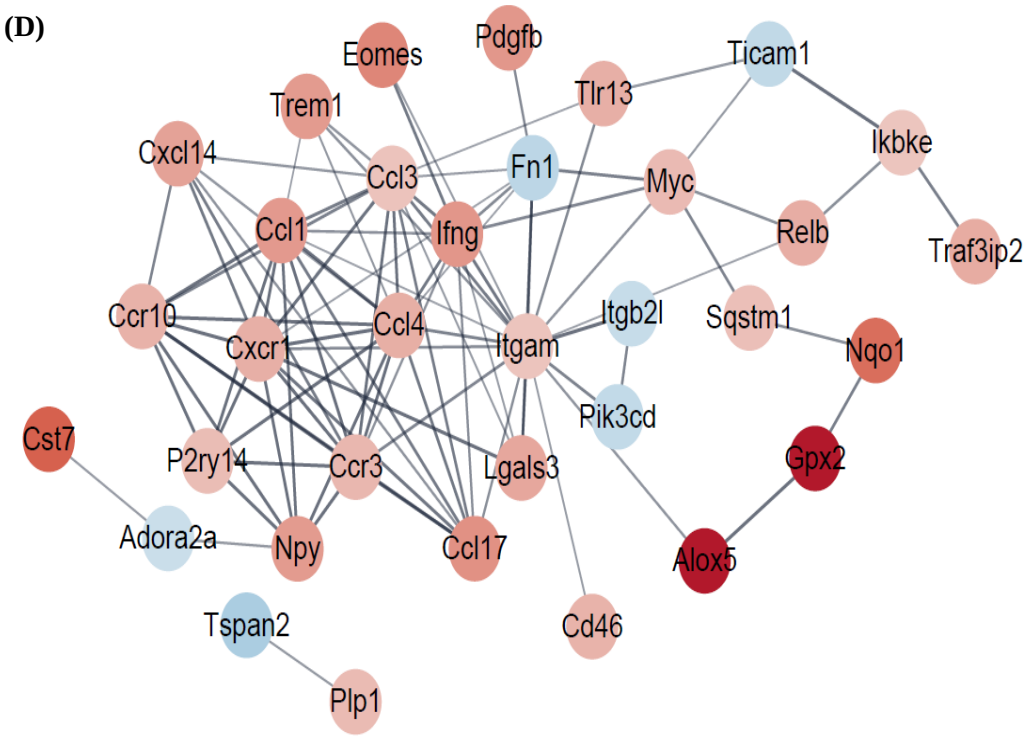

Fig. 39. Differential gene expression in ob/ob mice liver.

GO analysis of control ob/ob mice compared to the normal mice (A), SFN treated ob/ob mice compared to the normal mice (B), 500 mg/mL of BLE treated ob/ob mice compared to the normal mice (C), (The pie chart indicates functional categorization of the differentially expressed genes in ob/ob mice liver, and the bar graph represents the number of genes up and down-regulated). PPI network of normalized genes related to inflammation in BLE treated ob/ob mice (D). Red circles represent up-regulated genes, and blue circles represent down-regulated genes in control ob/ob mice.

3.5. Discussion

This study examined the anti-inflammatory effects of SFN enriched BLE on LPS-stimulated RAW 264.7 macrophage cells. The results showed that both SFN and BLE increased the DPPH free radical scavenging activity. In addition, SFN and BLE suppressed the expression of iNOS, COX-2, and pro-inflammatory cytokines (TNF-α, IL-6, and IL-1β) in LPS-stimulated RAW 264.7 cells. In particular, both SFN and BLE showed anti-inflammatory effects by normalizing the expression of the genes related to inflammation, including chemokine ligands (*Cxcl14*, *Ccl1*, *Ccl3*, *Ccl4*, and *Ccl17*) and chemokine receptors (*Cxcr1*, *Ccr3*, *and Ccr10*), which were perturbed in ob/ob mice liver.

In the present study, SFN and BLE showed antioxidant potential through a DPPH assay in a concentration-dependent manner. Previous studies reported that isothiocyanates extracted from broccoli were strongly correlated with DPPH radical scavenging activity [125, 126]. Similarly, in the present study, SFN had potent free radical scavenging activity compared to the GRN. Because oxidative stress induces inflammation [127], the antioxidant activity of SFN and BLE might improve the healing procedure of inflammation.

In this study, SFN and BLE inhibited the levels of COX-2 and iNOS expression in LPS-stimulated RAW 264.7 cells, with concomitant decreases in NO production. The production of NO by iNOS leads to the activation of macrophages against microorganisms [128]. On the other hand, overexpression of NO, a key biomarker of oxidative stress, causes oxidative damage during the inflammatory process [129]. COX-2 is involved in the production of prostaglandins, which causes an increase in

chemotaxis, blood flow, and subsequent dysfunction of tissues during inflammation [130]. The previous study reported that SFN enriched broccoli florets extract suppressed NO production and iNOS expression by inhibiting the NF-κB activity in LPS-stimulated RAW 264.7 cells [131]. In addition, SFN decreased the levels of COX-2 and prostaglandin E_2 in LPS-stimulated RAW 264.7 cells [132, 133]. Consistent with previous findings, the results confirmed that the biological activity of SFN is firmly attributed to the inhibitory effects on COX-2, iNOS, and NO production in LPS-stimulated RAW 264.7 cells. In addition, GRN, without enzymatic conversion to SFN, did not show significant anti-inflammatory effects on LPS-stimulated RAW 264.7 cells compared to SFN.

In the present study, SFN and BLE exhibited its anti-inflammatory effects by inhibiting the production of pro-inflammatory cytokines, including TNF-α, IL-6, and IL-1β in LPS-stimulated RAW 264.7 cells. A recent study reported that SFN inhibited the production of TNF-α, IL-6, and IL-1β through activation of the Nrf2/HO-1 pathway and inhibition of the JNK/AP-1/NF-κB pathway in LPS-activated microglia [134]. Therefore the anti-inflammatory effects of SFN and BLE might result from the inhibitory effects on the production of pro-inflammatory cytokines in LPS-stimulated RAW 264.7 cells.

In the present study, RNA sequencing analysis was conducted to reveal the molecular mechanism underlying the anti-inflammatory effect of SFN and BLE on the obesity-induced inflammation in ob/ob mice. The gene expression results showed that SFN and BLE normalized the expression levels of up-regulated genes related to the inflammation, including *Cxcl14*, *Ccl1*, *Ccl3*, *Ccl4*, *Ccl17*, *Cxcr1*, *Ccr3*, *Ccr10*, and Ifng genes in the ob/ob mice liver. *Cxcl14* mediated leukocyte migration and

differentiation [135]. In addition, *Cxcl14* involves the obesity-associated infiltration of macrophages into tissues and hepatic steatosis in obese mice [136]. *Ccl1* acts as a chemoattractant for NK cells, monocytes, immature B cells and dendritic cells [137]. Inhibition of *Ccl1* reduced liver inflammation and fibrosis progression [138]. Ccl3 promotes the recruitment of CD4+ T cells to the liver, and increased *Ccl3* expression was observed in the patient with liver injury [139]. *Ccl17* shows chemotactic activity for $CD4^+$ T cells and plays a role in trafficking and activation of mature T cells [140]. Furthermore, chemokine receptors (*Ccr1*, *Ccr10*, and *Ccr3*) interact with their specific chemokine ligands, which cause various cell responses, such as chemotaxis [141]. In the liver, IFN-γ activates resident macrophages [142] and stimulates hepatocyte apoptosis by enhancing ROS production [143].

Remarkably, in the present study, chemokine ligands (*Cxcl14*, *Ccl1*, *Ccl3*, *Ccl4*, and *Ccl17*) and chemokine receptors (*Cxcr1*, *Ccr3*, and *Ccr10*) were identified as hub genes because they formed a "functional cluster" within the PPI network. These results suggest that chemokine proteins might play key roles in the obesity-induced inflammation in ob/ob mice liver. Therefore, the treatment of SFN can normalize liver inflammation by normalizing the up-regulated genes related to chemokines in ob/ob mice liver.

In addition, the current results showed that SFN and BLE normalized the down-regulated genes related to inflammation, including *Fn1*, *Itgb21*, and *Pik3cd* in ob/ob mice liver. *Fn1* produces soluble plasma fibronectin-1, which is involved mainly in blood clotting, wound healing, and protects against excessive liver fibrosis [144]. *Itgb2* encodes CD18, which inhibits the capability of the immune system to fight off infection [145]. *Pik3cd* regulates the immune cell metabolism through the PI3K-

AKT-mTOR signaling pathway [146]. These findings suggest that down regulation of *Fn1*, *Itgb21*, and *Pikk3cd* genes might involve the progress of inflammation by dysregulating immune responses in the ob/ob mice liver.

In conclusion, SFN in BLE has a potent anti-inflammatory activity, as demonstrated by its ability to inhibit the NO, COX-2, iNOS, and pro-inflammatory cytokines (TNF-α, IL-6, and IL-1β) in LPS-stimulated RAW 264.7 cells. In particular, gene expression analysis showed that SFN restores the obesity-induced inflammation by normalizing the genes related to chemokine signaling, including chemokine ligands (*Cxcl14*, *Ccl1*, *Ccl3*, *Ccl4*, and *Ccl17*) and chemokine receptors (*Cxcr1*, *Ccr3*, and *Ccr10*) in ob/ob mouse livers. Overall, SFN in BLE has a potent anti-inflammatory effect by normalizing the expression levels of the genes related to inflammation that had been perturbed in ob/ob mice (Fig. 40).

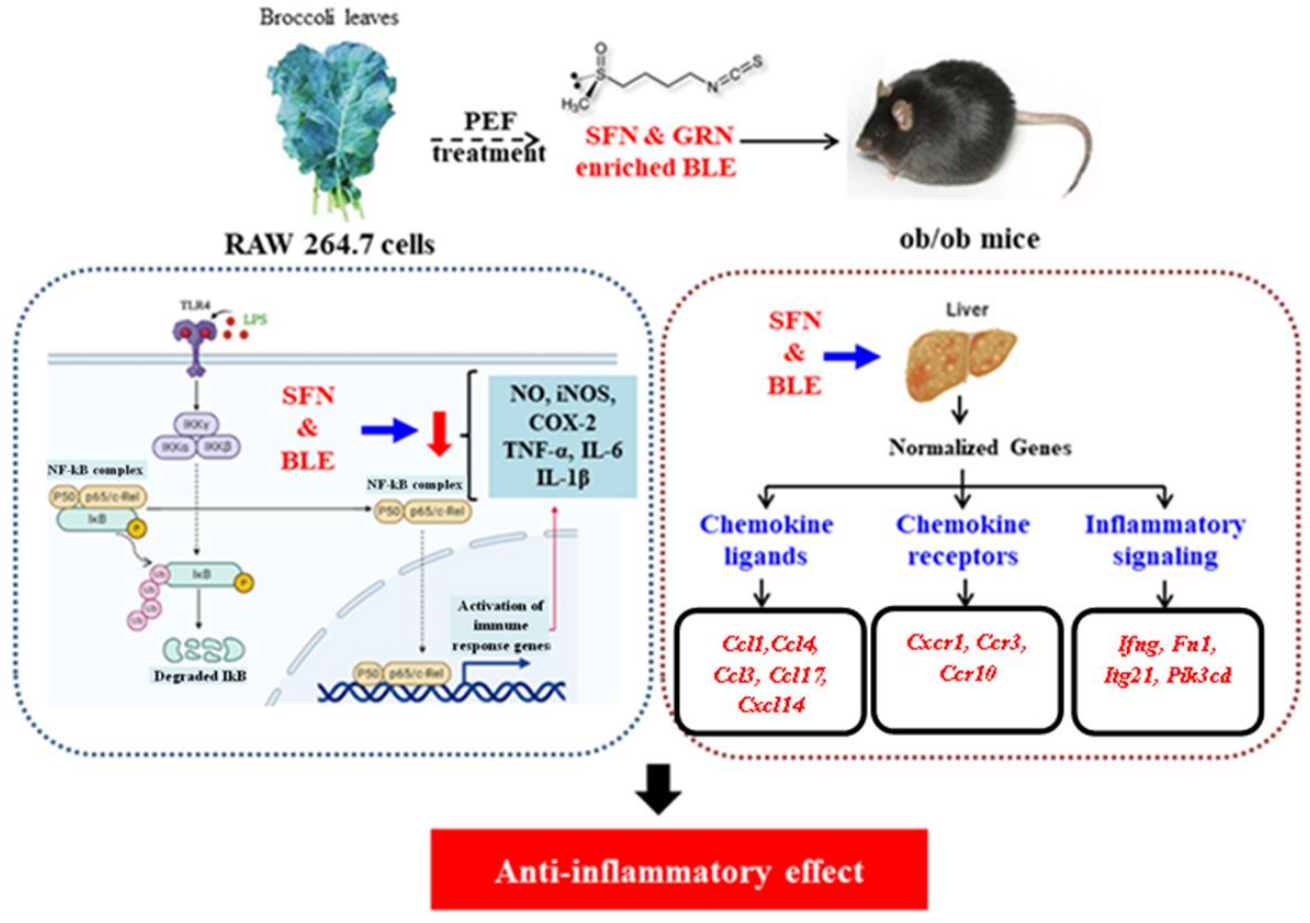

Fig. 40. Anti-inflammatory effect of SFN and BLE

General Conclusion

This research provides evidence that SFN in BLE exhibits anti-diabetic, anti-obesity, and anti-inflammatory effects by normalizing the expressions of genes involve in insulin signaling, lipid metabolism, and inflammation. Herein, PPI network analysis of differentially expressed genes was performed to reveal hub genes associated with diabetic, obesity, and inflammation which are up- and down-regulated in ob/ob mice and were normalized by SFN and BLE.

Anti-diabetic study in HepG2 cells and ob/ob mice exhibited that SFN and BLE increase insulin sensitivity by phosphorylation of Akt and GSK3β. In addition, SFN and BLE increased glucose uptake in HepG2 cells and enhanced glucose tolerance in ob/ob mice which reflects SFN and BLE affected glucose metabolism in diabetic condition. More importantly, differential gene expression analysis revealed that SFN and BLE improved systemic insulin sensitivity and glucose metabolism through normalizing the expression of insulin signaling related genes including *Atf3*, *Atf4*, *Foxc2*, and *Myc*, and glucose metabolism associated genes including *Phkg1*, *Phka1*, *Pygm*, *Gys1*, and *Pgc-1α* in ob/ob mice.

- **SFN & BLE exert Anti-diabetic effect by normalizing the expression of genes related to Insulin Signaling & Glucose Metabolism**

Anti-obesity study revealed that SFN and BLE reduced lipid accumulation and TG content, and increased glucose uptake by activating AMPK in 3T3-L1 adipocytes. In addition, SFN and BLE decreased serum lipid profile (TG, LDL, and TC), and hepatic lipid accumulation by activating the AMPK pathway in ob/ob mice. In

particular, differential gene expression analysis revealed that both SFN and BLE exert an anti-obesity effect by normalizing the expression of genes related to lipid metabolism including *Srebf2*, *Pla2g2c*, *Plb1*, *Ip6k3*, *Elovl5*, *Elovl7*, *Slc27a3*, *Plcg1*, *Fgfr1*, *Pik3cd*, *plcb4*, *Ctp1a*, and *Lipin1* genes in ob/ob mice

- **SFN & BLE exhibit Anti-obesity effect by normalizing the expression of genes involved in Lipid Metabolism**

Anti-inflammatory study showed that SFN and BLE inhibited the production of inflammatory mediators (TNF-α, IL-6, IL-1β, NO, COX-2, and iNOS) in LPS-stimulated RAW 264.7 cells. In addition, SFN and BLE restored the obesity-induced inflammation by normalizing the expression of genes related to chemokine signaling including chemokine ligands (*Cxcl14*, *Ccl1*, *Ccl3*, *Ccl4*, and *Ccl17*) and chemokine receptors (*Cxcr1*, *Ccr3*, and *Ccr10*) in ob/ob mice.

- **SFN & BLE exhibit Anti-inflammatory effect by normalizing the expression of genes involved in inflammation**

Overall, The present study provided evidence that SFN in BLE exhibits anti-diabetic, anti-obesity, and anti-inflammatory effects by restoring the disturbed gene expression related to diabetes, obesity, and inflammation to normal level (Fig. 41).

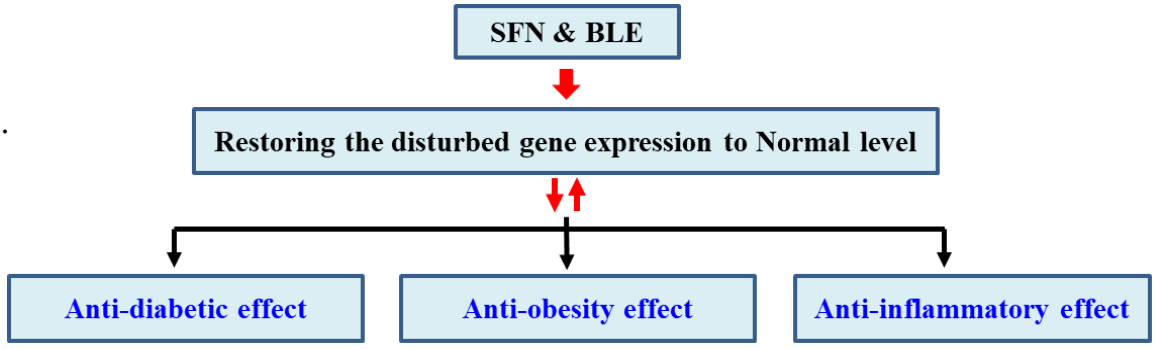

Fig. 41. SFN in BLE exerts anti-diabetic, anti-obesity, and anti-inflammatory effects by restoring the disturbed gene expression to normal level

However, further studies focusing on these hub genes are required to confirm the underlying mechanisms of SFN in BLE. In our future study, we will evaluate the expression of those genes at the protein level.

References

1. **Maahs DM, West NA, Lawrence JM, Mayer-Davis EJ**. Epidemiology of Type 1 Diabetes. Endocrinol Metab Clin 2010, **39**, 481–497.

2. **Alberti KGMM, Zimmet PZ**. Definition, diagnosis and classification of diabetes mellitus and its complications. Part 1: diagnosis and classification of diabetes mellitus. Provisional report of a WHO Consultation. Diabet Med 1998, **15**, 539–553.

3. **Bastaki S**. Diabetes mellitus and its treatment. Int J Diabetes Metab 2015, **13**, 111–134.

4. **Whiteman EL, Cho H, Birnbaum MJ**. Role of Akt/protein kinase B in metabolism. Trends Endocrinol Metab 2002, **13**, 444–451.

5. **Beg M, Abdullah N, Thowfeik FS, Altorki NK, McGraw TE**. Distinct Akt phosphorylation states are required for insulin regulated Glut4 and Glut1-mediated glucose uptake. Elife 2017, **6**, e26896.

6. **Esser N, Legrand-Poels S, Piette J, Scheen AJ, Paquot N**. Inflammation as a link between obesity, metabolic syndrome and type 2 diabetes. Diabetes Res Clin Pract 2014, **105**, 141–450.

7. **Spiegelman BM, Flier JS**. Obesity and the Regulation of Energy Balance. Cell 2001, **104**, 531–543.

8. **Ke R, Xu Q, Li C, Luo L, Huang D**. Mechanisms of AMPK in the maintenance of ATP balance during energy metabolism. Cell Biol Int 2018, **42**,

384–392.

9. **Hardie DG**. Minireview: The AMP-Activated Protein Kinase Cascade: The Key Sensor of Cellular Energy Status. Endocrinology 2003, **144**, 5179–5183.

10. **Daval M, Foufelle F, Ferré P**. Functions of AMP-activated protein kinase in adipose tissue. J Physiol 2006, **574**, 55–62.

11. **Henin N, Vincent MF, Gruber HE, Van den Berghe G**. Inhibition of fatty acid and cholesterol synthesis by stimulation of AMP-activated protein kinase. FASEB J 1995, **9**, 541–546.

12. **Wellen KE, Hotamisligil GS**. Inflammation, stress, and diabetes. J Clin Invest 2005, **115**, 1111–1119.

13. **Surmi BK, Hasty AH**. Macrophage infiltration into adipose tissue: initiation, propagation and remodeling. Future Lipidol 2008, **3**, 545–556.

14. **Sutter AG, Palanisamy AP, Lench JH, Jessmore AP, Chavin KD**. Development of steatohepatitis in Ob/Ob mice is dependent on Toll-like receptor 4. Ann Hepatol 2015, **14**, 735–743.

15. **Sun B, Karin M**. Obesity, inflammation, and liver cancer. J Hepatol 2012, **56**, 704–713.

16. **Owis AI**. Broccoli; the green beauty: A review. J Pharm Sci Res 2015, **7**, 696–703.

17. **Bahadoran Z, Tohidi M, Nazeri P, Mehran M, Azizi F, Mirmiran P**. Effect of broccoli sprouts on insulin resistance in type 2 diabetic patients: a

randomized double-blind clinical trial. Int J Food Sci Nutr 2012, **63**, 767–771.

18. **Aborehab NM, El Bishbishy MH, Waly NE**. Resistin mediates tomato and broccoli extract effects on glucose homeostasis in high fat diet-induced obesity in rats. BMC Complement Altern Med 2016, **16**, 225.

19. **Glade MJ, Meguid MM**. A Glance at… Broccoli, glucoraphanin, and sulforaphane. Nutrition 2015, **31**, 1175–1178.

20. **Lai R-H, Miller MJ, Jeffery E**. Glucoraphanin hydrolysis by microbiota in the rat cecum results in sulforaphane absorption. Food Funct 2010, **1**, 161–166.

21. **Choi KM, Lee YS, Kim W, Kim SJ, Shin KO, Yu JY, et al.** Sulforaphane attenuates obesity by inhibiting adipogenesis and activating the AMPK pathway in obese mice. J Nutr Biochem 2014, **25**, 201–207.

22. **Lee JH, Moon MH, Jeong JK, Park YG, Lee YJ, Seol JW, et al.** Sulforaphane induced adipolysis via hormone sensitive lipase activation, regulated by AMPK signaling pathway. Biochem Biophys Res Commun 2012, **426**, 492–497.

23. **de Souza CG, Sattler JA, de Assis AM, Rech A, Perry MLS, Souza DO**. Metabolic Effects of Sulforaphane Oral Treatment in Streptozotocin-Diabetic Rats. J Med Food 2012, **15**, 795–801.

24. **Xu Y, Fu JF, Chen JH, Zhang ZW, Zou ZQ, Han LY, et al.** Sulforaphane ameliorates glucose intolerance in obese mice via the upregulation of the insulin signaling pathway. Food Funct 2018, **9**, 4695–4701.

25. **Axelsson, Annika S., Emily Tubbs, Brig Mecham, Shaji Chacko, Hannah A, et al.** Sulforaphane reduces hepatic glucose production and improves glucose control in patients with type 2 diabetes. Sci Transl Med 2017, **9**, 4477.

26. **Nagata N, Xu L, Kohno S, Ushida Y, Aoki Y, Umeda R, et al.** Glucoraphanin ameliorates obesity and insulin resistance through adipose tissue browning and reduction of metabolic endotoxemia in mice. Diabetes 2017, **66**, 1222–1236.

27. **Farahmandi K, Khazdoozy S, Barati S**. The Effect of Hydro-Alcoholic Extract of Broccoli Leaves on Sugar and Lipids in Serum of Diabetic Rats. Asian J. Biomed. Pharm. Sci. 2013, **3**, 24.

28. **Lamb J, Crawford ED, Peck D, Modell JW, Blat IC, Wrobel MJ, et al.** The Connectivity Map: Using Gene-Expression Signatures to Connect Small Molecules, Genes, and Disease. Science 2006, **313**, 1929-1935.

29. **Kukurba KR, Montgomery SB**. RNA Sequencing and Analysis. Cold Spring Harb Protoc 2015, **2015**, 951–969.

30. **Liu X, Yang X, Chen X, Zhang Y, Pan X, Wang G, et al.** Expression Profiling Identifies Bezafibrate as Potential Therapeutic Drug for Lung Adenocarcinoma. J Cancer 2015, **6**, 1214–1221.

31. **Sirota M, Dudley JT, Kim J, Chiang AP, Morgan AA, Sweet-Cordero A, et al.** Discovery and Preclinical Validation of Drug Indications Using Compendia of Public Gene Expression Data. Sci Transl Med 2011, **3**, 9677 - 9677.

32. **Dudley JT, Sirota M, Shenoy M, Pai RK, Roedder S, Chiang AP, et al.** Computational repositioning of the anticonvulsant topiramate for inflammatory bowel disease. Sci Transl Med 2011, **3**, 9676.

33. **Safari-Alighiarloo N, Taghizadeh M, Rezaei-Tavirani M, Goliaei B, Peyvandi AA**. Protein-protein interaction networks (PPI) and complex diseases. Gastroenterol Hepatol from bed to bench 2014, **7**, 17–31.

34. **Jaeger S, Aloy P**. From protein interaction networks to novel therapeutic strategies. IUBMB Life 2012, **64**, 529–537.

35. **Mahdi T, Hänzelmann S, Salehi A, Muhammed SJ, Reinbothe TM, Tang Y, et al.** Secreted Frizzled-Related Protein 4 Reduces Insulin Secretion and Is Overexpressed in Type 2 Diabetes. Cell Metab 2012, **16**, 625–633.

36. **Zhang B, Horvath S**. A general framework for weighted gene co-expression network analysis. Stat Appl Genet Mol Biol 2005, **4**, Article17.

37. **Wang J, Wu T, Fang L, Liu C, Liu X, Li H, et al.** Anti-diabetic effect by walnut (Juglans mandshurica Maxim.)-derived peptide LPLLR through inhibiting α-glucosidase and α-amylase, and alleviating insulin resistance of hepatic HepG2 cells. J Funct Foods 2020, **69**, 103944.

38. **Shao J-W, Jiang J-L, Zou J-J, Yang M-Y, Chen F-M, Zhang Y-J, et al.** Therapeutic potential of ginsenosides on diabetes: From hypoglycemic mechanism to clinical trials. J Funct Foods 2020, **64**, 103630.

39. **Bahadoran Z, Mirmiran P, Hosseinpanah F, Rajab A, Asghari G, Azizi F**. Broccoli sprouts powder could improve serum triglyceride and oxidized

LDL/LDL-cholesterol ratio in type 2 diabetic patients: A randomized double-blind placebo-controlled clinical trial. Diabetes Res Clin Pract 2012, **96**, 348–354.

40. **Fahey JW, Holtzclaw WD, Wehage SL, Wade KL, Stephenson KK, Talalay P**. Sulforaphane Bioavailability from Glucoraphanin-Rich Broccoli: Control by Active Endogenous Myrosinase. PLoS One 2015, **10**, e0140963.

41. **Angelino D, Jeffery E**. Glucosinolate hydrolysis and bioavailability of resulting isothiocyanates: Focus on glucoraphanin. J Funct Foods 2014, **7**, 67–76.

42. **Axelsson AS, Tubbs E, Mecham B, Chacko S, Nenonen HA, Tang Y, et al.** Sulforaphane reduces hepatic glucose production and improves glucose control in patients with type 2 diabetes. Sci Transl Med 2017, **9**, 4477.

43. **Song MY, Kim EK, Moon WS, Park JW, Kim HJ, So HS, et al.** Sulforaphane protects against cytokine- and streptozotocin-induced β-cell damage by suppressing the NF-κB pathway. Toxicol Appl Pharmacol 2009, **235**, 57–67.

44. **Zhang HQ, Chen SY, Wang AS, Yao AJ, Fu JF, Zhao JS, et al.** Sulforaphane induces adipocyte browning and promotes glucose and lipid utilization. Mol Nutr Food Res 2016, **60**, 2185–2197.

45. **Teng W, Li Y, Du M, Lei X, Xie S, Ren F**. Sulforaphane Prevents Hepatic Insulin Resistance by Blocking Serine Palmitoyltransferase 3-Mediated Ceramide Biosynthesis. Nutrients 2019, **11**, 1185.

46. **Zang M, Zuccollo A, Hou X, Nagata D, Walsh K, Herscovitz H, et al.** AMP-activated protein kinase is required for the lipid-lowering effect of metformin in insulin-resistant human HepG2 cells. J Biol Chem 2004, **279**, 47898–47905.

47. **Nakajima K, Yamauchi K, Shigematsu S, Ikeo S, Komatsu M, Aizawa T, et al.** Selective attenuation of metabolic branch of insulin receptor down-signaling by high glucose in a hepatoma cell line, HepG2 cells. J Biol Chem 2000, **275**, 20880–20886.

48. **Teng JF, Lee CH, Hsu TH, Lo HC**. Potential activities and mechanisms of extracellular polysaccharopeptides from fermented Trametes versicolor on regulating glucose homeostasis in insulin-resistant HepG2 cells. PLoS One 2018, **13**, 1–18.

49. **Zou C, Wang Y, Shen Z**. 2-NBDG as a fluorescent indicator for direct glucose uptake measurement. J Biochem Biophys Methods 2005, **64**, 207–215.

50. **R. G, Carey VJ, D.M. B, Bolstad B, Dettling M, Dudoit S, et al.** Bioconductor: Open software development for computational biology and bioinformatics. Genome Biol 2004, **5**, R80.

51. **Heiss EH, Schachner D, Zimmermann K, Dirsch VM**. Glucose availability is a decisive factor for Nrf2-mediated gene expression. Redox Biol 2013, **1**, 359–365.

52. **Nagata N, Xu L, Kohno S, Ushida Y, Aoki Y, Umeda R, et al.** Glucoraphanin Ameliorates Obesity and Insulin Resistance Through Adipose

Tissue Browning and Reduction of Metabolic Endotoxemia in Mice. Diabetes 2017, **66**, 1222-1236.

53. **Kim JY, Park KJ, Hwang J-Y, Kim GH, Lee D, Lee YJ, et al.** Activating transcription factor 3 is a target molecule linking hepatic steatosis to impaired glucose homeostasis. J Hepatol 2017, **67**, 349–359.

54. **Zhang Q, Yu J, Liu B, Lv Z, Xia T, Xiao F, et al.** Central activating transcription factor 4 (ATF4) regulates hepatic insulin resistance in mice via S6K1 signaling and the vagus nerve. Diabetes 2013, **62**, 2230–2239.

55. **Seo J, Fortuno ES, Suh JM, Stenesen D, Tang W, Parks EJ, et al.** Atf4 Regulates Obesity, Glucose Homeostasis, and Energy Expenditure. Diabetes 2009, **58**, 2565-2573.

56. **Dahle MK, Grønning LM, Cederberg A, Blomhoff HK, Miura N, Enerbäck S, et al.** Mechanisms of FOXC2- and FOXD1-mediated regulation of the RIα subunit of cAMP-dependent protein kinase include release of transcriptional repression and activation by protein kinase bα and cAMP. J Biol Chem 2002, **277**, 22902–22908.

57. **Nian X, Zhang X, Wang Y, Li H, Li J, Liu H, et al.** Correlations of FOXC2 Gene Expression and Polymorphism with Type 2 Diabetes Mellitus. Clin Lab 2016, **62**, 781–791.

58. **Laybutt DR, Weir GC, Kaneto H, Lebet J, Palmiter RD, Sharma A, et al.** Overexpression of c-Myc in β-Cells of Transgenic Mice Causes Proliferation and Apoptosis, Downregulation of Insulin Gene Expression, and Diabetes.

Diabetes 2002, **51**, 1793-1804.

59. **Winchester JS, Rouchka EC, Rowland NS, Rice NA**. In Silico characterization of phosphorylase kinase: Evidence for an alternate intronic polyadenylation site in PHKG1. Mol Genet Metab 2007, **92**, 234–242.

60. **Burwinkel B, Hu B, Schroers A, Clemens PR, Moses SW, Shin YS, et al.** Muscle glycogenosis with low phosphorylase kinase activity: Mutations in PHKA1, PHKG1 or six other candidate genes explain only a minority of cases. Eur J Hum Genet 2003, **11**, 516–526.

61. **Agius L**. Role of glycogen phosphorylase in liver glycogen metabolism. Mol Aspects Med 2015, **46**, 34–45.

62. **Hunter RW, Zeqiraj E, Morrice N, Sicheri F, Sakamoto K**. Expression and purification of functional human glycogen synthase-1:glycogenin-1 complex in insect cells. Protein Expr Purif 2015, **108**, 23–29.

63. **Davit-Spraul A, Piraud M, Dobbelaere D, Valayannopoulos V, Labrune P, Habes D, et al.** Liver glycogen storage diseases due to phosphorylase system deficiencies: Diagnosis thanks to non invasive blood enzymatic and molecular studies. Mol Genet Metab 2011, **104**, 137–143.

64. **Ashcroft FM, Rohm M, Clark A, Brereton MF**. Is Type 2 Diabetes a Glycogen Storage Disease of Pancreatic β Cells? Cell Metab 2017, **26**, 17–23.

65. **Besse-Patin A, Jeromson S, Levesque-Damphousse P, Secco B, Laplante M, Estall JL**. PGC1A regulates the IRS1:IRS2 ratio during fasting to influence hepatic metabolism downstream of insulin. Proc Natl Acad Sci 2019,

116, 4285-4290.

66. **Koliaki C, Szendroedi J, Kaul K, Jelenik T, Nowotny P, Jankowiak F, et al.** Adaptation of hepatic mitochondrial function in humans with non-alcoholic fatty liver is lost in steatohepatitis. Cell Metab 2015, **21**, 739–746.

67. **Ahrens M, Ammerpohl O, von Schönfels W, Kolarova J, Bens S, Itzel T, et al.** DNA methylation analysis in nonalcoholic fatty liver disease suggests distinct disease-specific and remodeling signatures after bariatric surgery. Cell Metab 2007, **18**, 296–302.

68. **Gillberg L, Jacobsen SC, Ribel-Madsen R, Gjesing AP, Boesgaard TW, Ling C, et al.** Does DNA methylation of PPARGC1A influence insulin action in first degree relatives of patients with type 2 diabetes? PLoS One 2013, **8**, e58384.

69. **Westerbacka J, Kolak M, Kiviluoto T, Arkkila P, Sirén J, Hamsten A, et al.** Genes Involved in Fatty Acid Partitioning and Binding, Lipolysis, Monocyte/Macrophage Recruitment, and Inflammation Are Overexpressed in the Human Fatty Liver of Insulin-Resistant Subjects. Diabetes 2007, **56**, 2759-2765.

70. **Romieu I, Dossus L, Barquera S, Blottière HM, Franks PW, Gunter M, et al.** Energy balance and obesity: what are the main drivers? Cancer Causes Control 2017, **28**, 247–258.

71. **Sarwar R, Pierce N, Koppe S**. Obesity and nonalcoholic fatty liver disease: current perspectives. Diabetes Metab Syndr Obes 2018, **11**, 533–542.

72. **Hardie DG**. AMP-activated protein kinase: maintaining energy homeostasis at the cellular and whole-body levels. Annu Rev Nutr 2014, **34**, 31–55.

73. **Jeon S-M**. Regulation and function of AMPK in physiology and diseases. Exp Mol Med 2016, **48**, e245–e245.

74. **Hardie DG, Pan DA**. Regulation of fatty acid synthesis and oxidation by the AMP-activated protein kinase. Biochem Soc Trans 2002, **30**, 1064–1070.

75. **Carling D, Clarke PR, Zammit VA, Hardie DG**. Purification and characterization of the AMP-activated protein kinase. Copurification of acetyl-CoA carboxylase kinase and 3-hydroxy-3-methylglutaryl-CoA reductase kinase activities. Eur J Biochem 1989, **186**, 129–136.

76. **Luo T, Nocon A, Fry J, Sherban A, Rui X, Jiang B, et al.** AMPK Activation by Metformin Suppresses Abnormal Extracellular Matrix Remodeling in Adipose Tissue and Ameliorates Insulin Resistance in Obesity. Diabetes 2016, **65**, 2295–2310.

77. **Shaw RJ, Lamia KA, Vasquez D, Koo S-H, Bardeesy N, Depinho RA, et al.** The kinase LKB1 mediates glucose homeostasis in liver and therapeutic effects of metformin. Science 2005, **310**, 1642–1646.

78. **Karri S, Sharma S, Hatware K, Patil K**. Natural anti-obesity agents and their therapeutic role in management of obesity: A future trend perspective. Biomed Pharmacother 2019, **110**, 224–238.

79. **Liu Y, Sun M, Yao H, Liu Y, Gao R**. Herbal Medicine for the Treatment of Obesity: An Overview of Scientific Evidence from 2007 to 2017. Kismali G,

editor. Evidence-Based Complement Altern Med 2017, **2017**, 8943059.

80. **Rizzatti V, Boschi F, Pedrotti M, Zoico E, Sbarbati A, Zamboni M**. Lipid droplets characterization in adipocyte differentiated 3T3-L1 cells: size and optical density distribution. Eur J Histochem 2013, **57**, e24.

81. **Coleman DL**. Obese and diabetes: Two mutant genes causing diabetes-obesity syndromes in mice. Diabetologia 1978, **14**, 141–148.

82. **Langmead**. Bowtie2. Nat Methods 2013, **9**, 357–359.

83. **Choi K-M, Lee Y-S, Sin D-M, Lee S, Lee MK, Lee Y-M, et al.** Sulforaphane Inhibits Mitotic Clonal Expansion During Adipogenesis Through Cell Cycle Arrest. Obesity 2012, **20**, 1365–1371.

84. **Chen J, Bao C, Kim JT, Cho JS, Qiu S, Lee HJ**. Sulforaphene Inhibition of Adipogenesis via Hedgehog Signaling in 3T3-L1 Adipocytes. J Agric Food Chem 2018, **66**, 11926–11934.

85. **Liu D, Wang A, Liu J, Alkhalidy H, Zhen W, Moore W**. Genistein in Combination with Sulforaphane for the Treatment of Type 2 Diabetes. FASEB J 2019, **31**, 646-651.

86. **Yang G, Lee HE, Lee JY**. A pharmacological inhibitor of NLRP3 inflammasome prevents non-alcoholic fatty liver disease in a mouse model induced by high fat diet. Sci Rep 2016, **6**, 1–11.

87. **Xu X, Dai M, Lao F, Chen F, Hu X, Liu Y, et al.** Effect of glucoraphanin from broccoli seeds on lipid levels and gut microbiota in high-fat diet-fed

mice. J Funct Foods 2020, **68**, 103858.

88. **Armah CN, Derdemezis C, Traka MH, Dainty JR, Doleman JF, Saha S, et al.** Diet rich in high glucoraphanin broccoli reduces plasma LDL cholesterol: Evidence from randomised controlled trials. Mol Nutr Food Res 2015, **59**, 918–926.

89. **Tao R, Xiong X, DePinho RA, Deng CX, Dong XC**. Hepatic SREBP-2 and cholesterol biosynthesis are regulated by FoxO3 and Sirt6. J Lipid Res 2013, **54**, 2745–2753.

90. **Dennis EA, Cao J, Hsu Y-H, Magrioti V, Kokotos G**. Phospholipase A2 enzymes: physical structure, biological function, disease implication, chemical inhibition, and therapeutic intervention. Chem Rev 2011, **111**, 6130–6185.

91. **Chakraborty A, Koldobskiy MA, Bello NT, Maxwell M, Potter JJ, Juluri KR, et al.** Inositol pyrophosphates inhibit Akt signaling, thereby regulating insulin sensitivity and weight gain. Cell 2010, **143**, 897–910.

92. **Zhu Q, Ghoshal S, Rodrigues A, Gao S, Asterian A, Kamenecka TM, et al.** Adipocyte-specific deletion of Ip6k1 reduces diet-induced obesity by enhancing AMPK-mediated thermogenesis. J Clin Invest 2016, **126**, 4273–4288.

93. **Rao F, Xu J, Fu C, Cha JY, Gadalla MM, Xu R, et al.** Inositol pyrophosphates promote tumor growth and metastasis by antagonizing liver kinase B1. Proc Natl Acad Sci U S A 2015, **112**, 1773–1778.

94. **Moritoh Y, Oka M, Yasuhara Y, Hozumi H, Iwachidow K, Fuse H, et al.**

Inositol Hexakisphosphate Kinase 3 Regulates Metabolism and Lifespan in Mice. Sci Rep 2016, **6**, 1–13.

95. **Naganuma T, Sato Y, Sassa T, Ohno Y, Kihara A**. Biochemical characterization of the very long-chain fatty acid elongase ELOVL7. FEBS Lett 2011, **585**, 3337–3341.

96. **Anderson CM, Stahl A**. SLC27 fatty acid transport proteins. Mol Aspects Med 2013, **34**, 516–528.

97. **Steiling H, Wüstefeld T, Bugnon P, Brauchle M, Fässler R, Teupser D, et al.** Fibroblast growth factor receptor signalling is crucial for liver homeostasis and regeneration. Oncogene 2003, **22**, 4380–4388.

98. **Böhm F, Speicher T, Hellerbrand C, Dickson C, Partanen JM, Ornitz DM, et al.** FGF receptors 1 and 2 control chemically induced injury and compound detoxification in regenerating livers of mice. Gastroenterology 2010, **139**, 1385–1396.

99. **Ocker M**. Fibroblast growth factor signaling in non-alcoholic fatty liver disease and non-alcoholic steatohepatitis: Paving the way to hepatocellular carcinoma. World J Gastroenterol 2020, **26**, 279–290.

100. **Liu W, Struik D, Nies VJM, Jurdzinski A, Harkema L, De Bruin A, et al.** Effective treatment of steatosis and steatohepatitis by fibroblast growth factor 1 in mouse models of nonalcoholic fatty liver disease. Proc Natl Acad Sci U S A 2016, **113**, 2288–2293.

101. **Oliva-Vilarnau N, Hankeova S, Vorrink SU, Mkrtchian S, Andersson ER,**

Lauschke VM. Calcium Signaling in Liver Injury and Regeneration. Front Med 2018, **5**, 192.

102. **Rufer AC, Thoma R, Hennig M**. Structural insight into function and regulation of carnitine palmitoyltransferase. Cell Mol Life Sci 2009, **66**, 2489–2501.

103. **Chen Y, Rui BB, Tang LY, Hu CM**. Lipin family proteins - Key regulators in lipid metabolism. Ann Nutr Metab 2015, **66**, 10–18.

104. **Croce MA, Eagon JC, Lariviere LL, Korenblat KM, Klein S, Finck BN**. Hepatic Lipin 1 ᴺᴸ Expression Is Diminished in. Regulation 2007, **56**, 2395–2399.

105. **Perfield JW, Ortinau LC, Pickering RT, Ruebel ML, Meers GM, Rector RS**. Altered Hepatic Lipid Metabolism Contributes to Nonalcoholic Fatty Liver Disease in Leptin-Deficient Ob/Ob Mice. Almobarak A, editor. J Obes 2013, **2013**, 296537.

106. **Harrison DG, Guzik TJ, Lob HE, Madhur MS, Marvar PJ, Thabet SR, et al.** Inflammation, immunity, and hypertension. Hypertension 2011, **57**, 132–140.

107. **Shapiro H, Lutaty A, Ariel A**. Macrophages, meta-inflammation, and immuno-metabolism. ScientificWorldJournal 2011, **11**, 2509–2529.

108. **Biswas SK, Lewis CE**. NF-κB as a central regulator of macrophage function in tumors. J Leukoc Biol 2010, **88**, 877–884.

109. **Li Q, Verma IM**. NF-κB regulation in the immune system. Nat Rev Immunol 2002, **2**, 725–734.

110. **Ye J, McGuinness OP**. Inflammation during obesity is not all bad: evidence from animal and human studies. AJP Endocrinol Metab 2013, **304**, E466–477.

111. **Ellulu MS, Patimah I, Khaza'ai H, Rahmat A, Abed Y**. Obesity and inflammation: the linking mechanism and the complications. Arch Med Sci 2017, **13**, 851–863.

112. **Hotamisligil GS**. Inflammation and metabolic disorders. Nature 2006, **444**, 860–867.

113. **Lauterbach MAR, Wunderlich FT**. Macrophage function in obesity-induced inflammation and insulin resistance. Pflugers Arch 2017, **469**, 385–396.

114. **Perfield 2nd JW, Ortinau LC, Pickering RT, Ruebel ML, Meers GM, Rector RS**. Altered hepatic lipid metabolism contributes to nonalcoholic fatty liver disease in leptin-deficient Ob/Ob mice. J Obes 2013, **2013**, 296537.

115. **Santín-Márquez R, Alarcón-Aguilar A, López-Diazguerrero NE, Chondrogianni N, Königsberg M**. Sulforaphane - role in aging and neurodegeneration. GeroScience 2019, **41**, 655–670.

116. **Xu L, Nagata N, Ota T**. Glucoraphanin: a broccoli sprout extract that ameliorates obesity-induced inflammation and insulin resistance. Adipocyte 2018, **7**, 218–225.

117. **Galuppo M, Giacoppo S, De Nicola GR, Iori R, Mazzon E, Bramanti P**.

RS-Glucoraphanin bioactivated with myrosinase treatment counteracts proinflammatory cascade and apoptosis associated to spinal cord injury in an experimental mouse model. J Neurol Sci 2013, **334**, 88–96.

118. **Sotokawauchi A, Ishibashi Y, Matsui T, Yamagishi S**. Aqueous Extract of Glucoraphanin-Rich Broccoli Sprouts Inhibits Formation of Advanced Glycation End Products and Attenuates Inflammatory Reactions in Endothelial Cells. Ohta Y, editor. Evidence-Based Complement Altern Med 2007, **2018**, 9823141.

119. **Vo Q V, Nam P, Dinh T, Mechler A, Tran T**. Anti-inflammatory activity of synthetic and natural glucoraphanin. J Serbian Chem Soc 2019, **84**, 445-453.

120. **Dinkova-Kostova AT, Fahey JW, Kostov R V., Kensler TW**. KEAP1 and done? Targeting the NRF2 pathway with sulforaphane. Trends in Food Science and Technology 2017, **69,** 257–269.

121. **Li B, Cui W, Liu J, Li R, Liu Q, Xie X-H, et al.** Sulforaphane ameliorates the development of experimental autoimmune encephalomyelitis by antagonizing oxidative stress and Th17-related inflammation in mice. Exp Neurol 2013, **250**, 239–249.

122. **Sánchez-Moreno C, Larrauri J a., Saura-calixto F**. A procedure to measure the antiradical efficienc y of polyphenols. J Sci Food Agric 1998, **270**, 270–276.

123. **Vuong LD, Nguyen QN, Truong V-L**. Anti-inflammatory and anti-oxidant effects of combination between sulforaphane and acetaminophen in LPS-

stimulated RAW 264.7 macrophage cells. Immunopharmacol Immunotoxicol 2019, **41**, 413–419.

124. **Bai Y, Wang X, Zhao S, Ma C, Cui J, Zheng Y**. Sulforaphane Protects against Cardiovascular Disease via Nrf2 Activation. Oxid Med Cell Longev 2015, **2015**, 407580.

125. **Plumb GW, Price KR, Rhodes MJ, Williamson G**. Antioxidant properties of the major polyphenolic compounds in broccoli. Free Radic Res 1997, **27**, 429–435.

126. **Jang HW, Moon J-K, Shibamoto T**. Analysis and Antioxidant Activity of Extracts from Broccoli (*Brassica oleracea* L.) Sprouts. J Agric Food Chem 2015, **63**, 1169–1174.

127. **Salzano S, Checconi P, Hanschmann E-M, Lillig CH, Bowler LD, Chan P, et al.** Linkage of inflammation and oxidative stress via release of glutathionylated peroxiredoxin-2, which acts as a danger signal. Proc Natl Acad Sci 2014, **111**, 12157–12162.

128. **MacMicking J, Xie QW, Nathan C**. Nitric oxide and macrophage function. Annu Rev Immunol 2007, **15**, 323–350.

129. **Tripathi P, Tripathi P, Kashyap L, Singh V**. The role of nitric oxide in inflammatory reactions. FEMS Immunol Med Microbiol 1997, **51**, 443–452.

130. **Mitchell JA, Larkin S, Williams TJ**. Cyclooxygenase-2: Regulation and relevance in inflammation. Biochem Pharmacol 1995, **50**, 1535–1542.

131. **Hwang JH, Lim S Bin**. Antioxidant and anti-inflammatory activities of Broccoli florets in LPS-stimulated RAW 264.7 Cells. Prev Nutr Food Sci 2014, **19**, 89–97.

132. **Qi T, Xu F, Yan X, Li S, Li H**. Sulforaphane exerts anti-inflammatory effects against lipopolysaccharide-induced acute lung injury in mice through the Nrf2/ARE pathway. Int J Mol Med 2016, **37**, 182–188.

133. **Reddy SA, Shelar SB, Dang T-M, Lee BN-C, Yang H, Ong S-M, et al.** Sulforaphane and its methylcarbonyl analogs inhibit the LPS-stimulated inflammatory response in human monocytes through modulating cytokine production, suppressing chemotactic migration and phagocytosis in a NF-κB- and MAPK-dependent manner. Int Immunopharmacol 2015, **24**, 440–450.

134. **Subedi L, Lee JH, Yumnam S, Ji E, Kim SY**. Anti-Inflammatory Effect of Sulforaphane on LPS-Activated Microglia Potentially through JNK/AP-1/NF-κB Inhibition and Nrf2/HO-1 Activation. Cells 2019, **8**, 194.

135. **Lu J, Chatterjee M, Schmid H, Beck S, Gawaz M**. CXCL14 as an emerging immune and inflammatory modulator. J Inflamm (Lond) 2016, **13**, 1.

136. **Nara N, Nakayama Y, Okamoto S, Tamura H, Kiyono M, Muraoka M, et al.** Disruption of CXC Motif Chemokine Ligand-14 in Mice Ameliorates Obesity-induced Insulin Resistance. J Biol Chem 2007, **282**, 30794–30803.

137. **Roos RS, Loetscher M, Legler DF, Clark-Lewis I, Baggiolini M, Moser B**. Identification of CCR8, the receptor for the human CC chemokine I-309. J Biol Chem 1997, **272**, 17251–17254.

138. **Heymann F, Hammerich L, Storch D, Bartneck M, Huss S, Rüsseler V, et al.** Hepatic macrophage migration and differentiation critical for liver fibrosis is mediated by the chemokine receptor C-C motif chemokine receptor 8 in mice. Hepatology 2012, **55**, 898–909.

139. **Ajuebor MN, Hogaboam CM, Le T, Proudfoot AEI, Swain MG**. CCL3/MIP-1α is pro-inflammatory in murine T cell-mediated hepatitis by recruiting CCR1-expressing CD4+ T cells to the liver. Eur J Immunol 2004, **34**, 2907–2918.

140. **Gilet J, Chang Y, Chenivesse C, Legendre B, Vorng H, Duez C, et al.** Role of CCL17 in the Generation of Cutaneous Inflammatory Reactions in Hu-PBMC-SCID Mice Grafted with Human Skin. J Invest Dermatol 2009, **129**, 879–890.

141. **Murdoch C, Finn A**. Chemokine receptors and their role in inflammation and infectious diseases. Blood 2000, **95**, 3032–3043.

142. **Crispe IN**. The liver as a lymphoid organ. Annu Rev Immunol 2009, **27**, 147–63.

143. **Watanabe Y, Suzuki O, Haruyama T, Akaike T**. Interferon-gamma induces reactive oxygen species and endoplasmic reticulum stress at the hepatic apoptosis. J Cell Biochem 2003, **89**, 244–253.

144. **To WS, Midwood KS**. Plasma and cellular fibronectin: distinct and independent functions during tissue repair. Fibrogenesis Tissue Repair 2011, **4**, 21.

145. **Gjelstrup LC, Boesen T, Kragstrup TW, Jørgensen A, Klein NJ, Thiel S, et al.** Shedding of Large Functionally Active CD11/CD18 Integrin Complexes from Leukocyte Membranes during Synovial Inflammation Distinguishes Three Types of Arthritis through Differential Epitope Exposure. J Immunol 2010, **185**, 4154 -4168.

146. **Fruman DA, Chiu H, Hopkins BD, Bagrodia S, Cantley LC, Abraham RT**. The PI3K Pathway in Human Disease. Cell 2017, **170**, 605–635.

Acknowledgement

Foremost, I would like to express my sincere gratitude to my supervisor Prof. Chang-Hoon Han, for the continuous support of my PhD study and research with his patience, motivation, and immense knowledge. His guidance helped me in all the time of research and writing of this thesis.

Besides my supervisor, I would like to thank my thesis panel, Prof. Lee Young Jae, Prof. Jee Youngheun, Prof. Kim Se Jae, and Prof. Kim Min Young. Thank you for investing time and providing interesting and valuable feedback. I feel proud and honored that you have accepted to be on my committee.

In addition, I would like to thank my past and current lab members in the veterinary biochemistry lab, Mrs. Chanuri, Ms. Kyeong-Mi Yang, Mrs. Gyung Hye Yang, Mr. Daniel, Mrs. Priyanka, Miss Lakshi, and Mr. Kyungjun for their valuable support during my research and personal life in Jeju. I extended my gratitude to Miss. Suyama, Dr. Madushani and Korean friends who attached to other laboratories for their support during my research work and Jeju life. I am also so thankful to all Sri Lankan friends, who provided stimulating discussions as well as happy distractions to rest my mind outside of my research. My sincere thanks also goes to former and current Deans of the Center of International Affairs and their team members for their excellent encouragement and support during the stay at Jeju National University.

Of course, I also want to thank my mother and my late father, my husband, my son, my brothers, and in-laws for believing in me and being there for practical support in all those things of life beyond doing a PhD. I would like to thank all those

whom I have not mentioned above but helped me in various ways. I could not have completed this dissertation without the support of you all. Thank you so much for your encouragement.